DESIGN AND DEVELOPMENT OF PAPER-BASED MICROFLUIDICS FOR POINT-OF-CARE APPLICATIONS

A Thesis Submitted to
the Graduate School of İzmir Institute of Technology
in Partial Fulfillment of the Requirements for the Degree of

MASTER OF SCIENCE

in Bioengineering

by
Fatih ÖZEFE

December, 2020
İZMİR

I would like to dedicate this dissertation first to my dear grandmother, Fatma ÖZEFE, who I lost one month ago because of nCoV-2019. She was very supportive to me every time during my life. I also dedicate this to my parents for their love, patience, and support.

ACKNOWLEDGMENTS

I would like to express my sincere gratitude to my thesis committee members, Assoc. Prof. Arslan-Yildiz, Prof. Bulmus-Zareie, and Prof. Yesil-Celiktas. Special thanks are dedicated to my supervisor Dr. Arslan-Yildiz for her continuous guidance and support and for her patience and motivation during my thesis studies. Thank you for giving me opportunity to study in your research group. I would also thank my co-advisor Dr. Yildiz for opening his laboratory and for his knowledge, support and suggestions.

I would like to thank my colleagues in Biomimetics Laboratory and Biosens & Bioapps Laboratory for their help all the time. Baran, your help was very informative for me to learn computer coding and programming. Soner, you were so friendly and I am glad to work and study with you.

In addition, I thank to all my friends for providing support and friendship.

I would also like to thank my father, mother, and brother. Mom and dad, you were with me all the time and I know that there are not enough words to acknowledge. I totally know how much you have sacrificed your dreams to provide me a chance to achieve mine. I will never forget your support on me for my life. Furkan, you were always nice brother. Thanks to keep your eyes on our parents while I was away.

I especially want to give special thanks to Nilgün. Many thanks for your love and full support along this journey. You made me feel and believe everything possible. Never stop to smile. This accomplishment would not have been possible without you. Thank you.

Thank you.

ABSTRACT

DESIGN AND DEVELOPMENT OF PAPER-BASED MICROFLUIDICS FOR POINT-OF-CARE APPLICATIONS

Paper-based microfluidics is a subarea of microfluidics which is recently used in various applications from diagnostics to environmental monitoring, and to food safety. In such microfluidic systems, a test platform is formed from a paper substrate instead of silicon and polymers, such as poly-dimethylsiloxane, poly-methyl methacrylate, and etc. The main goal of this thesis is the development and fabrication of a paper-based microfluidic device (μPAD), which could be used in point-of-care (POC) applications. The characterizations of μPADs, which were fabricated via laser ablation methodology, were performed in terms of their surface and barrier characteristics, and liquid sample flows within μPADs. Depending on the characterization, nine different fabrication parameters, 10P40S (10%Power & 40%Speed), 10P60S, 20P90S, 30P50S, 30P100S, 40P80S, 40P100S, 70P80S, and 70P100S, were identified as optimized fabrication parameters. Also, two designed models of μPADs, 1S4T-Type2 and 1S4T-Type3, were selected to be used in the detection of BSA and recombinant Hepatitis C Virus (HCV) protein. The BSA and HCV (1 mg/ml) in PBS solution were successfully detected via naked eye depending on the colorimetric sensing through micro-paper enzyme linked immunosorbent assay (μP-ELISA) protocol. Moreover, the limit of detection (LoD) values for HCV were determined in 1S4T-Type2 μPAD as 1.000, 0.883, and 0.796 ng/ml when the detection was performed via naked eye, smart-phone, and bright-field microscope, respectively. Also, the easily-disposable 1S4T-Type2 μPAD provided 14 times faster and 45 times cheaper detection of HCV compared to conventional ELISA techniques. Consequently, the developed 1S4T-Type2 μPAD presented low-cost, easy-to-use, and rapid detection of HCV as POC devices.

ÖZET

HASTA-YANI UYGULAMALARI İÇİN KAĞIT TEMELLİ MİKROAKIŞKANLARIN DİZAYNI VE GELİŞTİRİLMESİ

Tanılama çalışmalarından çevresel izleme ve gıda güvenliğine kadar birçok farklı alanda kullanılan mikroakışkanların bir alt kolu da kağıt temelli mikroakışkanlardır (µPAD). Bu mikroakışkan sistemlerde, uygulamanın yapılacağı düzenekler silikon, polidimetilsiloksan ya da poli-metil metakrilat yerine kağıt kullanılarak elde edilmektedir. Bu tezin ana amacı hasta-yanı uygulamalarda (POC) kullanılabilecek kağıt temelli mikroakışkanların geliştirilmesidir. Tez çalışmaları süresince lazer kesim yöntemiyle elde edilen kağıt temelli mikroakışkanlar, yüzey ve kenar özellikleri ve ayrıca sistem içinde bulunan kanallardaki sıvı akışı açısından karakterize edildi. Yapılan karakterizasyon çalışmaları doğrultusunda, ideal üretim koşulları 10P40S (10% Güç & 40% Hız), 10P60S, 20P90S, 30P50S, 30P100S, 40P80S, 40P100S, 70P80S ve 70P100S olarak belirlendi. Ayrıca, BSA ve rekombinant Hepatit C Virüs (HCV) proteinin tespitinde kullanılacak kağıt temelli mikroakışkan modelleri, 1S4T-Type2 ve 1S4T-Type3 olarak belirlendi. Belirlenen koşullarda üretilen 1S4T-Type2 ve 1S4T-Type3 model kağıt temelli mikroakışkan sistemlerinde uygulanan mikro-kağıt ELISA testi (µP-ELISA) doğrultusunda fosfat tamponlu tuz (PBS) solüsyonu içerisinde bulunan BSA ve HCV proteinleri (1 mg/ml) başarılı bir şekilde renk değişimine bağlı olarak tespit edildi. Buna ek olarak, 1S4T-Type2 model kağıt temelli mikroakışkan sistemlerde, HCV proteini için tespit sınırı (LoD) gözle tespit için 1.000 ng/ml, akıllı telefon ile tespit için 0.883 ng/ml ve ışık mikroskopu ile tespit için 0.796 ng/ml olarak belirlendi. Kolay bir şekilde yok edilebilen bu 1S4T-Type2 model kağıt temelli mikroakışkan sistemler konvansiyonel ELISA testlerine göre HCV proteininin tespitini 14 kat daha hızlı ve 45 kat daha ucuz olacak şekilde gerçekleştirdi. Sonuç olarak geliştirilen 1S4T-Type2 model kağıt temelli mikroakışkan sistem aynı hasta-yanı uygulamalarında kullanılan cihazlar gibi HCV proteinin tespitini ucuz, kolay ve hızlı bir şekilde sağladı.

TABLE OF CONTENTS

LIST OF FIGURES

LIST OF TABLES

Table **Page**

LIST OF SYMBOLS AND/OR ABBREVIATIONS

µL: Microliter

µm: Micrometre

µPADs: Microfluidic paper-based analytical devices

µP-ELISA: Micro-Paper Enzyme Linked Immunosorbent Assay

100P10S: 100%Power & 10%Speed

10P100S: 10%Power & 100%Speed

10P10S: 10%Power & 10%Speed

10P20S: 10%Power & 20%Speed

10P30S: 10%Power & 30%Speed

10P40S: 10%Power & 40%Speed

10P50S: 10%Power & 50%Speed

10P60S: 10%Power & 60%Speed

10P70S: 10%Power & 70%Speed

10P80S: 10%Power & 80%Speed

10P90S: 10%Power & 90%Speed

1S1T µPAD: µPAD, which contains one sample inlet and one test zone

1S2T µPAD: µPAD, which contains one sample inlet and two test zone

1S4T-Type1 µPAD: Type1-µPAD, which contains one sample inlet and four test zone

1S4T-Type2 µPAD: Type2-µPAD, which contains one sample inlet and four test zone

1S4T-Type3 µPAD: Type3-µPAD, which contains one sample inlet and four test zone

1S8T µPAD: µPAD, which contains one sample inlet and eight test zone

20P10S: 20%Power & 10%Speed

20P90S: 20%Power & 90%Speed

2D µPADs: Two dimensional microfluidic paper-based analytical devices

30P100S: 30%Power & 100%Speed

30P10S: 30%Power & 10%Speed

30P50S: 30%Power & 50%Speed

3D µPADs: Three dimensional microfluidic paper-based analytical devices

40P100S: 40%Power & 100%Speed

40P10S: 40%Power & 10%Speed

40P80S: 40%Power & 80%Speed

50P10S: 50%Power & 10%Speed

60P10S: 60%Power & 10%Speed

70P100S: 70%Power & 100%Speed

70P10S: 70%Power & 10%Speed

70P80S: 70%Power & 80%Speed

80P10S: 80%Power & 10%Speed

90P10S: 90%Power & 10%Speed

AKD: Alkenyl ketene dimer

BSA: Bovine serum albumin

CL: Chemiluminescence

CO_2: Carbon dioxide

DBAE: 2-(dibutylamino)-ethanol

EC: Electrochemical

ECL: Electrochemiluminescence

ELISA: Enzyme Linked Immunosorbent Assay

ePADs: Electrochemical μPADs

H_2O_2: Hydrogen peroxide

HCV: Hepatitis C Virus

HPLC: High-pressure liquid chromatography

HRP: Horse radish peroxidase

LFIA: Lateral flow immunoassays

LOC: Lab-on-a-chip

LoD: Limit of Detection

MS: Mass spectroscopy

NADH: Nicotinamide adenine dinucleotide

OH^-: Hydroxyl group

PBS: Phosphate buffered saline

PDMS: Poly(dimethylsiloxane)

PEDs: Paper-based electrochemical devices

P-ELISA: Paper-ELISA

PMMA: Poly-methyl methacrylate

POC: Point-of-Care

POCT: Point-of-care testing

PoNBMA: Poly(o-nitrobenzyl methacrylate)

REDOX: Reduction-Oxidation

$Ru(bpy)_3^{2+}$: tris(2,2′-bipyridyl)ruthenium(II)

SEM: Scanning electron microscope

SERS: Surface-enhanced raman spectroscopy

TBPB: Tetrabromophenol blue

TMB: Tetramethylbenzidine

w/v: weight/volume

WHO: World Health Organization

μTAS: Miniaturized total analysis systems

CHAPTER 1.

INTRODUCTION

1.1. Microfluidics

Microfluidics is well established in the wide areas of science where the fluids in nanoliters to attoliters (10^{-9} to 10^{-18}) are processed and/or manipulated within the micro-sized channels.[1] It is an interdisciplinary arena which covers the science and technology to develop microstructured devices used in diverse fields of applications, such as biomolecules analysis and detection, diagnostics, drug development, environmental analysis, and microelectronics.[2] The unique properties of microfluidic systems are their portability (small dimensions), capability to work with low amounts of samples, ability to perform rapid and robust detection and separations with high sensitivity, and also their cost-effectiveness.[3] Depending on the unique properties of microfluidic systems, the microfluidic platforms and devices provide many advantages compared to macro-sized fluidic systems by allowing the investigation of micro-sized volume of samples in short period of time with low cost and high sensitivity.[4] On the other hand, the fluid phenomena for the liquid domination at the microscale are noticeably different from the macroscale. While the effect provided by the force of gravity is exceedingly decreased at microscale, the effects provided by the force of surface tension and capillary forces are conversely increased.[5]

The development of microfluidic technology was started at 1950s with the study that provides the basics of ink-jet technology.[3] However, the work which was performed at the end of 1970s by S. C. Terry *et al*. to produce miniaturized gas chromatograph on silicon is considered as the origins of microfluidics. According to the authors, the size of sensor to detect each individual component in mixture containing nitrogen gas, n-pentane, and n-hexane was reduced from laboratory instruments to pocket-size.[6] Until 1990s, the microfluidic technologies were improved by integrating the micro-sized elements, such as microvalves and micropumps.[7,8] After the integration and progression of microvalves

and micropumps into the microfluidic technologies, many silicon-based microfluidic devices were produced for different medical and industrial purposes.[4,9] Manz *et al*. defined the miniaturized total analysis systems (μTAS) for chemical sensing[10] and fabricated the microfluidic device which consisted of silicon chip (including an open-tubular column and conductometric detector), a chip holder, injector, and valves to perform the high-pressure liquid chromatography (HPLC).[11] Manz *et al*. also fabricated μTAS chip from Pyrex glass by micromachining to perform capillary electrophoresis-based separation of amino acids in short period of time.[12] Simultaneously, the test strips were produced to be used as microfluidic device for simpler biochemical analysis, such as pH measurement, pregnancy and drug abuse tests.[13,14]

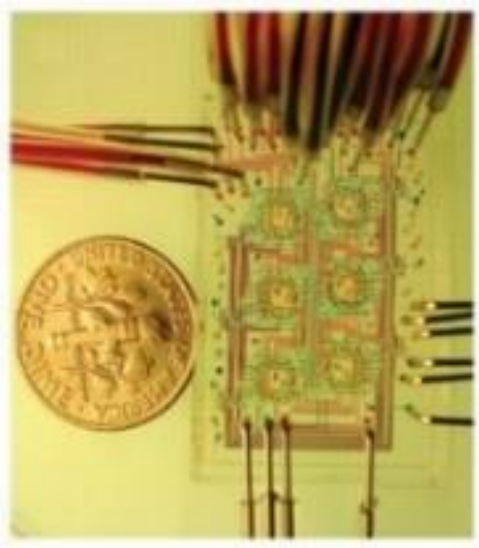

Figure 1.1. Microfluidic device which contains six independent micro-chemostats that provide semi-continuous planktonic growth.[15]

Silicon[8] and glass[16] were used in the fabrication of microfluidic devices until the late 1990s; however, these materials have many disadvantages. Silicon is an expensive and opaque material which has low gas permeability; while glass has low gas permeability, too.[5,17] Also, these materials required a clean room facility to be fabricated as microfluidic devices.[5] These disadvantages caused the limitations on the usage of microfluidics in many biological studies.[17] The researchers investigated different materials to eliminate these limitations of microfluidic devices. Whitesides *et al*. defined

the new concept in 1998 by using silicon-based organic polymer -poly(dimethylsiloxane) (PDMS)- instead of silicon and/or glass materials to fabricate the microfluidic device easier with lower cost.[18] Because of the biocompatible properties of PDMS,[19,20] the microfluidic devices were used in varied cell biology applications.[21–23] Folch *et al.* fabricated micro-sized channels from PDMS for the patterning of biological components, such as cells and proteins. In one of their studies, they directly patterned 3T3-J2 fibroblasts cell line on the substrate;[24] however, they needed to coat collagen and fibronectin onto the surface of substrate before patterning hepatocyte/fibroblast co-cultures in another study.[23] In addition to studies of cell patterning, many on-chip tissue/organ models were introduced for biological processes, such as drug discovery and development, to eliminate the limitations which were caused by *in vitro* and *in vivo* systems.[25] Huh *et al.* fabricated a PDMS microfluidic chip device which structurally, functionally, and mechanically mimics the microenvironment of lung alveolar-capillary interface in 2010. In that microfluidic device, the human breath was mimicked by seeding human alveolar epithelial cells on upper side of porous PDMS membrane and human pulmonary endothelial cells onto the bottom.[26]

There has been a progressive attention in the area of microfluidics, caused by the development lab-on-a-chip (LOC) systems.[9] LOCs are microstructured systems which have a capability to integrate entire biological and/or chemical laboratories within a chip that contains micro-sized elements, such as microchannels, filters, microvalves, micromixers, microsorters, and micropumps.[1,9,27] By controlling the flow of samples in LOCs systems, biological and industrial applications are performed at reduced scales with low sample consumption and high-throughput.[28] After introduction of PDMS to microfluidics by Whitesides *et al.*,[18] PDMS used in LOC devices for many applications; however it causes several limitations.[29–33] To eliminate these limitations, the researchers studied on alternative materials instead of PDMS.[5] Thermoplastic materials, such as polystyrene-cyclic olefin copolymer,[34] poly-methyl methacrylate (PMMA) and polycarbonate;[35,36] paper,[37] and wax[38] were used as substrate materials instead of PDMS.

Paper was started to be used as substrate material in the fabrication of micro-sized analytical devices because of its (i) availability around the World,[37] (ii) low-cost,[2,37] (iii) ability to provide passive transport by capillary action,[2] (iv) biocompatibility,[2,37,39] (v) biodegradability,[2] (vi) disposability by combustion,[2,37] and (vi) chemically modifiability to provide covalently immobilization of chemical compounds onto its surface.[40] By the usage of paper with these advantages, many microfluidic paper-based analytical devices

(µPADs) and paper-based biosensor chips which could easily be operated in resource limited environments as point-of-care (POC) devices were developed.[41–43] Even if the paper was already used in analytical and clinical chemistry since 19th century, the term of "paper-based microfluidics", also called "lab-on-a-paper", has great attention in the research field of microfluidics since 2007. Whitesides *et al.*[44] fabricated first microfluidic paper-based analytical devices by lithography for simultaneous detection of glucose and protein in urine.

For 20 years, the microfluidic devices which perform small-scale analysis were a topic of interest in scientific area and also used in POC applications in clinical studies.[45]

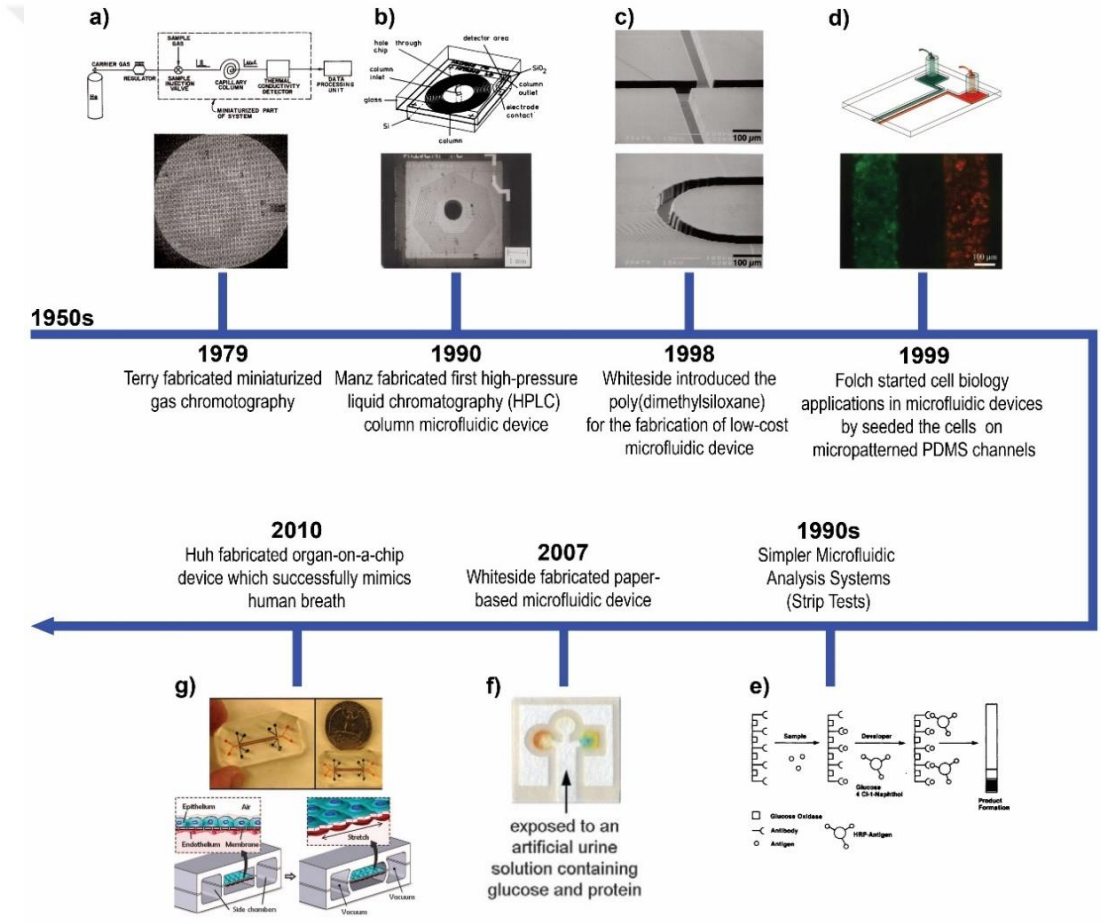

Figure 1.2. History of microfluidics. a) Miniaturized gas chromatography fabricated in Silicon,[6] b) HPLC column microfluidic device involving a silicon chip,[11] c) Using PDMS as substrate material in the fabrication of microfluidic device,[18] d) Cell patterning within PDMS channels,[24] e) An enzyme-channelling immunochemical test strip,[13] f) A paper-based microfluidic device which was fabricated by photolithography for simultaneous detection of glucose and protein,[44] g) An organ-on-chip which mimics the human breath.[26]

1.2. Paper-Based Microfluidics

Paper-based microfluidics, also called lab-on-a-paper, is the subarea of microfluidics in which cellulose paper is used to fabricate µPADs that flow of fluid from input to reaction zone is provided by capillary force within microchannels (patterned hydrophilic regions).[46] The paper-based microfluidics became an essential point-of-care testing (POCT) platform, which is mainly used for rapid diagnosis, environmental monitoring, and food safety detection in resource limited regions over time, because of its advantages compared to silicon, glass, PDMS, thermoplastic, and/or other materials.[47,48]

Microfluidic paper-based analytical devices with the advantages of simple fabrication and using processes, rapid and robust operation, portability, and low-cost[47–49] satisfy ASSURED (A: affordable; S: sensitive; S: specific; U: user-friendly; R: rapid and robust; E: equipment-free; and D: deliverable to end-users) criteria which are the determined requirements of diagnostic devices in developing countries by World Health Organization (WHO).[37,50]

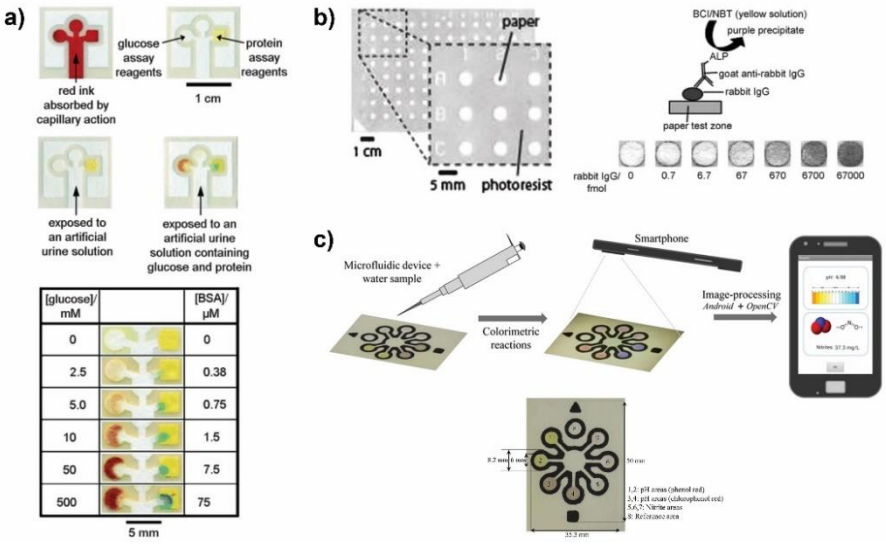

Figure 1.3. Examples of microfluidic paper-based analytical devices. a) A µPAD for simultaneous detection of glucose and protein,[44] b) Demonstration of indirect enzyme linked immunosorbent assay (ELISA) within a 96-microzone plate made from paper (P-ELISA),[51] c) A µPAD which is coupled with smart-phone for measurement of nitrite concentration and pH determination.[52]

The development of microfluidic paper-based analytical devices was provided by previous studies in paper-based bioanalyses which were performed starting from early 20th centuries. The first study, which the fabrication technique was defined to create spot testing on paper was performed by Yagoda in 1937.[53] By following this study, Müller *et. al.* produced paraffin patterned paper, which is defined as first paper-based assay, to in 1949.[54] While Martin and Synge invented a paper chromatograph which is the study that was awarded Nobel Prize in 1952,[55] the paper strip tests were started to be developed as biodetection tools, such as glucose measurements. Comer developed a test paper to semi-quantitatively measure the glucose level in urine sample in 1956.[56]

The adaptation of nitrocellulose paper in molecular detection studies[57] provided significant improvements in lateral flow immunoassays (LFIA) in 1970s. By the following studies, the immunochromatographic tests, such as pregnancy test strip, were developed[58] and then the commercial lateral flow tests were produced for many area, such as clinical diagnostic, food and environmental applications, and biodefence.[59–61]

In 2007, Whitesides' group inspired from previous paper-based bioanalysis[53–61] introduced microfluidic paper-based analytical devices, which is the concept of using paper as substrate in microfluidic structure for the simultaneously detection of more than one analyte in sample.[44] Whitesides *et. al.* patterned the PDMS onto the surface of hydrophilic paper by photolithography to fabricate microfluidic device for simultaneous glucose and protein detection. External equipments, such as micro-pumps, were not required for flow of fluid, because the micro-sized channels in device provided the capillary action for flow of fluid.[44] The concept, which was defined by Whiteside, meet the ASSURED criteria for POC diagnostics.[46]

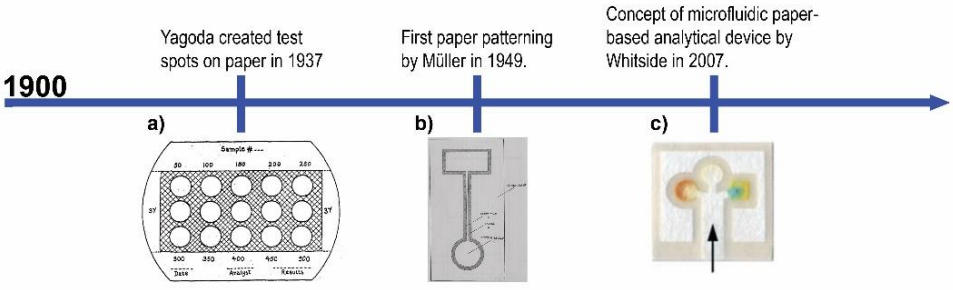

Figure 1.4. History of microfluidic paper-based analytical devices. a) First study on the fabrication of test spots on paper,[53] b) First paper-based assay by paraffin patterned paper,[54] c) A µPAD was fabricated by Whitesides' group.[44]

1.2.1. Fabrication Methodologies of Paper-Based Microfluidic Devices

The microfluidic paper-based analytical devices have had many developments after 2007. The process of device fabrication became the main point, which determines the novelty of µPADs.[62] In literature, there are 2D (two dimensional) and 3D (three dimensional) µPADs, which are used for various purposes. In 2D µPADs, single layer of cellulose paper is patterned; however, more than one paper is stacked together in 3D µPADs to provide vertical motion of fluids, in addition to the horizontal motion.[41,63,64]

There are two different categories, (i) 2D-shaping/cutting of paper and (ii) hydrophilic/hydrophobic contrast on paper, for the fabrication of the microfluidic paper-based analytical devices. The microfluidic channels are obtained by X-Y plotter or CO_2 laser in the category of shaping/cutting of paper,[41] however, there are technically three different patterning techniques in the category of hydrophilic/hydrophobic contrast on paper. The hydrophilic/hydrophobic contrast is provided by surrounding the hydrophilic pattern with hydrophobic borders. To create hydrophilic/hydrophobic contrast on paper, different patterning strategies, which are the (i) physical blocking of pores, (ii) physical deposition of hydrophobising agent on the paper, and (iii) chemical modification of paper surface are used.[47]

In 2D-shaping/cutting method, there are two different ways to fabricate the microfluidic paper-based analytical devices, such as using (i) X–Y knife plotters[65] and (ii) CO_2 laser cutters. The computer controlled X–Y knife plotters contain a knife which rotates around a turret to provide the cutting of paper for patterning different shapes on a paper. However, the paper is cut and shaped via CO_2 laser cutters in laser ablation methodology.[66]

Photolithography is one of the techniques, which depends on physical blocking of pores by using a photoresist. In this technique, paper is entirely hydrophobized and then selectively dehydrophobized by UV exposure.[47] Whitesides' group used the SU-8 2010 photoresist to pattern chromatography paper by photolithography.[44] In this concept, the µPAD was produced in small dimension with high resolution.[44,47] However, (i) the usage of photoresist, (ii) complex fabrication instruments, such as lithography equipments, and (iii) requirement of clean room facility generally prevent this technique to be ideal for the fabrication of µPADs.[44,46]

The wax-based patterning techniques, which depend on physical deposition of hydrophobising agent on the paper, are used for fabrication of microfluidic paper-based analytical devices. The µPADs are fabricated by selective hydrophobisation[41] with non-toxic reagents in wax-based fabrication methods, such as wax screen printing, wax dipping, and wax printing. In wax screen printing, hydrophobic barriers are formed by diffusion of melted wax (by hot plate) onto the paper, after solid wax is patterned onto surface of paper. Dungchai *et. al.* fabricated µPADs by wax screen-printing method to determine glucose and total iron in serum sample. In this concept, the µPADs could simply be fabricated at a low cost, because neither complex equipment nor clean room facilities were required for fabrication of µPADs.[67] In wax dipping, the designed pattern is produced by using iron mould and molten wax.[68,69] Songjaroen *et. al.* fabricated µPADs by wax dipping method to determine glucose and protein in the real sample. The iron mould which was produced via laser cutting was dipped into melted wax to fabricate designed pattern on the paper.[68] In wax printing, wax printer and heater (hot plate or oven) are used to fabricate µPADs. To pattern desired design on paper, the paper is placed into wax printer and then heated.[67,70] Wax printer (FUJIXEROX Phaser 8560DN, Japan) was used by Lu *et. al.* to fabricated µPADs, whose performance was verified via horse radish peroxidase (HRP), bovine serum albumin (BSA), and glucose assays. In this concept, the whole process for µPAD fabrication was simply and rapidly operated without using any chemical solvents and clean room facilities; however, a wax printer was required.[70]

PDMS printing, which depends on the physical blockage of pores in paper, is also a technique to fabricate microfluidic paper-based analytical devices. In this technique, PDMS was printed onto paper via desktop plotter.[71] Whitesides *et. al.* fabricated µPADs from PDMS, which was dissolved in hexanes, by using the modified X-Y plotter. The hydrophilic channels on paper were produced by generating hydrophobic walls, as result of the penetration of PDMS to the depth of paper. Even if PDMS printing did not require expensive materials and clean room facilities, this technique still need computer-aided design, and usage of chemical reagents.[71]

The ink stamping and double side ink methods are also the techniques, which were used to fabricate the microfluidic paper-based analytical devices. In these techniques, the hydrophobic channels in paper are produced by using a PDMS stamp and inerasable inks.[47] Curto *et. al.* used PDMS stamp and indelible ink to fabricate µPADs, which were used in the colorimetric glucose detection. The cost-effective µPADs were rapidly fabricated without any requirement of cleanroom facilities and complex instruments.[72]

However, Akyazi *et. al.* used double side stamping method for the fabrication of µPADs to eliminate low reproducibility of standard ink-stamping method, which was caused by non-uniform penetration of the ink to the back side of the paper.[73]

In addition to techniques, which depend on physical deposition of hydrophobising agent on the paper, there are also some other techniques, which depend on chemical modification of paper surface. In such techniques, the cellulose reactive agents react with the hydroxyl group (-OH) in the cellulose structure of paper. The alkenyl ketene dimer (AKD) is a common cellulose reactive agent, which is used in fabrication of µPADs. Li *et. al.* firstly hydrophobized paper via the AKD solution and the solution was cured by heating. Hydrophilic patterns in paper that was hydrophobized with AKD were formed by plasma treatment method in which paper samples that were sandwiched between masks were placed into a vacuum plasma reactor.[74] Instead of using plasma treatment, hydrophobic AKD channels in µPADs were also fabricated via ink-jet printing method by Li *et. al.* For printing process, ink in cartridge was replaced by AKD solution, and then the solution was cured onto the paper by heating. [75] On the other hand, polystyrene,[76] polyacrylate,[77] hydrophobic sol-gel-derived methylsilsesquioxane,[78] and teflon[79] were also used ink-jet printing method.

Haller *et. al.* fabricated the microfluidic paper-based analytical devices by chemical vapour-phase deposition. The hydrophilic channels surrounded by hydrophobic walls were obtained after UV light was exposed to the paper, which was coated with Poly(o-nitrobenzyl methacrylate) (PoNBMA). The absence of the using organic solvent in vapour-phase deposition makes this technique environmentally friendly; however, the usage of complex equipment incurs high cost for the fabrication of µPADs.[80]

Other methods, such as flexographic printing,[81] ink-jet etching,[82] silane and UV/O_3 patterning,[83] printed circuit technology,[84] and subtractive laser treatment,[85] are also considered to create hydrophilic/hydrophobic contrast in the fabrication of µPADs. However, these methods are limited because of their requirements, such as (i) multistep fabrication processes, (ii) requirements of clean room facility, complex equipment, and organic solvents, and (iii) high fabrication costs.

The detailed information about the fabrication techniques, which are generally used in the fabrication of microfluidic paper-based analytical devices (µPADs) in literature, is shown in Table 1.1

Table 1.1. Fabrication techniques for paper-based microfluidic devices.

Fabrication Technique	Equipments	Advantages	Drawbacks	Refs.
Shaping/Cutting	X-Y plotter or CO_2 laser cutter	Sharp barriers	Expensive equipments; Low-mechanical stability;	65,66
Photolithography	Lithography equipments; UV lamp; Hot plate	High resolution; Sharp barriers	Requires complex equipments, photoresist and organic solvents; High cost; Requires clean room facilities;	44,46,47
Wax screen printing	Hot plate	Simple operation; Low cost	Inconsistent deposition of wax; Low resolution; Rough barriers	67
Wax dipping	Iron mould (Mask); Heater	Simple and rapid steps; Low cost;	Inconsistency between batches	68,69
Wax printing	Wax printer; Heater	Simple operation; Rapid process	Expensive equipments; Poor availability in resource limited area; Low resolution; Nonstable at high temperature	70
PDMS printing	Computer; Desktop plotter	Flexible device; Cheap consumables (PDMS)	Inconsistency in the formation of barriers; Low resolution; Requires additional steps for curing	71
Stamping	PDMS stamp or stainless steel stamp; Heater	Simple steps; Low cost;	Low resolution; Requires additional pre-heating step;	47,72,73
Plasma treatment	Vacuum plasma reactor; Masks; Heater;	Cheap consumables (AKD)	Requires the customized masks; Poor availability in resource limited area;	74
Ink-jet printing	Modified inkjet printer; Heater	High resolution; Cheap consumables (AKD)	Requires modified ink-jet printers; Requires additional steps for curing	75–79
Vapour-phase deposition	Vapour deposition chamber	Simple operation	Requires complex equipments; High cost	80
Flexographic printing	Specialized printer	Single roll-to-roll process; No pre-heating step	Requires complex equipments, templates, and reagents; High cost;	81
Ink-jet etching	Specialized ink-jet printer	Requires only one printing apparatus;	Multiple printing steps; Requires organic solvents	82
Silane and UV/O_3 patterning	Mask and clamps; UV lamb	Simple operation; Low cost	Requires organic solvents	83
Printed circuit technology	Computer; Printer; Thermal transfer printer;	Rapid process; Low cost; Reproducible	Requires complex equipments; Multiple printing steps;	84
Subtractive laser treatment	Computer-controlled CO_2 laser cutting system	Simple operation; Sharp barriers	Requires complex equipment;	85

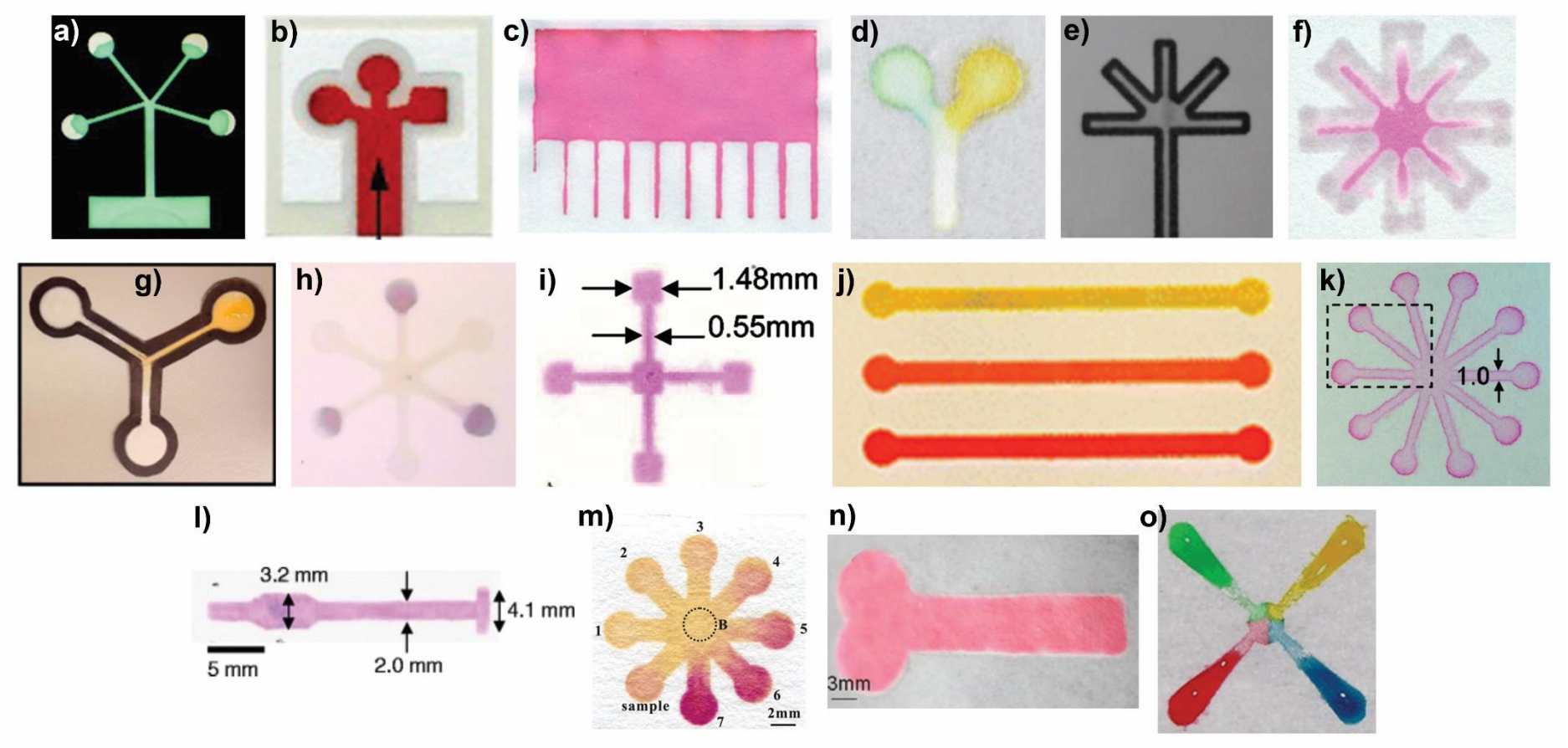

Figure 1.5. Fabrication of microfluidic paper-based analytical devices via different fabrication techniques. The fabrication of µPADs via (a) 2D-shaping,[65] b) photolithography,[44] c) wax screen printing,[67] d) wax dipping,[68] e) wax printing,[70] f) PDMS printing,[71] g) stamping,[73] h) plasma treatment,[74] i) ink-jet printing,[76] j) vapour-phase deposition,[80] k) flexographic printing,[81] l) ink-jet etching,[82] m) alkylsilane self-assembling and UV/O_3-patterning,[83] n) printed circuit technology,[84] and o) subtractive laser treatment.[85]

1.2.2. Sensing Technologies in Paper-Based Microfluidic Devices

Microfluidic paper-based analytical devices, which are used in analysis of samples, are one type of the miniaturized total analysis systems (μTAS). To detect the analyte for their analysis, different types of sensing technologies are applied to μPADs.[41,47,48,62,86] The most commonly used sensing technologies in μPADs are colorimetric sensing, electrochemical (EC) sensing, fluorescence sensing, chemiluminescence (CL) sensing and electrochemiluminescence (ECL) sensing; however, there are also other available techniques, which were already mentioned in literature, such as surface-enhanced raman spectroscopy (SERS), mass spectroscopy (MS), and nanoparticle-based sensors.

1.2.2.1. Colorimetric Sensing

The colorimetric sensing is the main sensing technique for detection of analytes in μPADs, because paper has a bright and colourless background, which provides an easy readout of generated signals even in the absence of any instruments. The signals in test zones of μPADs that have the colorimetric sensing technologies are obtained by visible colour formations resulting from enzymatic or chemical reactions.[41,47,48] Sample fluids, which are loaded to μPADs from the inlet, firstly reaches the test zones of μPADs, and then it reacts with its target reagents, resulting in colour-change that could be possibly determined by naked eye.[48] In μPADs, which colorimetric assays are performed, qualitative, semi-quantitative or quantitative results are obtained.[47,62] The qualitative results (yes/no answer), which can be visually achieved by naked eyes, are evaluated without using any additional instrumentation.[47] However, semi-quantitative results can be obtained by the colour charts that are used to approximately determine relative amounts of analytes based on their specified calibration curves.[41,47,62] On the other hand, the colour signal intensities are calculated by additional instruments, which process image-processing software, in μPADs to obtain quantitative results.[62,87]

The pH, glucose and protein assays were performed in early examples of μPADs, which have colorimetric sensing technologies.[44,71] In such assays, the formations of colour changes in test zones provide detection of analyte, visually. The brown colour is formed by enzymatic oxidation of iodide to iodine in the test zone of μPADs during glucose assays. Similar to glucose assay, the colour change of tetrabromophenol blue (TBPB) from yellow to blue occurs in the presence of proteins during protein assays. Nowadays, qualitative and quantitative colorimetric sensing technologies in μPADs are used in a wide range of applications, from detection of biomolecules[88–92] and metal particles,[93–95] to immunoassays,[51,96,97] to food and environmental applications.[98,99]

The colorimetric sensing is the most frequently used sensing mechanism in μPADs because signals are read easily even without using any additional instruments.[48] However, there are some drawbacks, such as high detection limits with low selectivity and sensitivity, caused by nonhomogeneous distribution of colour and presence background noise on paper. Moreover, analysis of real samples via colorimetric sensing technologies requires more improvements in sample manipulation and isolation of molecules.[71,76] In addition, improvements on capturing the image and image analysis are required in colorimetric sensing-based μPADs to obtain quantitative results.[87]

1.2.2.2. Electrochemical Sensing

The electrochemical (EC) sensing is the most extensively investigated technique for detection of analytes in μPADs, because it provides a low detection limits with high selectivity and sensitivity, in contrast to colorimetric sensing.[47,62] In addition, μPADs, which have EC sensing technology, are commonly insensitive to light and ambient conditions, providing more stable signals.[100] EC sensing is provided by three electrodes, which are deposited onto paper to build three-electrode system. This three-electrode system includes a counter electrode, a working electrode, and a reference electrode.[41,48] While the counter and working electrodes are fabricated from carbon inks; reference electrodes are fabricated from silver/silver chloride ink.[41] In these devices, the electrical outputs, which are induced by REDOX (reduction-oxidation) reactions on electrodes' surface, are obtained as detection signals.[41,48]

The glucose, lactate, and uric acid were detected in the early examples of μPADs, which have EC sensing technologies.[101] In such assays, signals, resulted by oxidase enzyme reactions that occurred on Prussian Blue (redox mediator)-improved working electrode, were obtained via chronoamperometry. For production of electrochemical μPADs (ePADs) or paper-based electrochemical devices (PEDs), photolithography and screen-printing technology were used in fabrication of microfluidic channels and fabrication of electrodes on paper, respectively. On the other hand, ePADs, which are used for detection of cholesterol, tumour markers, dopamine, and drugs, are also considered as early examples of EC sensing. Today, the ePADs are still used in a wide range of applications, from detection of biomolecules[102–104] and metal particles[105] to immunoassays.[106–108]

As EC sensing provides some advantages over the colorimetric sensing, it is one of the most typically used detection techniques. However, there are some drawbacks, which are the EC sensing requires (i) additional steps for fabrication of electrodes,[41] and (ii) detection instruments.[47] During production of ePADs, additional fabrication steps are required for production of electrodes by deposition of conductive inks. Moreover, additional detection instruments are also needed, causing an increase in the complexity of ePADs, also increasing its cost.

1.2.2.3. Fluorescence Sensing

Detection of analyte is also performed with μPADs, which contain fluorescence sensing technologies.[41,47,48] Fluorescence sensing depends on intensity measurement of emitted light from a substance, which has already absorbed light and/or electromagnetic radiation.[47]

In early examples of fluorescence sensing-based μPADs, fluorescein isothiocyanate-labelled BSA was detected. The limit of detection was 125 fmol for fluorescein isothiocyanate-labelled BSA in paper microzone plates, which required a small amount of sample.[109] In addition to this study, fluorescence sensing-based μPADs were used in varied applications from detection of biomolecules[110,111], pathogens,[112] and cells[113] to immunoassays.[114]

The fluorescence sensing-based μPADs provide a low limit of detection;[115] although they have some difficulties, which are (i) presence of additives in paper which can have fluorescence properties, (ii) background noise caused by paper that increases the average relative standard deviation, and (iii) requirement of some instruments, such as fluorescence readers to measure the florescence intensity.[47,62]

1.2.2.4. Chemiluminescence Sensing

The chemiluminescence (CL) sensing depends on the intensity measurement of emitted light, which is generated by chemical reactions. During the chemical reaction, the products and light are produced in the presence of catalyst or excited intermediate. For example, luminol being oxidized by hydrogen peroxide (H_2O_2) to 3-aminophthalate, results in emission of light.[41]

Although there are some drawbacks for CL sensing, which are (i) need of chemiluminescence readers, (ii) high cost, and (iii) requirement of dark room to carry out measurement;[47,115] these sensing mechanisms have some advantages, such as (i) simplicity and high sensitivity, (ii) compatibility with micromachining systems, (iii) possibility for a low limit of detection, and (iv) reduced background noise.[47,62,116]

The advantages of CL sensing-based μPADs lead to usage of this detection mechanism in a wide spectrum of applications, these applications ranged from detection of biomolecules and metals,[117–119] to the measurement of DNA hybridization,[120] to immunoassays.[121,122]

1.2.2.5. Electrochemiluminescence Sensing

Electrochemiluminescence (ECL) sensing is established by combining the sensing mechanisms of CL and EC.[47] The mechanisms of ECL sensing depend on luminescence, which is generated by electrochemical reactions. In this detection mechanism, the electrochemically generated intermediates undergo exergonic reactions,

resulting in an electronically excited state that emits the light at the electrode surface by relaxation of excited state to lower level state.[41,47,123]

In first study of ECL sensing mechanism, the 2-(dibutylamino)-ethanol (DBAE) and nicotinamide adenine dinucleotide (NADH) were detected by readouts of orange luminescence via conventional photodetector. Orange luminescence was provided by ECL reaction of tris(2,2′-bipyridyl)ruthenium(II) ($Ru(bpy)_3^{2+}$) with its analyte. During this ECL reaction, DBAE is oxidized and deprotonated, resulting in formation of radical DBAE at electrode. The radical DBAE then reduced the $Ru(bpy)_3^{2+}$ to $Ru(bpy)_3^{3+}$, which is the excited state. By the relaxation of excited state to ground state, $Ru(bpy)_3^{3+}$ emitted at 620 nm. While the fluidic channels in ECL sensing-based μPAD was fabricated via ink-jet printing, electrodes were introduced by screen-printed method.[124] In addition, ECL sensing-based μPADs were widely used in a variety of applications from detection of biomolecules[124,125] to immunoassays, to food and environmental monitoring.[126,127]

Combining CL and EC sensing in ECL sensing mechanism resulted in higher sensitivity by preserving simplicity and stability of μPADs.[128] In addition to providing higher sensitivity, ECL sensing have other advantages, such as (i) almost zero background noises, and (ii) easily controllable electrode potentials.[47,62] Nevertheless, the readouts should be carried out in a dark room with additional power source, which limit the applicability of ECL sensing mechanisms in resource-limited areas.[41,47]

1.2.2.6. Other Sensing Mechanisms

In addition to the common sensing mechanisms in μPADs, such as colorimetric sensing, electrochemical (EC) sensing, fluorescence sensing, chemiluminescence (CL) sensing and electrochemiluminescence (ECL) sensing, there are also other mechanisms of sensing, which are surface-enhanced raman spectroscopy (SERS),[129] mass spectroscopy (MS),[47] and nanoparticle-based sensors.[82,130,131] Although these sensing mechanisms were studied in some studies and mentioned in literature, they are less-frequently used sensing technologies in the applications.

1.2.3. Applications of Paper-Based Microfluidics

The microfluidic paper-based analytical devices are one type of μTAS. The main purpose of the μPADs is to present to owner a low-cost and easy-to-use analytical platform. There are different types of μPADs, which have different working principle and function. The μPADs are currently used in the different groups of applications. The applications performed by μPADs can be categorized into the three main groups, such as health diagnostics, environmental monitoring, and water and food safety.[47]

The high amounts of effort are made on the μPADs, which are used in health diagnostics, because the μPADs have critical importance and a high possibility for commercialization.[47] For example, μPADs, which were manufactured for pregnancy tests, were the one of the main breakthroughs in this field.[132] The critical importance of μPADs has come from their suitability for the POC applications, which are used in resource-limited countries that people preponderantly die because of curable infectious diseases. That's why; the μPADs have critical importance for POC detection by meeting the ASSURED criteria of WHO. According to WHO, the ideal rapid test should be affordable, sensitive, specific, user-friendly, rapid and robust, equipment free, and deliverable to end users.[133] In addition, μPADs have commercial importance in developed countries in which people survive longer. In the branch of health diagnostics, μPADs are used in (i) the analysis of biomolecules (proteins, hormones, neurotransmitter, etc.),[88,96] small molecules (glucose, uric acid, etc.),[72,92,118,119] nucleic acids (DNA and RNA),[102,110,112,120] (ii) immunoassay studies for disease and cancer diagnostics,[51,97,102,108,110,112,113,120] (iii) pregnancy tests,[134] (iv) blood typing,[135] and (v) drug sensing.[136]

In addition to health care studies, μPADs are developed and fabricated for studies of environmental monitoring, such as (i) analysis of water, soil, and air, and (ii) metal detection. [93–95,99,105]

Lastly, the μPADs are also used to control water and food safety. The quality of drinking water in resource limited countries could be easily determined by using μPADs. Moreover, the quality of foods could be controlled with μPADs by the consumer, resulting in prevention of some diseases.[137,138]

CHAPTER 2

MATERIALS & METHODS

2.1. Materials

2.1.1. Consumable Materials

The filter paper (MN 615, Macherey-Nagel), aluminium band, and red ink (Ponceau 4r E124) were purchased for the fabrication and characterization of µPADs. The monoclonal anti-BSA antibody (Sigma-Aldrich, B2901), BSA (Sigma-Aldrich, A2153), ELISA diluent buffer (BioLegend, 421203), ELISA wash buffer (BioLegend, 421601), anti-mouse IgG/HRP antibody (Abcam, ab205719), tetramethylbenzidine (TMB) (Abcam, ab210902), anti-Hepatitis C Virus NS3 antibody (Abcam, ab21124), recombinant Hepatitis C Virus NS3 protein (Abcam, ab49022), anti-goat IgG/HRP antibody (Abcam, ab205723), and phosphate buffered saline (PBS, Sigma-Aldrich, P4244) were purchased for the optimization and detection studies.

2.1.2. Computer Programs & Instruments

CorelDRAW X7, Epilog Zing 16, Fei Quanta 250 FEG, Axio Observer Zeiss, Smart-phone (Samsung, A705FN), and timer were used in the fabrication and characterization of µPADs. The statistical analysis was performed via GraphPad (Prism 6.0) and Origin Pro 2020b. The colour intensity was measured with MATLAB R2018b.

2.2. Methods

2.2.1. Design and Fabrication of Paper-Based Microfluidic Devices

Fabrication of microfluidic paper-based analytical devices consist several steps, which are preparation of papers, design and drawing of µPADs, and patterning the design onto the surface of prepared papers.

In the beginning of µPADs fabrication, papers were prepared. For that purposes, the backsides of standard filter paper (MN 615, Macherey-Nagel), which has 70 g. of weight and 0.16 mm of thickness, was covered by aluminium band. Here, we decided to use standard filter paper in µPADs instead of other specialized papers to decrease the cost. As aluminium is not ablated by laser in contrast to paper, the backside of paper was coated with aluminium to create barriers around the hydrophilic micro-sized channels (Figure 2.1).

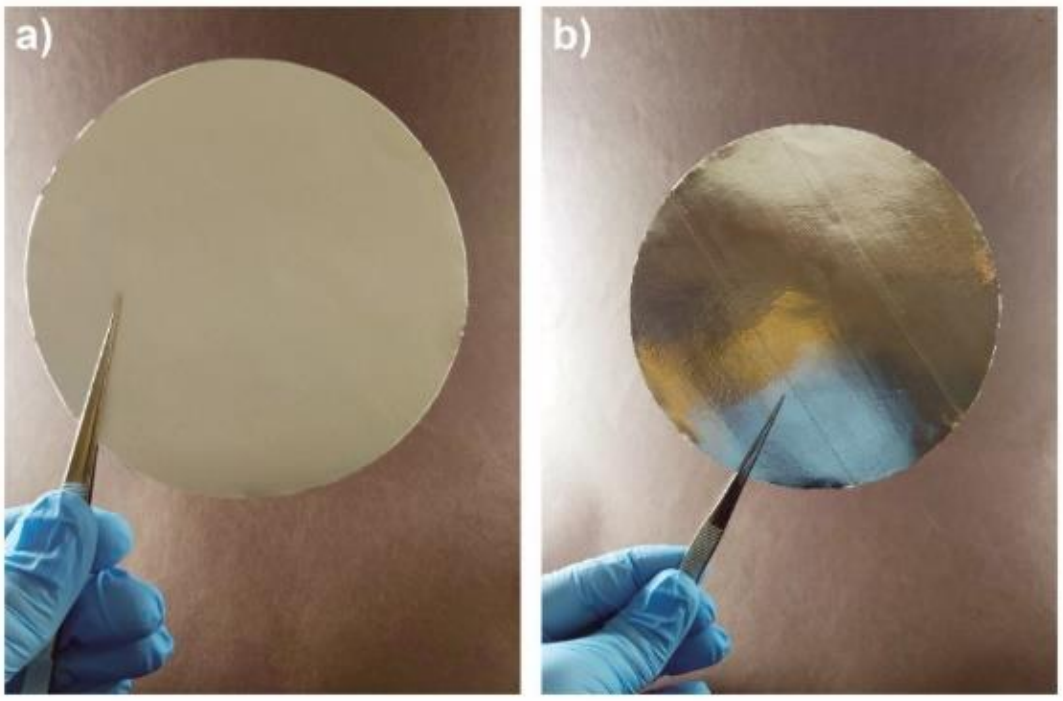

Figure 2.1. Modification of filter paper. a) Front-side of paper, b) Back-side of paper after coating with aluminium band.

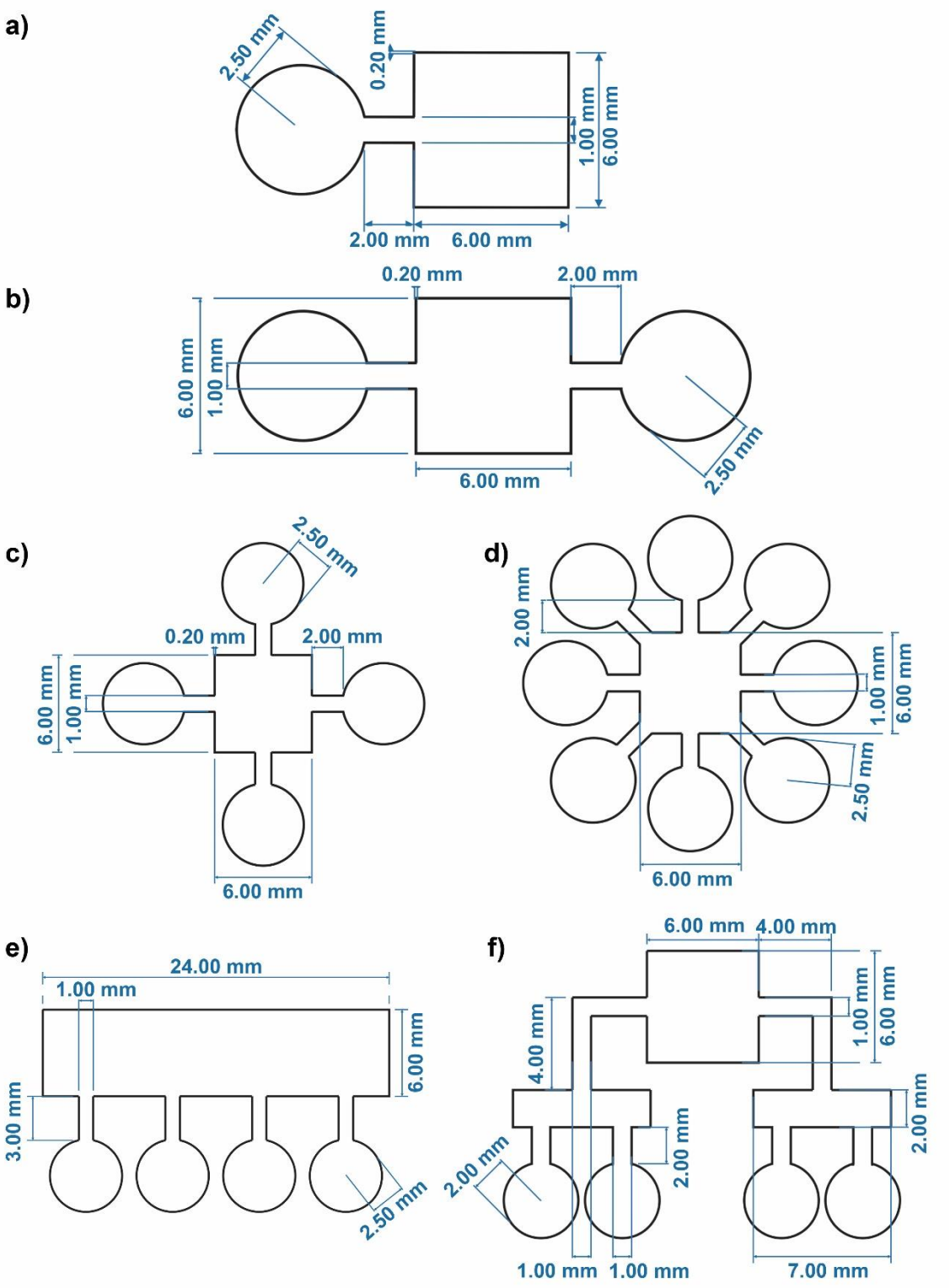

Figure 2.2. Technical drawings for different models of µPADs. a) 1S1T µPAD (one sample inlet and one test zone), b) 1S2T µPAD (one sample inlet and two test zones), c) 1S4T-Type1 µPAD (one sample inlet and four test zones), d) 1S8T µPAD (one sample inlet and eight test zones), e) 1S4T-Type2 µPAD (one sample inlet and four test zones), f) 1S4T-Type3 µPAD (one sample inlet and four test zones).

After the modification of paper, the several models of µPADs (1S1T, 1S2T, 1S4T-Type1, 1S4T-Type2, 1S4T-Type3, and 1S8T µPADs) were designed and drawn by using CorelDRAW X7, which is graphic design software for vectorial illustrations (Figure 2.2). For fabrication of µPADs, each designed models were patterned onto the front-side of modified filter paper via laser ablation methodology by using of Epilog Zing 16. During the fabrication process of µPADs, a hundred different fabrication parameters, which were the combination of speed and power values, were examined (Table 2.1).

Table 2.1. Ranges of speed and power in fabrication process.

Power	**Speed (%)**									
Power (10%)	10	20	30	40	50	60	70	80	90	100
Power (20%)	10	20	30	40	50	60	70	80	90	100
Power (30%)	10	20	30	40	50	60	70	80	90	100
Power (40%)	10	20	30	40	50	60	70	80	90	100
Power (50%)	10	20	30	40	50	60	70	80	90	100
Power (60%)	10	20	30	40	50	60	70	80	90	100
Power (70%)	10	20	30	40	50	60	70	80	90	100
Power (80%)	10	20	30	40	50	60	70	80	90	100
Power (90%)	10	20	30	40	50	60	70	80	90	100
Power (100%)	10	20	30	40	50	60	70	80	90	100

2.2.2. Characterization of Paper-Based Microfluidic Devices

Fabricated µPADs were characterized in many perspectives, such as surface properties of modified filter paper, integrity and thickness of barriers, and liquid sample flows within µPADs. Also, the required amount of sample and time for full sample saturation of test zones were determined for each µPAD.

In the beginning, the differences in the surface properties of filter paper were examined before and after modifying the backside of filter paper with aluminium band. For that purpose, front-side of standard (aluminium free) and modified (aluminium coated) filter papers were coated with thin gold layer and then observed under scanning electron microscope (FEI QUANTA 250 FEG) with varied magnification level (from

120X to 1000X). In addition, the barriers and corners in 1S1T µPADs were visualized via scanning electron microscope.

Later, 1S1T µPADs, which were fabricated in a hundred different parameters (Table 2.1), were used to analyse the effects of speed and power values on the integrity and thickness of barriers. The integrity and thickness of barriers within 1S1T µPADs were observed via inverted fluorescence microscope (Axio Observer-Zeiss). In addition to observation of barriers, the thicknesses of barriers were measured at six different positions in 1S1T µPADs to quantify their barrier thicknesses. By analysing the data with GraphPad Prism (6.0 version), average values of barrier thickness for each 1S1T µPAD were calculated as mean ± standard deviation. Depending on the barrier integrities and widths with low standard deviations, the optimized fabrication parameters were determined for next experimental section.

After the optimized fabrication parameters were identified, different models of µPADs (1S1T, 1S2T, 1S4T-Type1, 1S4T-Type2, 1S4T-Type3, and 1S8T µPADs), shown in Figure 2.2, were fabricated in each optimized parameters (Table 2.2). After, the fabricated µPADs were used in the observation of the liquid sample flows within the µPADs by using red ink. The red ink, which was produced by dissolving Ponceau 4r E124 in distilled water (5% w/v), were separately injected into the sample input areas of µPADs via pipette to observe the liquid sample flow within µPADs. Then, the varied amounts of red ink (Table 2.3) was injected to sample input area of each type of µPADs to determine the required amounts of fluid sample for the saturation of test zones in each µPAD.

Table 2.2. Optimized parameters for the fabrication of µPADs via laser ablation methodology.

Power (%)	**Speed (%)**
10	40
10	60
20	90
30	50
30	100
40	80
40	100
70	80
70	100

Table 2.3. The range of Ponceau 4r E124 amounts, which are used in determining the required amount of liquid sample for each type of µPADs.

Type of µPADs	Range of Ponceau 4r E124 amount
1S1T	3-15 µL
1S2T	5-15 µL
1S4T-Type1	8-20 µL
1S4T-Type2	15-30 µL
1S4T-Type3	13-30 µL
1S8T	10-20 µL

After the determination of required amounts of fluid sample, the required time for the saturation of test zones with liquid sample in each µPAD was investigated. For this purpose, the determined amounts of Ponceau 4r E124 (6, 7, 10, 22, 20, and 16 µL) were respectively loaded into the sample entry area of 1S1T, 1S2T, 1S4T-Type1, 1S4T-Type2, 1S4T-Type3, and 1S8T µPADs. Each µPADs was then incubated at room temperature until they dried. The time was recorded via timer to calculate the required time for the saturation of test zones within µPADs.

2.2.3. Micro-Paper Enzyme Linked Immunosorbent Assay (µP-ELISA)

2.2.3.1. Optimization of µP-ELISA Protocol

Before the fabricated (1S1T, 1S2T, 1S4T-Type1 and 1S8T) µPADs (Figure 2.3a) were used in HCV detection, the µP-ELISA protocol was optimized, using BSA as a model antigen.

In BSA detection, µP-ELISA contained six main steps, which were (i) coating the surface of test zones with monoclonal anti-BSA antibody (Sigma-Aldrich, B2901), (ii) blocking test zones via ELISA diluent buffer (BioLegend, 421203), (iii) addition of BSA (1 mg/ml) (Sigma-Aldrich, A2153) to test zone and washing to remove unbound BSA via ELISA wash buffer (BioLegend, 421601), (iv) primary antibody (anti-BSA antibody) addition to test zone and washing to remove unbound antibody via ELISA wash buffer,

(v) enzyme-conjugated detection antibody (Anti-mouse IgG/HRP) (Abcam, ab205719) addition to test zone and washing to remove unbound secondary antibody via ELISA wash buffer, and (vi) adding the substrate (3,3',5,5'-Tetramethylbenzidine, TMB) (Abcam, ab210902) and incubating about 20 minutes for colorimetric detection (Figure 2.3b).

In this section, we tried to optimize washing step in µP-ELISA protocol to decide proper models of µPADs for µP-ELISA application. We here considered and tried to prevent problems, which could be caused by undesired accumulation of BSA protein and enzyme-conjugated secondary antibody at input region. As test zones and input area are connected to each other with small hydrophilic channel, the BSA protein and secondary antibody could possibly flow into the sample entry area by washing step of µP-ELISA in improper µPAD models.

2.2.3.2. Evaluation of µP-ELISA via BSA Detection

The µP-ELISA protocol (Method 2.2.3.1) was evaluated via BSA detection. BSA detection was performed in 1S4T-Type2 and 1S4T-Type3 µPADs, which were determined as usable models for µP-ELISA applications. Here, the 1S4T-Type2 and 1S4T-Type3 µPADs were fabricated in 20P90S (20%Power & 90%Speed) and 40P80S (40%Power & 80%Speed) parameters by laser ablation methodology.

In the beginning, test zones in each fabricated µPADs were coated with monoclonal anti-BSA antibody (Sigma-Aldrich, B2901). For this purpose, 1 µL of an anti-BSA antibody solution in phosphate buffered saline (PBS) (1:250 diluted) was separately spotted in the test zones of µPADs to immobilize anti-BSA antibody. After the coating of test zones with anti-BSA antibody, each µPADs was dried for 10 minutes under ambient conditions.

Then, each test zones in µPADs were impregnated with 1 µL of ELISA diluent buffer (BioLegend, 421203) and the µPADs were again dried for 10 minutes at same conditions.

After the blocking of test zones in µPADs, 1 µL of BSA (Sigma-Aldrich, A2153) solution (1 mg/ml) was added to test zones and µPADs was dried for 10 minutes. After

10 minutes, the µPADs were properly washed by ELISA wash buffer (BioLegend, 421601) from top to bottom part of µPADs when the µPADs were held vertically.

Next, 1 µL of an anti-BSA antibody solution in PBS (1:250 diluted) was again added to test zone in µPADs and then the µPADs was incubated to become dry. After the µPADs were dried, the µPADs were washed by ELISA wash buffer to remove unbound primary antibody.

After that, 1 µL of HRP-conjugated secondary antibody (Anti-mouse IgG/HRP antibody, Abcam, ab205719) solution in PBS (1:250 diluted) was added to test zones. This secondary antibody, which has an affinity for anti-BSA antibody, could therefore bind any anti-BSA antibodies immobilized by the antigens. At the end of ten-minute incubation, test zones were washed by ELISA wash buffer.

Lastly, 20 µL (for 1S4T-Type2) and 22 µL (for 1S4T-Type3) of a colorimetric substrate (Tetramethylbenzidine(TMB), Abcam, ab210902) solution for HRP enzyme were separately added to µPADs from sample input areas. To complete the reaction in the test zones of µPADs, the µPADs were incubated under dark environment for 20 minutes. After the time period of incubation (20 minutes), the colour changes (blue colour formation) within test zones of each µPADs were observed by naked and imaged via camera of smart-phone (Samsung, A705FN).

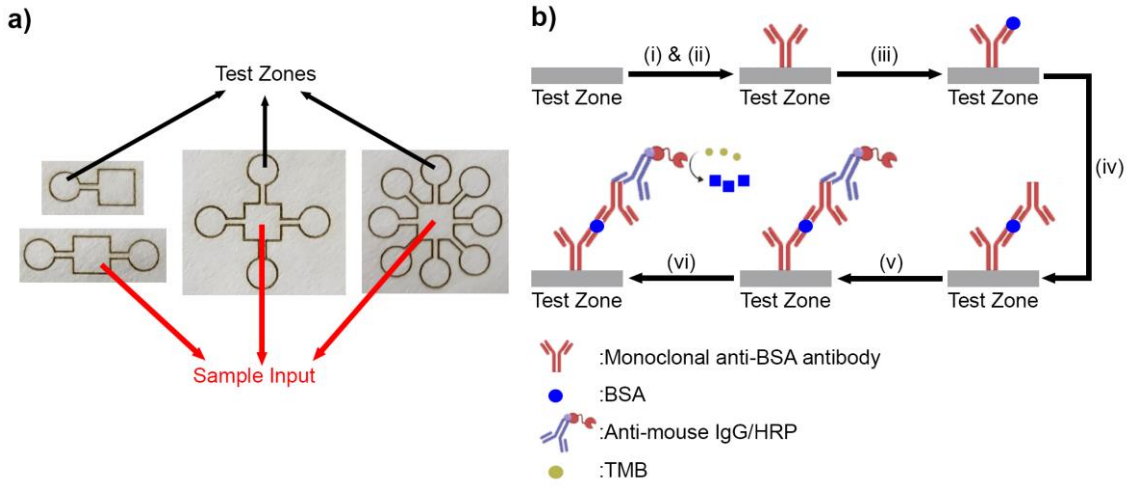

Figure 2.3. Demonstration of µP-ELISA protocol. a) Sample inlet area and test zones in different models of µPADs, b) µP-ELISA protocol which was used in the optimization of µP-ELISA.

2.2.3.3. Hepatitis C Virus (HCV) Detection via µP-ELISA

For the HCV detection, the µP-ELISA protocol, which was performed for BSA detection (Method 2.2.3.2) was followed in general. The recombinant Hepatitis C Virus NS3 protein (1 mg/ml in PBS solution) (Abcam, ab49022) was detected in 1S4T-Type2 and 1S4T-Type3 µPADs, which were fabricated in eight optimized fabrication parameters, such as 10P40S (10%Power & 40%Speed), 20P90S (20%Power & 90%Speed), 30P50S (30%Power & 50%Speed), 30P100S (30%Power & 100%Speed), 40P80S (40%Power & 80%Speed), 40P100S (40%Power & 100%Speed), 70P80S (70%Power & 80%Speed), and 70P100S (70%Power & 100%Speed).

The main differences between the BSA and HCV detection were the using of different primary and secondary antibodies, which were the anti-Hepatitis C Virus NS3 antibody (Abcam, ab21124) and anti-goat IgG/HRP antibody (Abcam, ab205723) instead of the anti-BSA antibody and anti-mouse IgG/HRP antibody, respectively. However, the colorimetric changes, which were caused by the reaction between HRP and TMB were captured via camera of smart-phone (Samsung, A705FN), as similar to BSA detection.

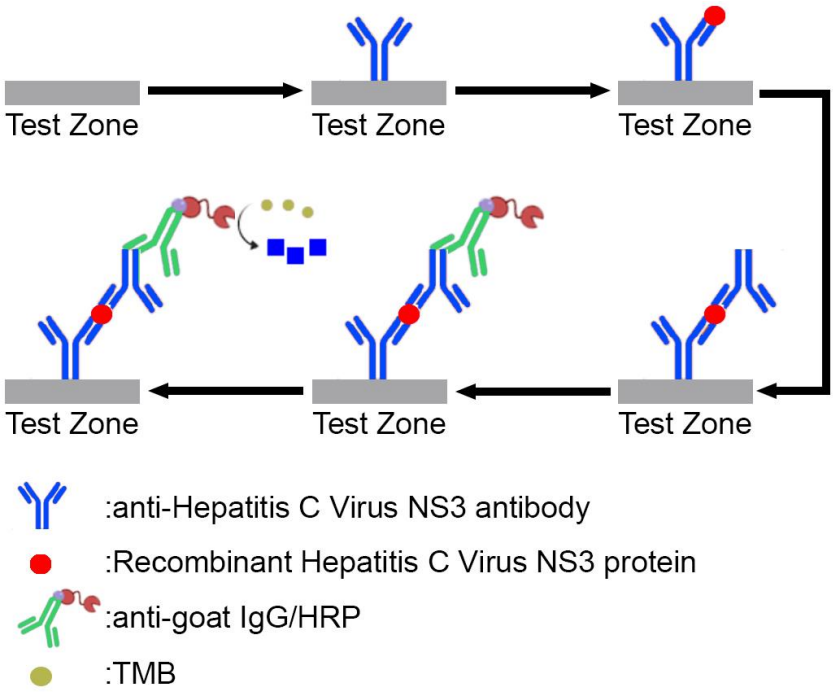

Figure 2.4. HCV detection with µP-ELISA.

2.2.3.4. Limit of Detection for HCV via Colorimetric Analysis

The limit of detection (LoD) for HCV in µP-ELISA was determined by colorimetric analysis. In this section, the varied amounts of recombinant Hepatitis C Virus NS3 protein (0-1 mg/ml) in PBS solution were tried to be detected in 1S4T-Type2 µPADs, which were fabricated in 20P90S (20%Power & 90%Speed) parameter, by following the same procedure in Method 2.2.3.3. At end of the µP-ELISA protocol, the colorimetric changes were captured via camera of smart-phone (Samsung, A705FN) and bright-field microscope (Axio Observer Zeiss).

The mean colour intensities in the images, which were captured via smart-phone and bright-field microscope, were analysed with MatLab R2018b. For this purposes, the images were uploaded to the program and the area in which the colour formation occurred were selected. After analysing the colour intensities on the selected regions, the data were recorded to Origin Pro (2020b) and GraphPad Prism (6.0 version). While the limit of detection (LoD) curves were generated via Origin Pro 2020b; the statistical analysis of data was performed via GraphPad Prism (6.0 version) (Figure 2.5).

Data for LoD experiments, which were analysed via GraphPad Prism (6.0 version), are expressed as mean ± SD. One-way ANOVA and Dunnett's multiple comparisons tests were used for comparison of experimental groups when appropriate. P values of less than 0.05 were considered as statistically significant.

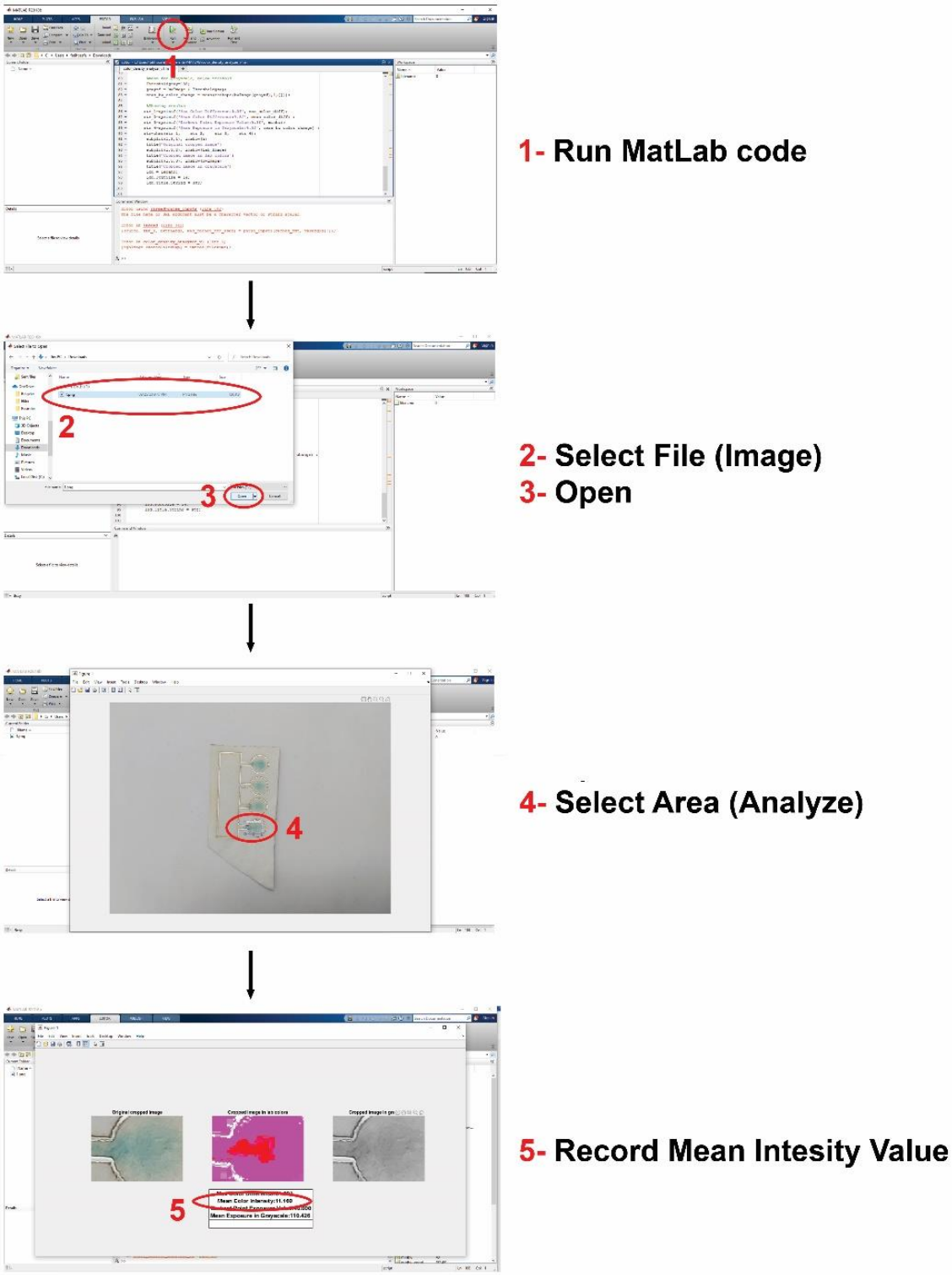

Figure 2.5. Colour intensity analysis via MatLab R2018b. In the first step, MatLab R2018b is executed and MatLab code, which was already written, is run. Then, the image file is selected. The area, which the colour change is observed, is selected on the appeared window. Lastly, the mean intensity value is recorded.

CHAPTER 3

RESULTS & DISCUSSIONS

3.1. Fabrication and Characterization of Paper-based Microfluidic Devices

Paper-based microfluidics, called µPADs, were fabricated via laser ablation methodology after coating of paper with adhesive aluminium film. And the designs of µPAD models were accomplished via CorelDraw software. First, the papers were coated by adhesive aluminium film on one side, as shown in Figure 2.1. After that, the designed models of µPADs were fabricated by patterning the designs onto opposite-side of aluminium coating. For the fabrication process, 100 different parameters, as given in Table 2.1, were used.

In the beginning of the study, surface characterizations of standard and modified filter papers, and 1S1T µPAD were done via scanning electron microscope (SEM). As shown in Figure 3.1, there were no differences among the standard and modified filter papers, and 1S1T µPAD in terms of their surface properties. Physical surface appearances for each one were observed as similar and there were no sign damages on cellulose fibres even after the fabrication process through laser ablation methodology.

On the other hand, channel formation and thickness, barriers and corners of 1S1T µPAD, which was fabricated by 10P60S (10%Power & 60%Speed) parameter, were also visualized with scanning electron microscope in varied magnifications. As seen in Figure 3.1d-f, the barriers in µPAD was distinct, neat, and straight, while the corners, in which vertical and horizontal barriers are intersected, were sharp. Also no melting or collapsing was observed during fabrication of channels, while a consistent and homogeneous barrier thickness (241.96 µm) was observed. This fabrication technique ensured consistent and high resolution patterning at low cost, which provide advantages compared to other patterning techniques, such as wax screen printing,[67] PDMS printing,[71] and stamping.[72]

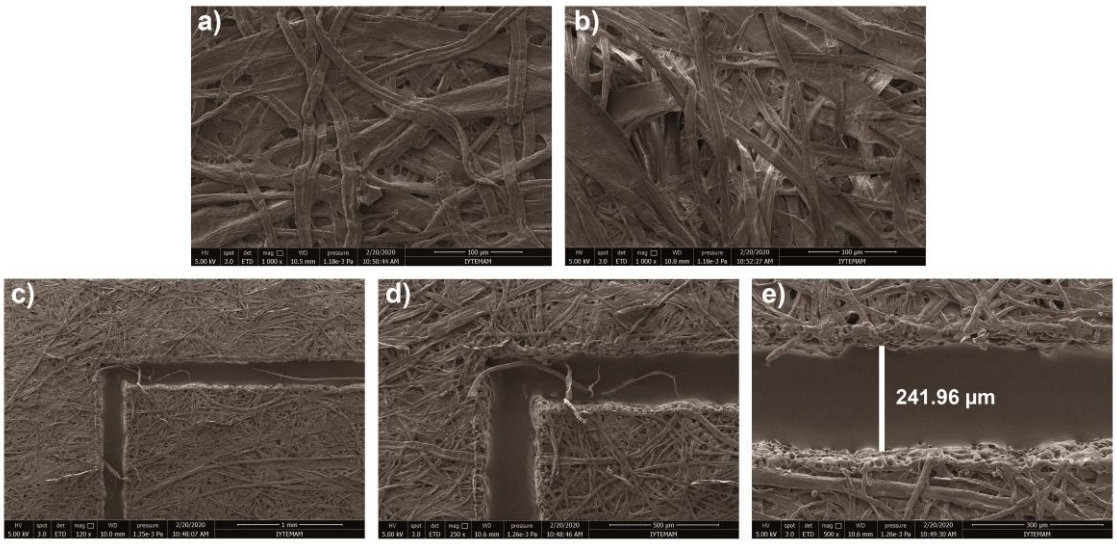

Figure 3.1. SEM images of standard and modified filter papers, and 1S1T µPAD. a) Visualization of standard filter paper at 1000X b) Visualization of modified filter paper whose one-side was coated with aluminium band at 1000X, c-e) Visualization of the barriers and corner in 1S1T µPAD at 120X, 250X, and 500X.

After characterization of surface properties, 1S1T µPADs were fabricated via laser ablation methodology in 100 different fabrication parameters (Table 2.1). Integrities of barrier were observed and then thickness of barriers in fabricated 1S1T µPADs were measured via microscopy. Integrity and thickness of barriers in 1S1T µPADs were substantially affected by the speed and power values (Figure 3.2 and Figure 3.3). It is clearly seen that barriers in 1S1T µPADs became thinner by increasing the speed at constant power. While 213.83 ± 13.83 µm of barrier thickness was obtained as minimum (10P100S, Figure 3.2j), the maximum barrier thickness was 384.19 ± 42.12 µm (10P10S, Figure 3.2a). Moreover, the integrity of barriers was becoming more tethered, when the speed was increased at constant power (Figure 3.2). On the other hand, the barriers dramatically became thicker by increasing the power at constant speed. While the minimum barrier thickness was achieved as 384.19 ± 42.12 µm (10P10S, Figure 3.2a), the maximum barrier thickness was 1009.31 ± 301.14 µm (100P10S, Figure 3.3j). The dramatic increase in the barrier thickness caused the deteriorations of the integrities of barriers (Figure 3.3). Moreover, microchannels between test zone and sample inlet area were almost closed in some 1S1T µPADs because of the improper fabrication parameters, such as 90P10S and 100P10S (Figure 3.3).

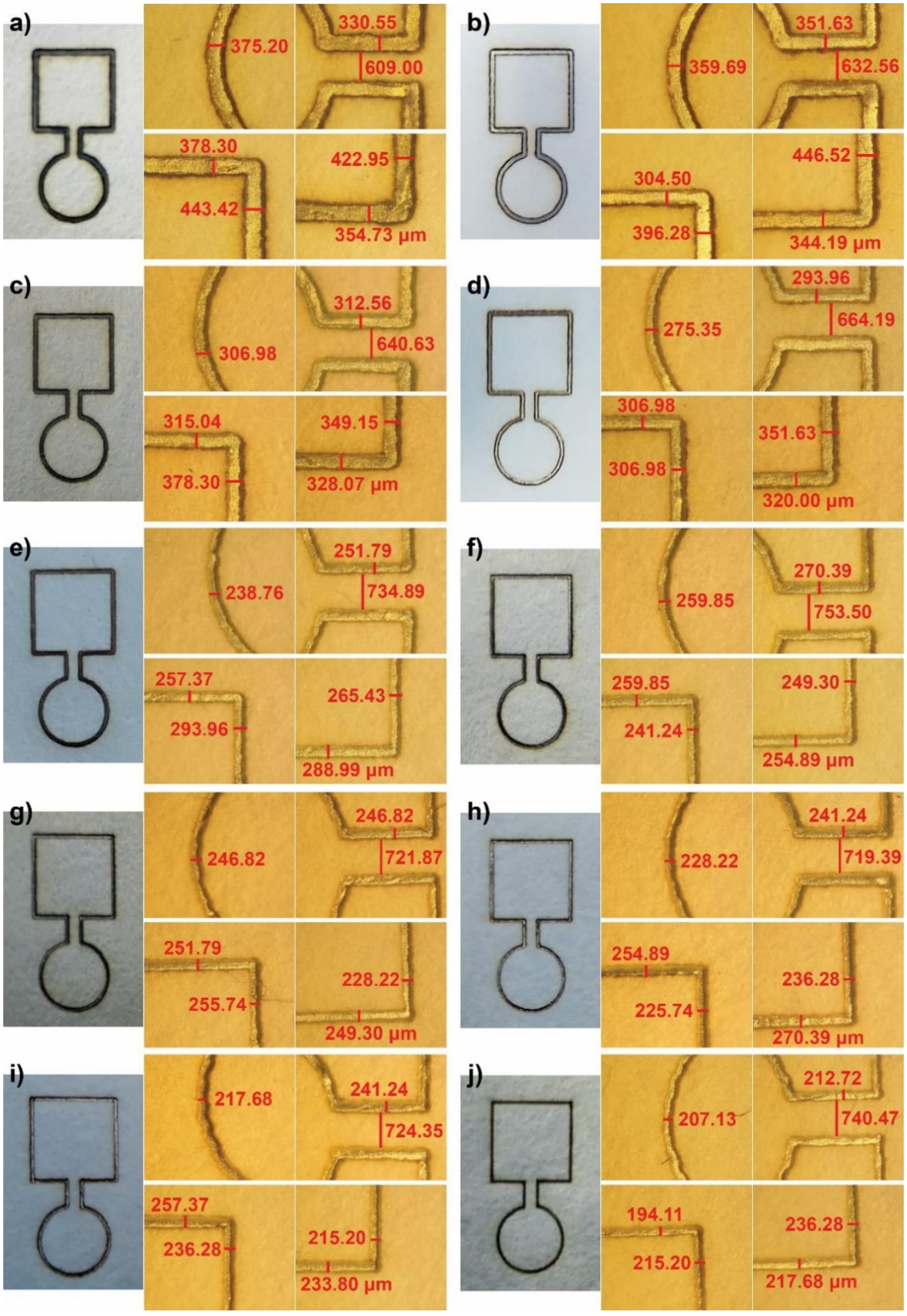

Figure 3.2. 1S1T µPADs were fabricated in the constant power (10%) and varied speed (10-100%) values. a) 10P10S (10%Power & 10%Speed), b) 10P20S, c) 10P30S, d) 10P40S, e) 10P50S, f) 10P60S, g) 10P70S, h) 10P80S, i) 10P90S, j) 10P100S.

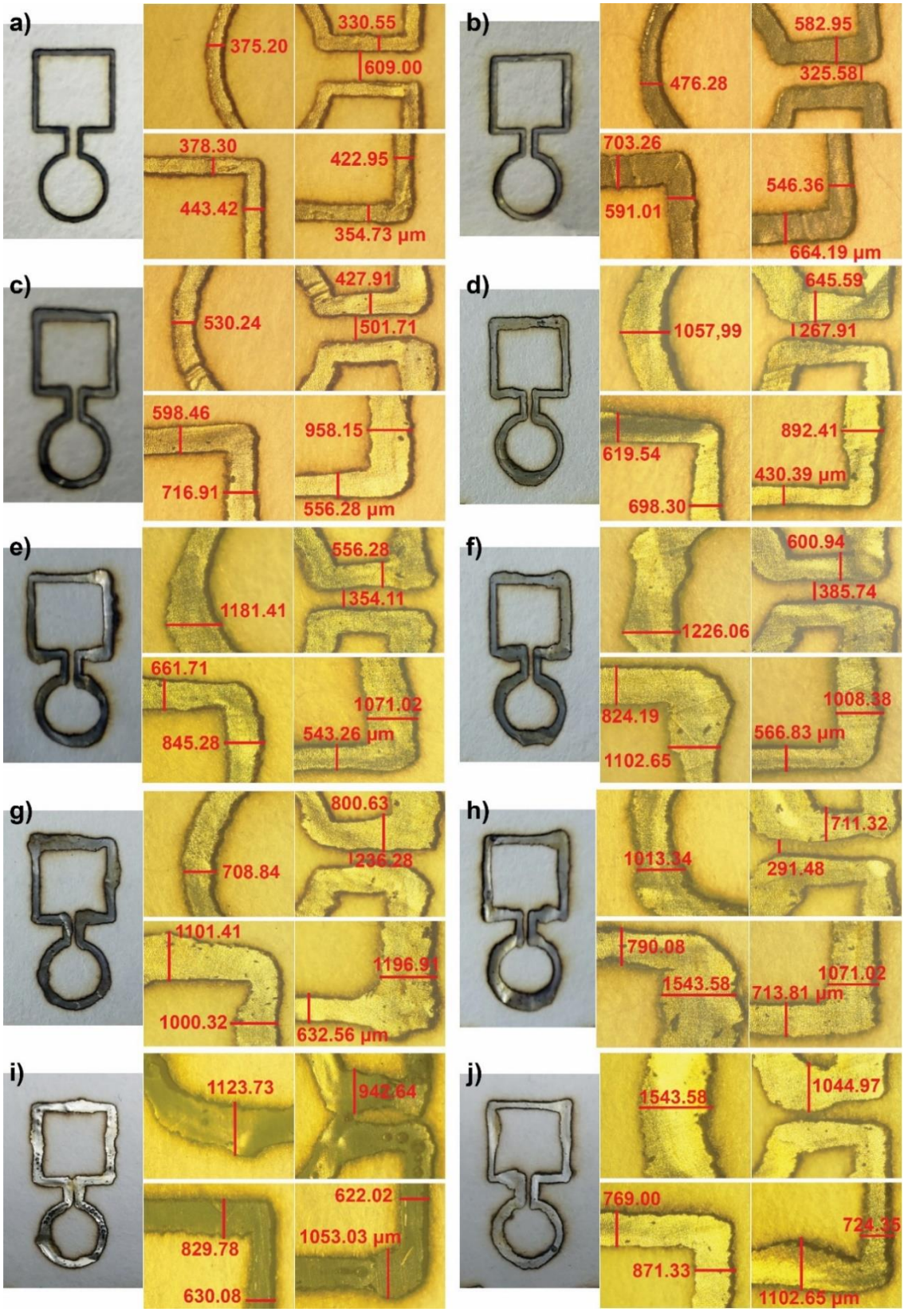

Figure 3.3. 1S1T µPADs were fabricated in the constant speed (10%) and varied power (10-100%) values. a) 10P10S (10%Power & 10%Speed), b) 20P10S, c) 30P10S, d) 40P10S, e) 50P10S, f) 60P10S, g) 70P10S, h) 80P10S, i) 90P10S, j) 100P10S.

To determine the optimized fabrication parameters, 1S1T µPADs were fabricated in 100 different fabrication parameter, and were analysed in terms of their barrier integrities and average barrier thickness. The average barrier thickness for each 1S1T µPADs were calculated from microscopy images and the analysis was done via GraphPad Prism.

As expected and shown in Figure 3.4, the thicker barriers were obtained at (i) high power with the constant speed, and (ii) low speed with the constant power. In contrast, the thinner barriers were achieved at (i) low power with the constant speed, and (ii) high speed with the constant power. Moreover, increasing the power values in the fabrication process deteriorated the barrier integrities.

After analysing the border integrities and thickness in each 1S1T µPAD (Figure 3.4), nine different fabrication parameters, which were 10P40S (10%Power & 40%Speed), 10P60S, 20P90S, 30P50S, 30P100S, 40P80S, 40P100S, 70P80S, and 70P100S, were determined as optimal fabrication parameters. The average barrier thickness of these µPADs were given in Table 3.1. In the µPADs, which were fabricated in these fabrication parameters, it was observed that there were (i) less deteriorations in the barriers, and (ii) low standard deviation around the barrier. The barrier integrities of 1S1T µPAD models, which were fabricated in optimal fabrication parameters, were also observed (Figure 3.5).

Table 3.1. The average of barrier thicknesses in 1S1T µPADs, which were fabricated in optimized fabrication parameters.

Optimized Fabrication Parameters	**Average Barrier Thickness (µm)**
10P40S (10%Power & 40%Speed)	309.15 ± 25.71
10P60S (10%Power & 60%Speed)	255.92 ± 10.01
20P90S (20%Power & 90%Speed)	332.10 ± 16.89
30P50S (30%Power & 50%Speed)	446.72 ± 29.59
30P100S (30%Power & 100%Speed)	358.87 ± 14.61
40P80S (40%Power & 80%Speed)	400.93 ± 21.21
40P100S (40%Power & 100%Speed)	377.99 ± 22.44
70P80S (70%Power & 80%Speed)	482.20 ± 25.32
70P100S (10%Power & 100%Speed)	427.91 ± 30.34

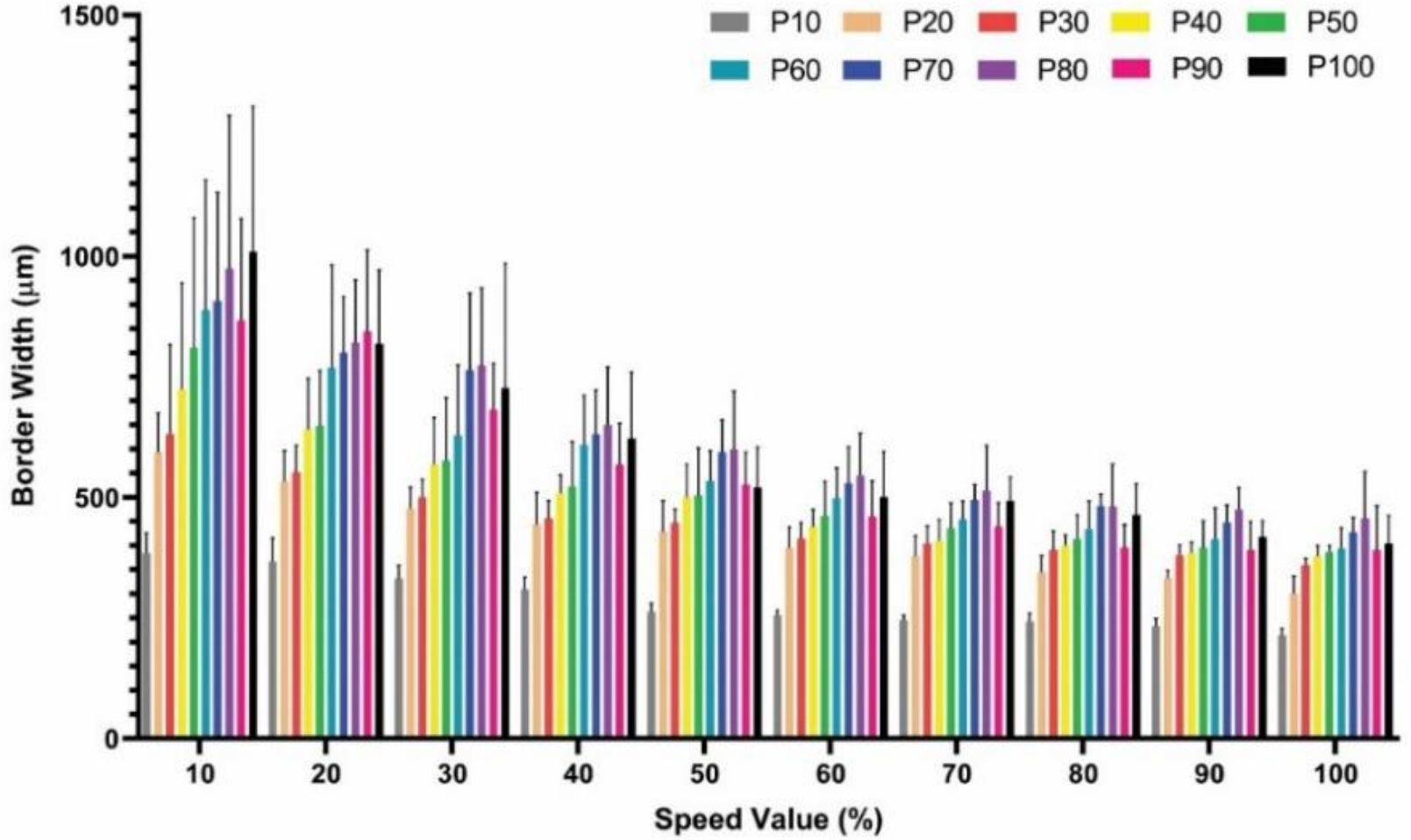

Figure 3.4. The barrier thickness in the 1S1T µPADs, which were fabricated in 100 different fabrication parameters (10-100%). The bars represent the average of eighteen measurements from three independent experiments and the error bars indicate the standard deviation.

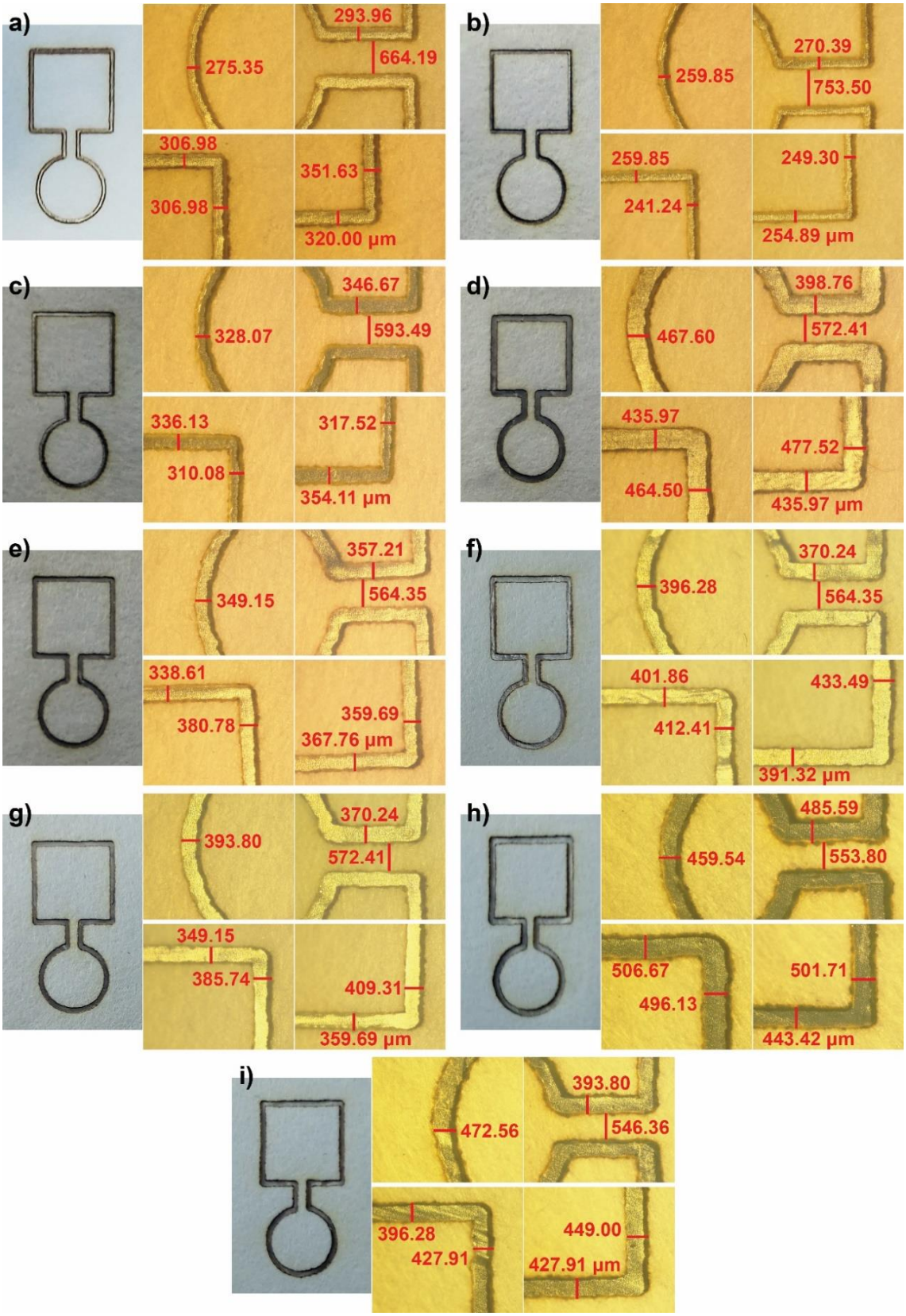

Figure 3.5. 1S1T µPADs were fabricated in the optimized fabrication parameters. a) 10P40S (10%Power & 40%Speed), b) 10P60S, c) 20P90S, d) 30P50S, e) 30P100S, f) 40P80S, g) 40P100S, h) 70P80S, i) 70P100S.

After fabrication parameters were optimized through 1S1T µPAD, varied µPAD models, which are 1S2T, 1S4T-Type1, 1S4T-Type2, 1S4T-Type3, and 1S8T, were investigated, and fabricated via laser ablation methodology based on previous designs (Figure 2.2). As these µPADs contain more than one test zone, they allow us to analyse more than one analytes in sample. Figure 3.6 represents different models of µPADs, which were successfully fabricated by laser ablation methodology. This results also show that well-defined patterns could be achieved by this technique.

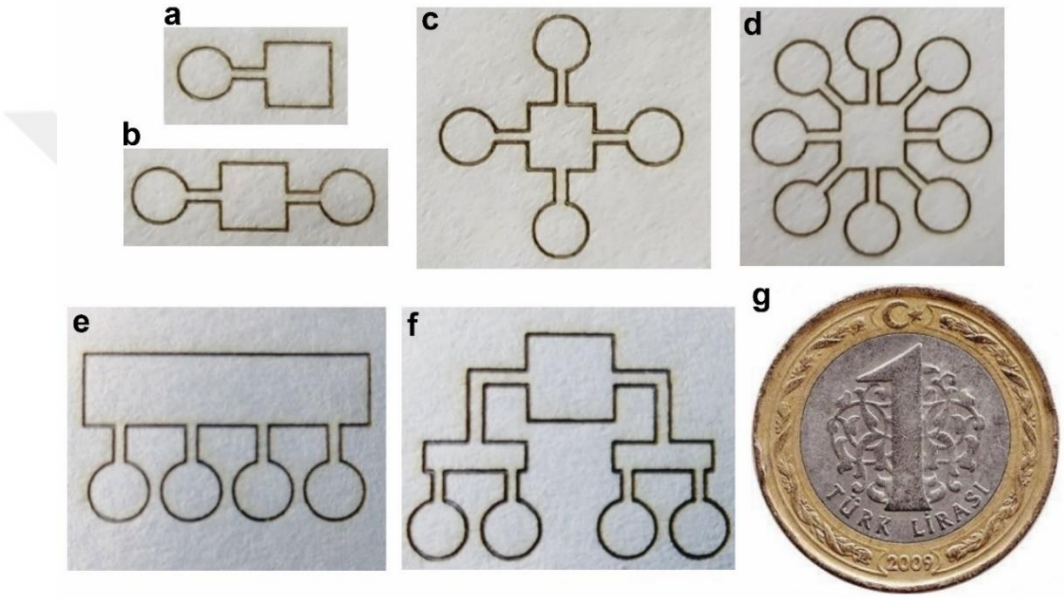

Figure 3.6. Different models of µPADs which were fabricated in 10P40S (10% Power & 40% Speed) parameter by laser ablation methodology. a) 1S1T µPAD, b) 1S2T µPAD, c) 1S4T-Type1 µPAD, d) 1S8T µPAD, e) 1S4T-Type2 µPAD, f) 1S4T-Type3 µPAD, g) 1 Turkish Lira which has diameter as 26.15 mm.

3.2. Liquid Flow and Confinement in µPADs

Fabricated µPADs were used for; (i) observation of fluid flow and (ii) determination of required sample volume. For that purposes, Ponceau 4r E124 [5% (w/v)] was separately loaded onto the 1S1T, 1S2T, 1S4T-Type1, 1S4T-Type2, 1S4T-Type3, and

1S8T µPADs through the sample input area by direct pipetting, and then the fluid flow was observed.

As seen in Figure 3.7-9, the 1S1T, 1S2T, 1S4T-Type1, and 1S8T µPADs fabricated in the 10P60S (10%Power & 60%Speed) parameter were not able to hold the sample within the test zones. The low values of barrier width (255.92 ± 10.01 µm, Table 3.1) of these µPADs could possibly be a main reason for these flow problems in µPADs. That's why, the barrier width in µPADs should be higher than 255.92 µm.

On the other hand, the required sample volume for complete saturation and absorption of test zones in each µPAD was determined by changing the injected sample volume where red food dye (Ponceau 4r E124) was used as ink. As shown in Figure 3.7, samples ranging between 3-15 µL was injected onto the 1S1T µPADs. It was observed that 5 µL sample volume was quite enough for filling the test zones in 1S1T µPADs; however, with 6 µL sample volume provided the full absorption of test zones in 1S1T µPADs for varied fabrication parameters. 5-15 µL sample volumes were used to determine the required sample amount for full saturation of test zones in 1S2T µPADs. As seen in Figure 3.8, the test zones were not completely filled by sample until 6 µL was used. It was seen that 6 µL was quite enough for filling the test zones in 1S2T µPADs; however, 7 µL sample volume provided the full saturation of test zones in 1S2T µPADs for varied fabrication parameters. Moreover, 8-20 µL sample volumes were tested for 1S4T-Type1 µPADs. As shown in Figure 3.9, the test zones were not completely filled and saturated until 10 µL sample is used. Additionally, 15-30 µL sample volumes were tested for 1S4T-Type2 µPADs, 13-30 µL sample volumes were tested for 1S4T-Type3 µPADs, and 10-20 µL sample volumes were tested for 1S8T µPADs. Saturation was observed at 22 µL for 1S4T-Type2 (Figure 3.10), 20 µL for 1S4T-Type3 (Figure 3.11), and 16 µL for 1S8T (Figure 3.12) µPADs.

The required amounts of sample volume for each µPADs was determined as given in Table 3.2. Even if the required sample volume differs for different models, the sample volume was not different for same models, which were fabricated by using different fabrication parameters. That's why, it can be commented that the required sample volume for full saturation is not affected by varied fabrication parameters.

In addition to the (i) observation of fluid flows within µPADs and (ii) determination of required sample volume, the required time for the saturation of test zones for each µPAD was also investigated. Optimized sample volumes (6, 7, 10, 22, 20, and 16 µL) were separately loaded onto the surface of sample inlet area in 1S1T, 1S2T, 1S4T-

Type1, 1S4T-Type2, 1S4T-Type3, and 1S8T µPADs, respectively. As it is clearly seen in Figure 3.13, the liquid samples were completely absorbed at the test zones in different rates. 1S1T, 1S2T, 1S4T-Type1, and 1S8T µPADs required 30 seconds for full saturation of test zones. However, saturation time was 90 seconds for 1S4T-Type2 µPAD, and 240 seconds for 1S4T-Type3 µPAD (Table 3.3).

Table 3.2. The required amounts of liquid sample for each type of µPADs.

µPAD Model	**Required Liquid Sample**
1S1T	6 µL
1S2T	7 µL
1S4T-Type1	10 µL
1S4T-Type2	22 µL
1S4T-Type3	20 µL
1S8T	16 µL

Table 3.3. The required time for full saturation of test zones in each type of µPADs.

µPAD Model	**Required Time for Test Zone Saturation**
1S1T	30 sec
1S2T	30 sec
1S4T-Type1	30 sec
1S4T-Type2	90 sec
1S4T-Type3	240 sec
1S8T	30 sec

As a summary of this section, 1S1T, 1S2T, 1S4T-Type1, 1S4T-Type2, 1S4T-Type3, and 1S8T µPADs were successfully fabricated by using varied parameters 10P40S (10%Power & 40%Speed), 10P60S, 20P90S, 30P50S, 30P100S, 40P80S, 40P100S, 70P80S, and 70P100S. For each fabricated µPAD, liquid sample flow was observed and the required amount of sample was determined. Each fabricated µPAD had an ability to hold liquid sample within the test zones with the exception of 10P60S, which were not able to hold the liquid sample because of its low barrier width. That's why, we decided to not continue with µPADs, which were fabricated in the 10P60S parameter.

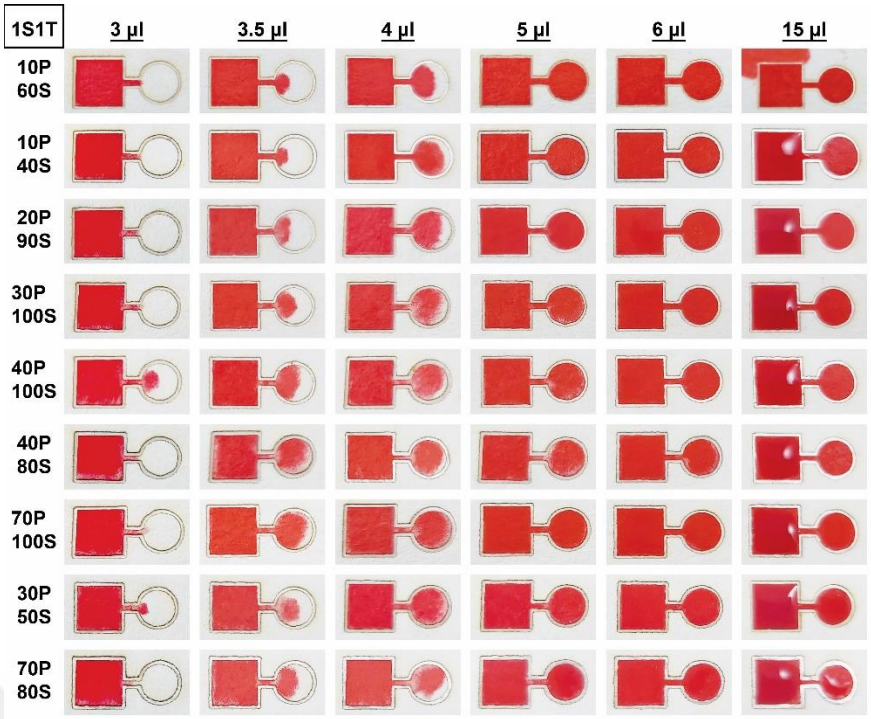

Figure 3.7. Determination of the required sample volume for 1S1T µPADs, which were fabricated in optimized fabrication parameters.

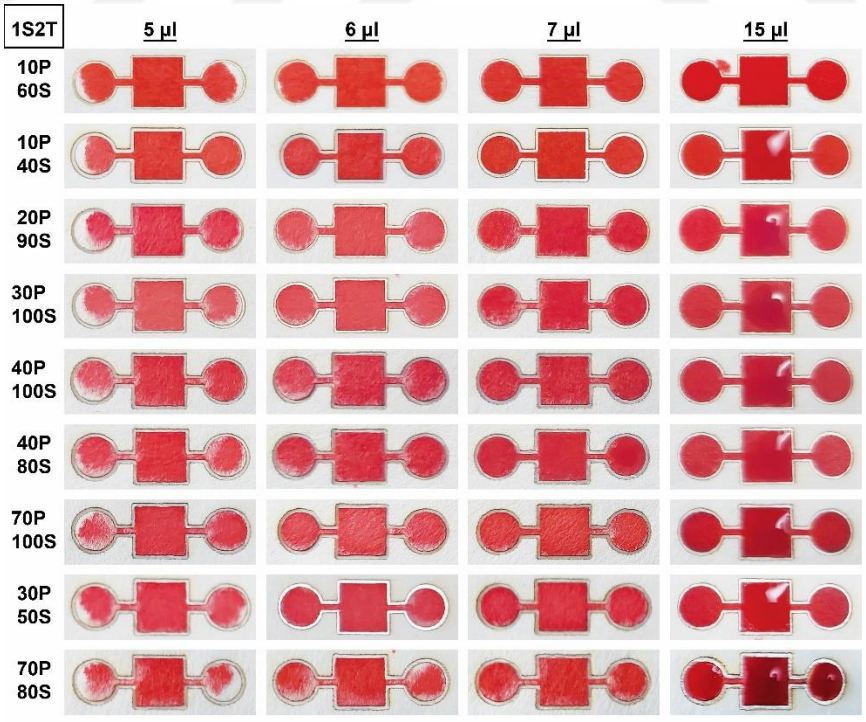

Figure 3.8. Determination of the required sample volume for 1S2T µPADs, which were fabricated in optimized fabrication parameters.

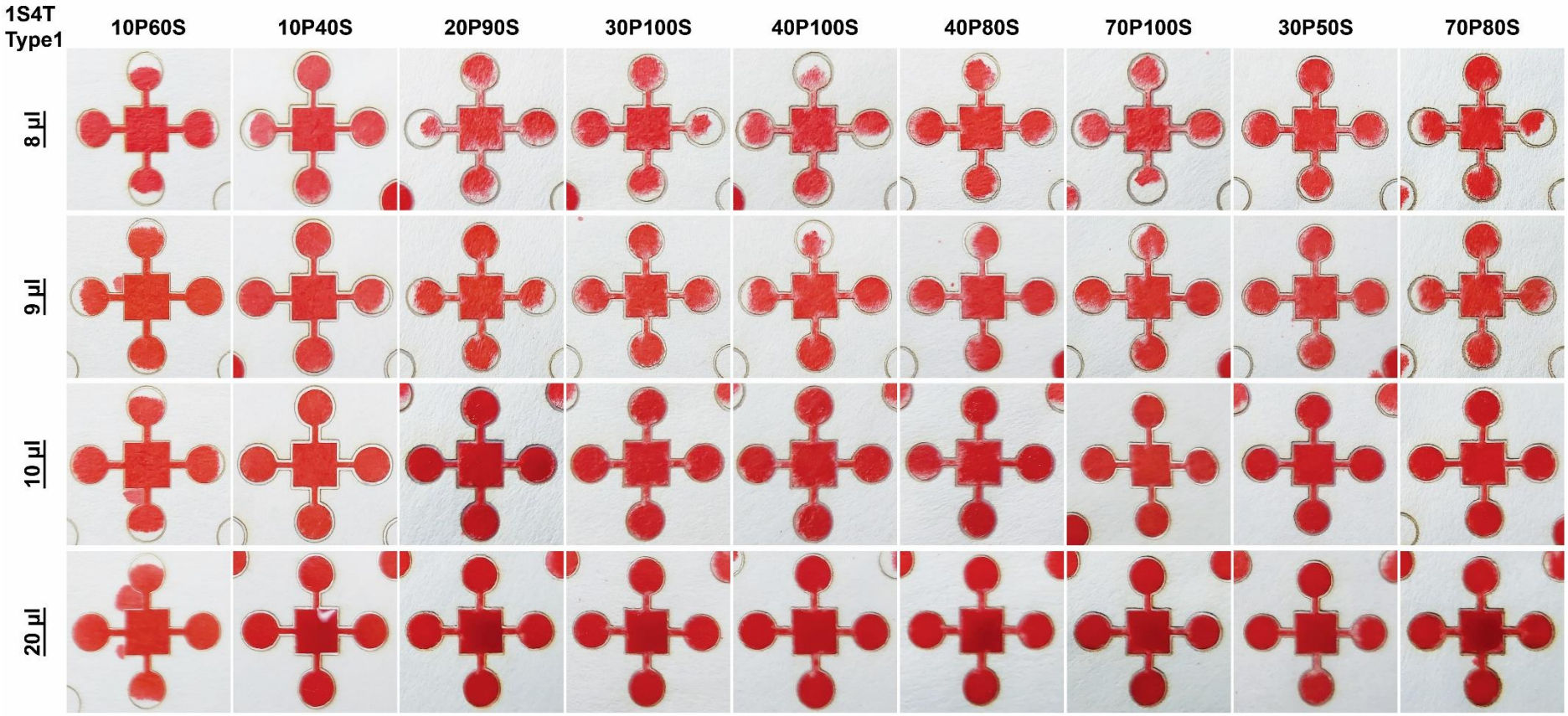

Figure 3.9. Determination of the required sample volume for 1S4T-Type1 µPADs, which were fabricated in optimized fabrication parameters.

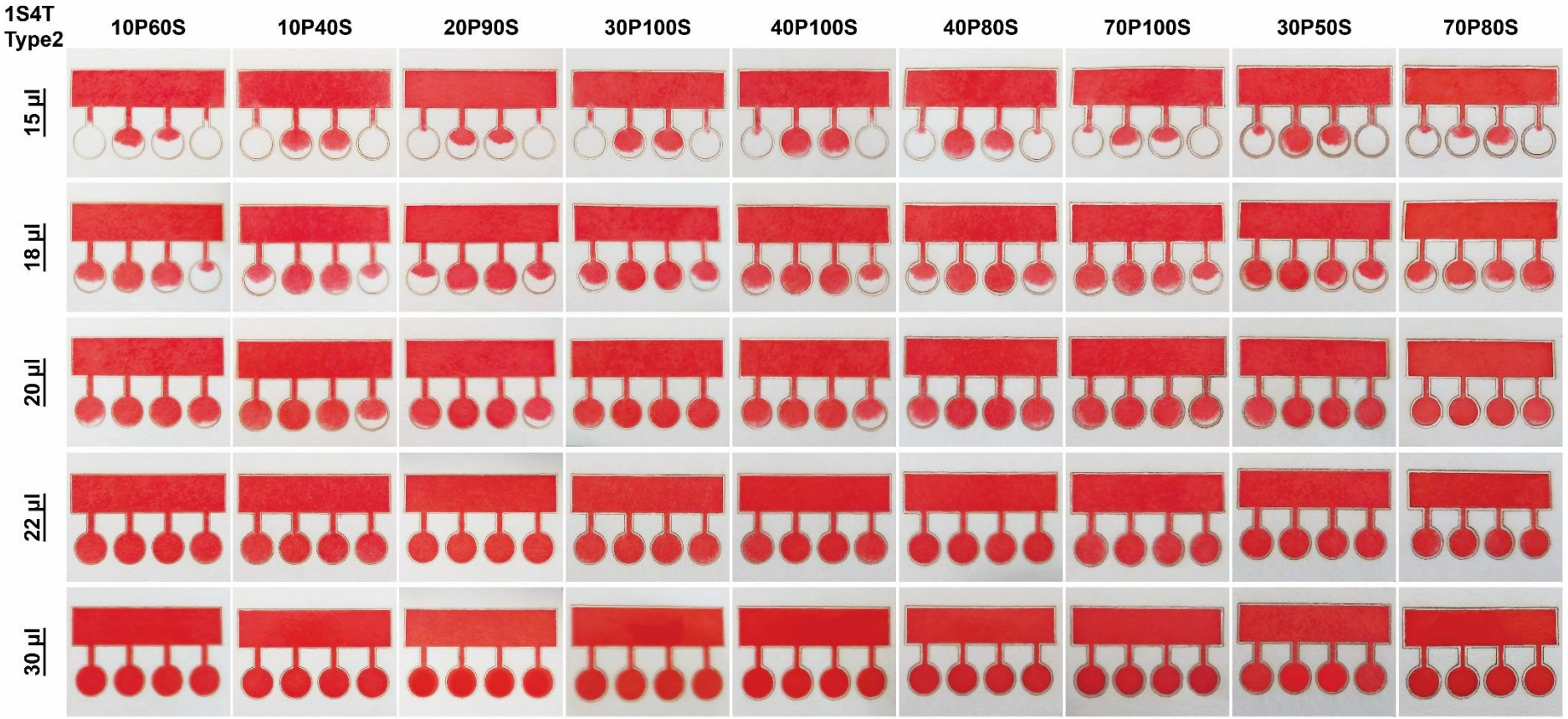

Figure 3.10. Determination of the required sample volume for 1S4T-Type2 µPADs, which were fabricated in optimized fabrication parameters.

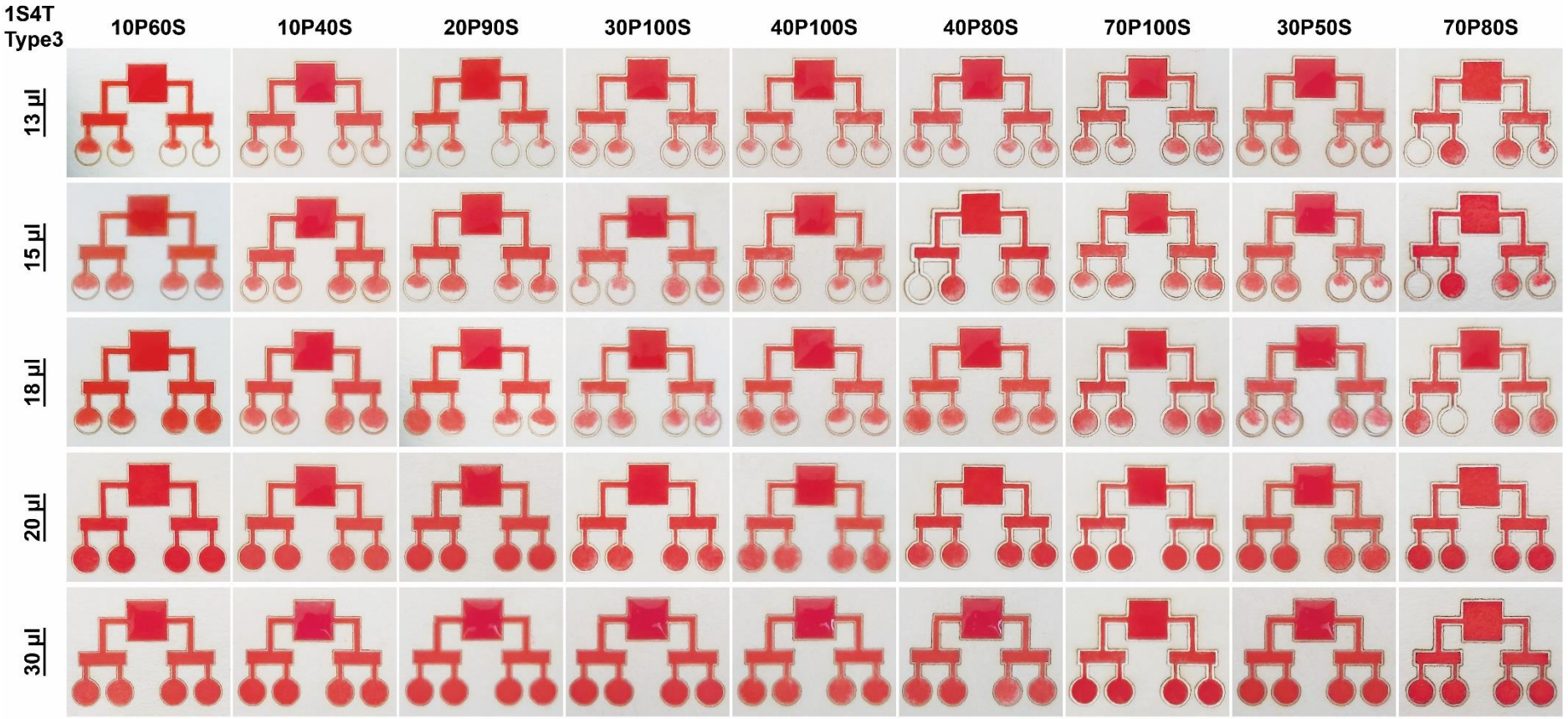

Figure 3.11. Determination of the required sample volume for 1S4T-Type3 µPADs, which were fabricated in optimized fabrication parameters.

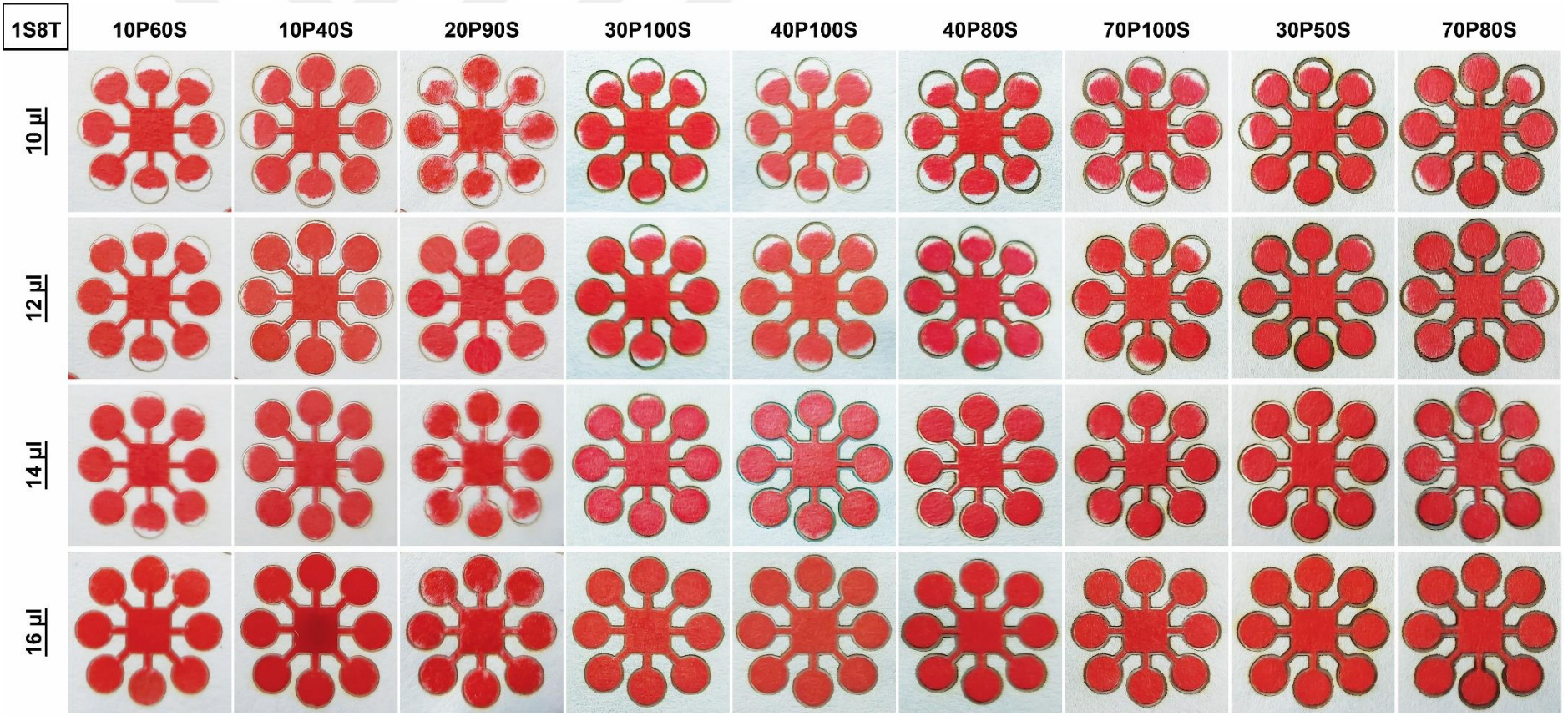

Figure 3.12. Determination of the required sample volume for 1S8T µPADs, which were fabricated in optimized fabrication parameters.

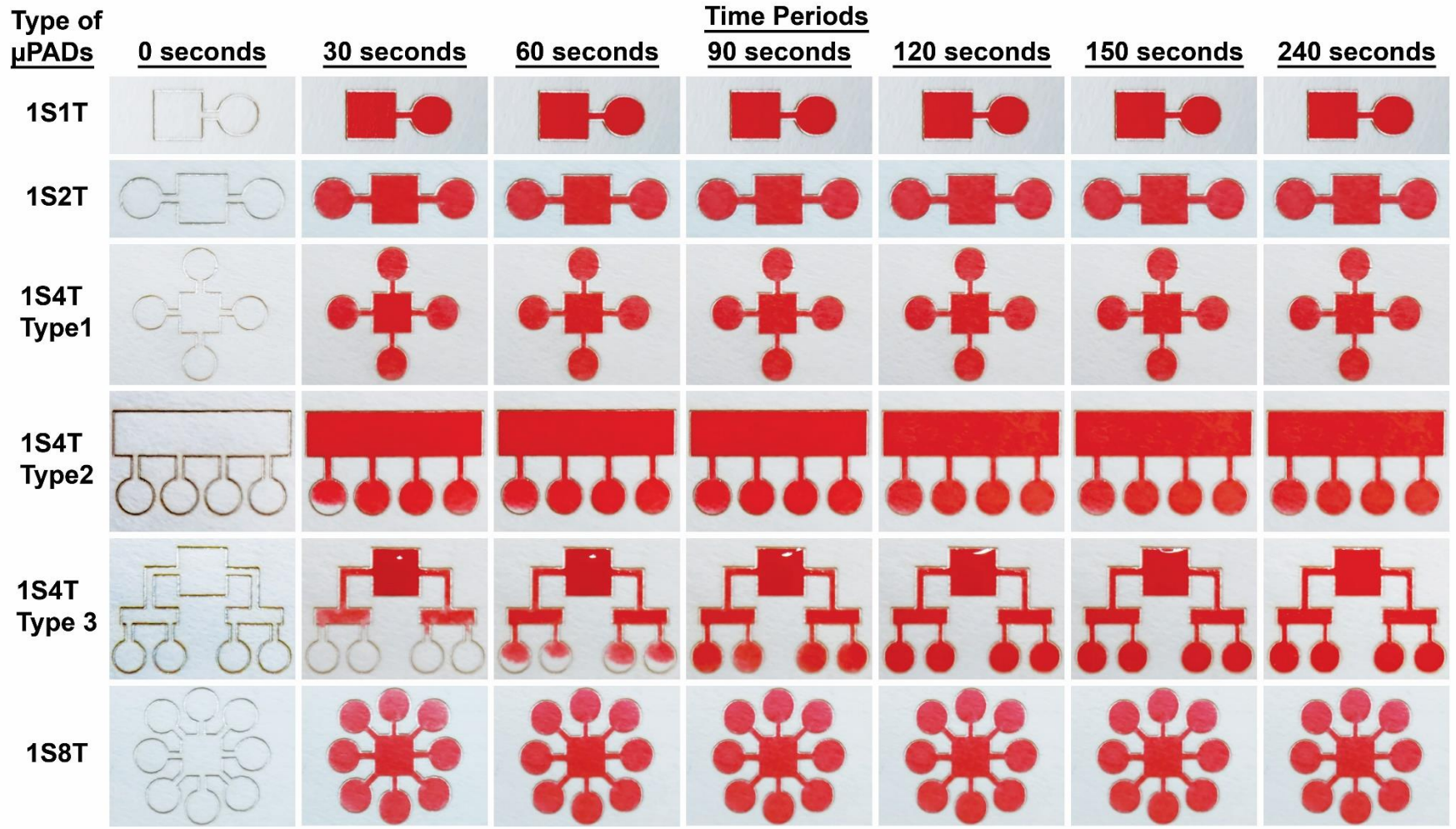

Figure 3.13. Liquid sample (Ponceau 4r E124) flow in each type of µPADs.

3.3. Optimization of Micro-Paper Enzyme Linked Immunosorbent Assay (µP-ELISA) Protocol

For optimization of µP-ELISA protocol, the 1S1T, 1S2T, 1S4T-Type1 and 1S8T µPADs (Figure 2.3a) were fabricated via laser ablation methodology. These fabricated µPADs were used to detect BSA, which was used as model antigen for calibration of µP-ELISA protocol.

As shown in Fig 2.3, there were six steps in µP-ELISA; (i) coating the test zones with 1 µL of monoclonal anti-BSA antibody (1:250 diluted), (ii) blocking the test zones, (iii) 1 µL of BSA addition (1 mg/ml) to test zone and washing, (iv) 1 µL of primary antibody (anti-BSA antibody - 1:250 diluted) addition to test zone and washing, (v) 1 µL of enzyme-conjugated secondary antibody (Anti-mouse IgG/HRP - 1:250 diluted) addition to test zone and washing, and (vi) adding around 20 µL of substrate (3,3',5,5'-Tetramethylbenzidine, TMB) and incubate for 20 minutes to observe the colorimetric signals.

In 1S1T µPADs, the µP-ELISA was performed and, the BSA was successfully detected via colour change (blue colour formation) (Figure 3.14a). However, when the µP-ELISA was performed in 1S4T-Type1 and 1S8T µPADs (Figure 3.14b-d), colour formation at the sample entry area was observed. This is caused by the secondary antibodies (Anti-mouse IgG/HRP), which were falsely accumulated at these parts of µPADs. The false accumulation of secondary antibodies was possibly caused by the flow from test zones to sample entry areas of µPADs during the washing steps. For the washing the µPADs were vertically held and the ELISA wash buffer was added from top, and solution allowed flowing through the bottom part of µPADs. This uncontrolled loading of wash buffer could be a reason for undesired flow of secondary antibodies through the sample inlet area in 1S2T, 1S4T-Type1 and 1S8T µPADs; that's why the colour formations, which were caused by enzymatic reaction of HRP with TMB, were observed.

To eliminate these problems, µPADs, which have four test zones were redesigned (Figure 2.2e-f), and 1S4T-Type2 and 1S4T-Type3 µPADs were fabricated (Figure 3.6e-f) to be used in µP-ELISA for BSA and HCV detections.

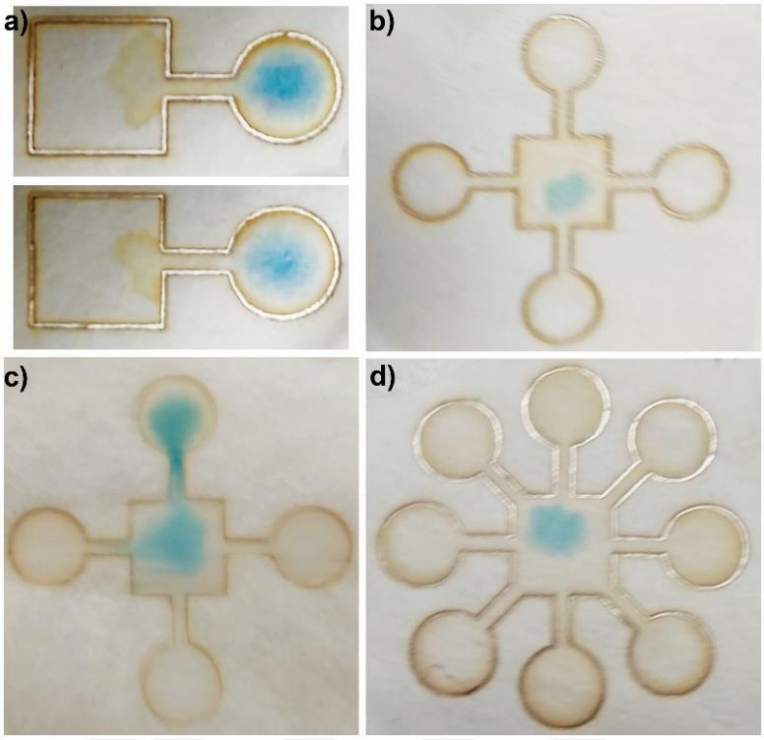

Figure 3.14. Problems, which were related to colour formation at sample entry area of µPADs as results of µP-ELISA. The µP-ELISA in a) 1S1T, b-c) 1S4T-Type1, and 1S8T µPADs.

3.4. Evaluation of µP-ELISA via BSA Detection

After the optimization of µPAD designs, µP-ELISA was evaluated by detection of the BSA. For that purposes, 1S4T-Type2 and 1S4T-Type3 µPADs were fabricated via laser ablation methodology in two different fabrication parameters, which were 20P90S (20%Power & 90%Speed) and 40P80S (40%Power & 80%Speed). In this section of study, some serial experiments were performed to reveal the necessity of each ELISA components in µPADs and, to evaluate the efficiency of µP-ELISA protocol to detect the BSA (Figure 3.15a).

The previously optimized µP-ELISA protocol was performed in the first test zones of each µPADs to detect the BSA in the PBS solution (Figure 3.15a). As clearly seen in Figure 3.15b, the colour formations were observed by naked eyes; the BSA (1 mg/ml), found in first test zones of each µPADs, was successfully detected. Interestingly, the distributions of colour formation were different in first test zones of each µPADs even

if the same amount of BSA was added to them. This could be explained by the differences in microchannel properties of µPADs. The thickness of the microfluidic channels in each µPADs, which provide connection between sample inlet and test zones, are different than each other. For example, 20P90S (20%Power & 90%Speed) had microchannel thickness as 593.49 ± 11.23 µm, and 40P80S (40%Power & 80%Speed) had microchannel thickness as 564.35 ± 12.18 µm.

Also, as a control group of, which the BSA was not added to the test zones, were performed in the second test zones of each µPADs (Figure 3.15). As there was no BSA as an antigen, consequently the blue colour formation was not observed in the second test zones of any µPADs, as expected (Figure 3.15b). By this control experiment, it was also confirmed that non-specific binding was not observed as well. On the other hand, as another control group, which secondary antibody (anti-mouse IgG/HRP) was not added to test zones, were performed in the third test zones of each µPADs (Figure 3.15). As there was no secondary antibody that contains HRP enzyme, the reaction that produces blue colour could not be occurred even in the presence of TMB substrate. That's why, the blue colour formation was not observed in the third test zones of each µPADs, as expected (Figure 3.15b).

In the fourth test zone of each µPADs, the µP-ELISA protocols were performed as the protocol, which was done in first test zones. The only difference between these protocols was about the addition of the primary and secondary antibodies. In fourth zone, primary and secondary antibodies were added together to eliminate one washing step in µP-ELISA protocol (Figure 3.15a). For this process, the primary and secondary antibodies were mixed and incubated for 20 minutes, before loading into the test zones. After incubation, the mixture of antibodies was added to test zones. The blue colour formation was also observed in fourth test zones as well as in first test zone; however, the distributions of blue colour were again different in fourth test zones of each µPADs (Figure 3.15b).

To sum up, BSA (1 mg/ml) was successfully detected in the first and fourth test zones of µPADs via naked eyes through µP-ELISA protocol in which the colorimetric changes occur. Moreover, it was also demonstrated that there were no blue color formation in negative control groups µP-ELISA protocol within the developed µPADs (Figure 3.15).

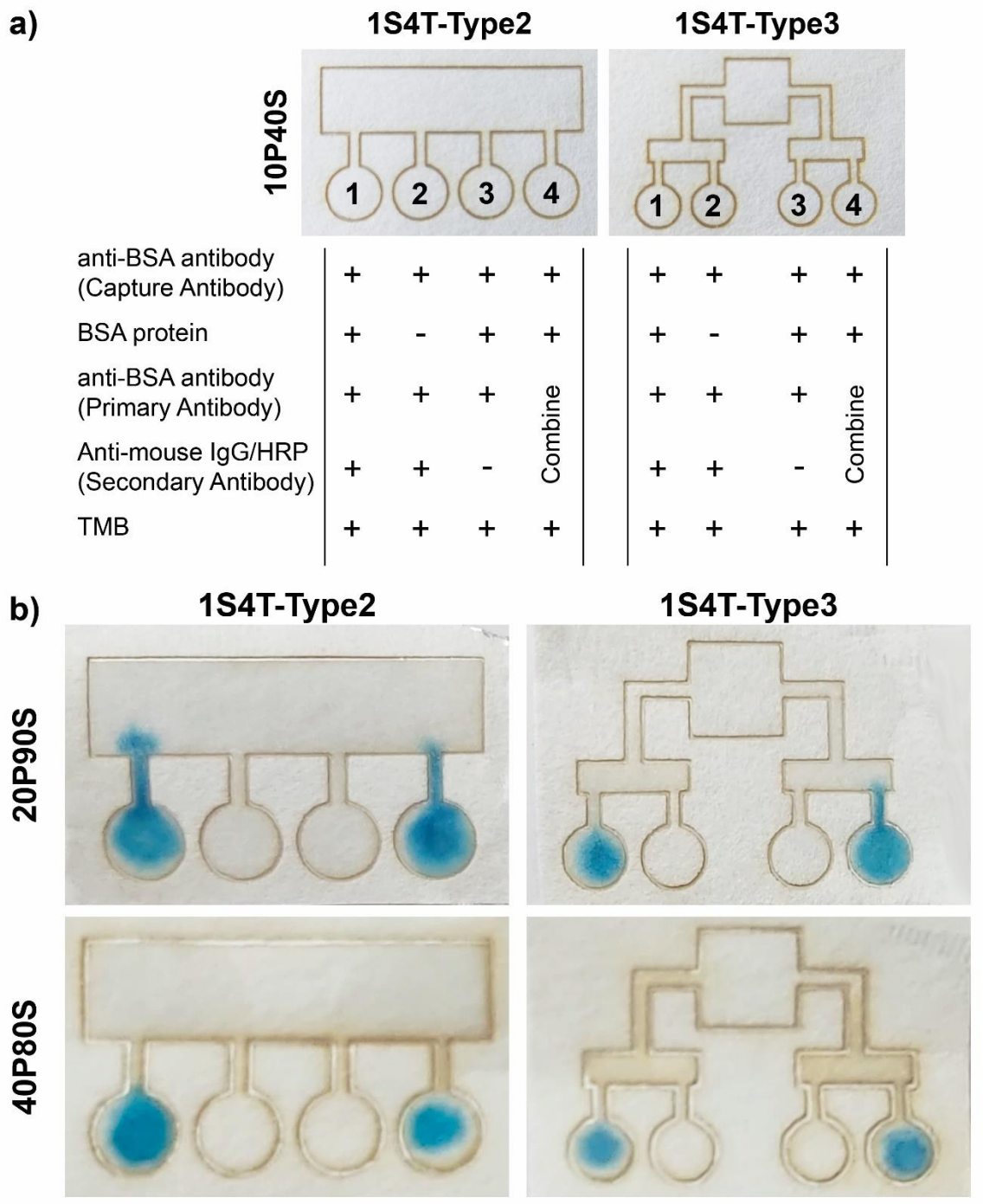

Figure 3.15. Evaluation of µP-ELISA via BSA Detection. a) µP-ELISA protocols, which were performed in the test zones of µPADs. First test zone: standard protocol; Second test zone: no BSA; Third test zone: no secondary antibody; Fourth test zone: mixed antibodies. b) µP-ELISA for BSA detection in 1S4T-Type2 and 1S4T-Type3 µPADs, which were fabricated in the 20P90S (20% Power & 90%Speed) and 40P80S (40% Power & 80%Speed) fabrication parameters.

3.5. Hepatitis C Virus (HCV) Detection via µP-ELISA

1S4T-Type2 and 1S4T-Type3 µPADs, which were optimized previously, were fabricated via laser ablation methodology in eight different fabrication parameters as shown in Table 2.2 (excluding 10P60S), and then each fabricated µPAD was used in the detection of recombinant Hepatitis C Virus NS3 protein through the µP-ELISA protocol.

For this part of study, the serial experiments that were mentioned in the previous section were performed similarly; however, specific primary and secondary antibodies were used against recombinant Hepatitis C Virus NS3 protein (Figure 3.16a). Similar to the BSA detection, in HCV detection experiments, colorimetric changes (blue colour formation) in the first and fourth test zones of 1S4T-Type2 and 1S4T-Type3 µPADs were clearly observed by naked eye; however, there were no blue colour formations in second and third test zones, which were designated as a control groups (Figure 3.16b).

As shown in Figure 3.16b, the recombinant Hepatitis C Virus NS3 protein (1 mg/ml) was successfully detected; when (i) the µP-ELISA protocol was performed in the first test zones of each µPADs, and (ii) the primary and secondary antibodies were added as mixture, which was already incubated for 20 minutes, in the fourth test zones of each µPADs. Distributions of blue colour were different even if the same amounts of recombinant Hepatitis C Virus NS3 protein were used. It could again be commented that the thickness property of microfluidic channels in each µPADs affect the distribution of sample in the µPADs. For example, 10P40S (10%Power & 40%Speed), 20P90S (20%Power & 90%Speed), 30P100S (30%Power & 100%Speed), 40P100S (40%Power & 100%Speed), 40P80S (40%Power & 80%Speed), 70P100S (70%Power & 100%Speed), 30P50S (30%Power & 50%Speed), and 70P80S (70%Power & 80%Speed) had microchannel thickness as 664.19 ± 8.73 µm, 593.49 ± 11.23 µm, 564.35 ± 18.72 µm, 572.41 ± 14.78 µm, 564.35 ± 12.18 µm, 546.36 ± 16.48 µm, 572.41 ± 21.87 µm, and 553.80 ± 20.19 µm.

As expected, there were no colour formations for the control groups; when (i) the recombinant Hepatitis C Virus NS3 protein was not added to the second test zones of each µPADs, and (ii) the secondary antibody (anti-goat IgG/HRP) was not added to the third test zones of each µPADs.

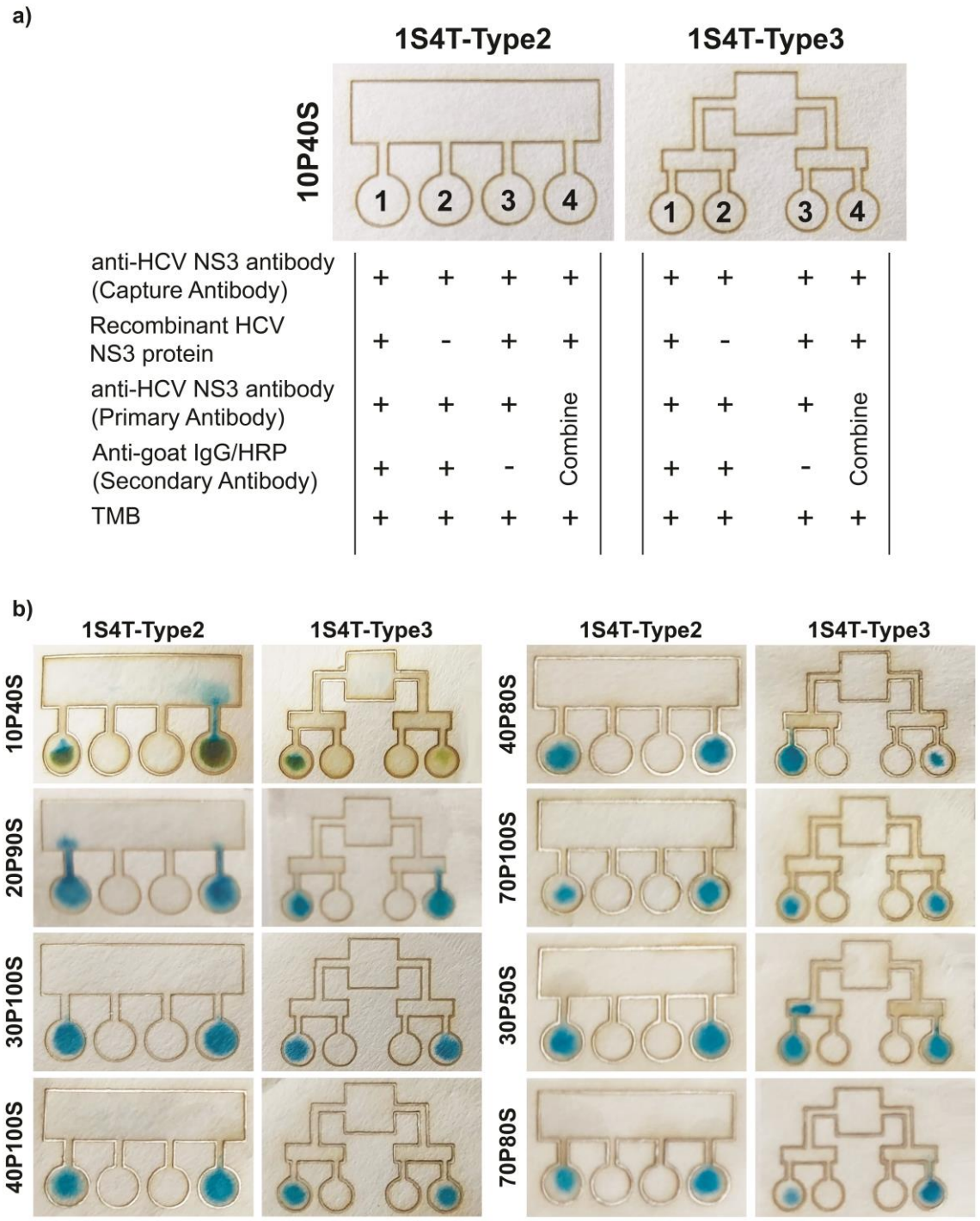

Figure 3.16. Hepatitis C Virus (HCV) detection via µP-ELISA. a) µP-ELISA protocols in the test zones of µPADs, b) µP-ELISA for HCV detection in 1S4T-Type2 and 1S4T-Type3 µPADs, which were fabricated in the 10P40S (10%Power & 40%Speed), 20P90S, 30P100S, 40P100S, 40P80S, 70P100S, 30P50S, and 70P80S parameters.

In addition to colorimetric detection of HCV by naked eye, the limit of detection value for HCV was investigated by using the same µP-ELISA protocol in 1S4T-Type2 µPAD, which was fabricated with 20P90S (20%Power & 90%Speed) fabrication parameter. For that purposes, different concentration of recombinant HCV NS3 protein solution in PBS ranging from 10^{-2} to 10^{6} ng/ml were prepared, and these samples were analysed via µP-ELISA. As a first step, the concentration-dependent responses in the test zones of 1S4T-Type2 µPAD were defined. Then, at the end of µP-ELISA, images were captured from the test zones via smart-phone and bright-field microscope for further colorimetric analysis. For colorimetric analysis, the captured images were analysed by using MatLab R2018b to determine the mean colour intensities in the test zones. By the analysis of images, the limit of detection (LoD) curves for HCV were established based on the changes of the mean colour intensities, which were driven with the chemical reaction between HRP and TMB.

The images of the test zones, which were captured via smart-phone, were given in Figure 3.17. The blue-colour formation, which is resulted from the reaction between HRP enzyme and TMB, was obviously seen in the test zones where the concentration of recombinant HCV NS3 protein varies from 1 mg/ml to 1 ng/ml (Figure 3.17a). Moreover, the blue colour intensity in test zones was proportional to the concentration of recombinant HCV NS3 protein. While the intensity of blue-colour was minimum in the test zone where 1 ng/ml recombinant HCV NS3 analysed, the readout reached a plateau at the concentration that was around 10 µg/ml. Figure 3.17b shows (i) the limit of detection (LoD) curve with R^2=0.993 for recombinant HCV NS3, and (ii) strong linear relationship between the concentration of recombinant HCV NS3 protein (10^{-1}-10^{4} ng/ml) and mean colour intensities, with a R^2=0.983.

The LoD was calculated as 8.83 X 10^{-1} ng/ml (883 pg/ml) for recombinant HCV NS3 protein by using three times the standard deviation (3σ) of the intensity of the zero concentration solution (PBS solution).[139,140]

Consequently, 1S4T-Type2 µPAD was successfully utilized in µP-ELISA application for the detection of recombinant HCV NS3 protein. The protein was successfully detected by naked eye at concentration of 1 ng/ml or higher; however, the limit of detection value was calculated as 8.83 X 10^{-1} ng/ml after a processing of images that were captured with smart-phone in MatLab.

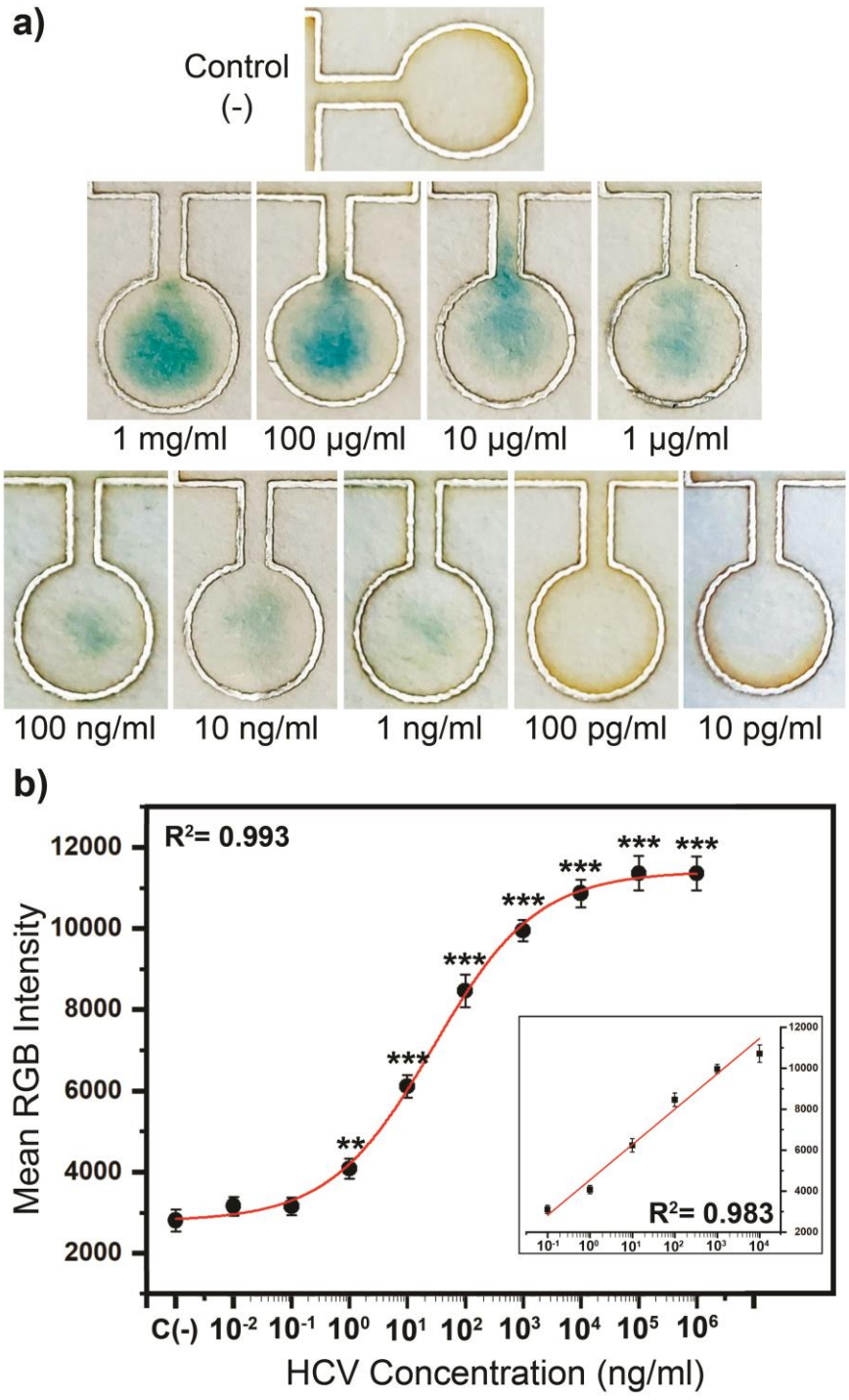

Figure 3.17. Limit of detection (LoD) measurement for HCV protein via smart-phone in 1S4T-Type2 µPADs. a) The colour bars represent the colour intensity of recombinant HCV NS3 protein with varying concentrations (from 0 to 1 mg/ml) in the presence of TMB substrate, b) The LoD curve was based on the mean RGB intensity of the test zones plotted against the various concentrations of recombinant HCV NS3 protein (from 0 to 1 mg/ml) in PBS. The error bars represent the standard deviations of eight replicates from two independent experiments. The inset chart shows the lineal calibration curve of HCV detection, and the lineal range was from 100 pg/ml to 10 µg/ml.

Additionally, the images of the test zones, which were captured via bright-field microscope, were analysed. Again, different concentration of recombinant HCV NS3 protein solution in PBS ranging from 10-2 to 106 ng/ml were prepared, and these samples were analysed via µP-ELISA. Figure 3.18a shows that the blue-colour formation was clearly seen in the test zones where the concentration of recombinant HCV NS3 protein varies from 1 mg/ml to 1 ng/ml. The colour intensity that is developed in test zones was again proportional to the concentration of recombinant HCV NS3 protein. The intensity of blue-colour was minimum in the test zone where 1 ng/ml recombinant HCV NS3 analysed; however, the readout reached a plateau at the concentration that was around 10 µg/ml. Figure 3.17b shows (i) the LoD curve with R^2=0.978 for recombinant HCV NS3 protein, and (ii) strong linear relationship between the concentration of recombinant HCV NS3 protein (10^{-1}-10^4 ng/ml) and mean colour intensities, with R^2=0.992.

The LoD was calculated as mentioned previously (in page 65). The LoD was determined as 7.96 X 10^{-1} ng/ml (796 pg/ml) for recombinant HCV NS3, when the bright-field microscope was used as a detection platform. Here, the determined LoD value was lower and the standard deviations were higher in the microscope compared to smart-phone. The possible reason of high standard deviations could be the higher resolution ability of microscope. As it has higher resolution properties than smart-phone camera, it provides high-resolution images that the colour intensities could be analysed in more details.

In summary, the HCV detection was successfully performed via µP-ELISA. The presented results show that the 1S4T-Type2 µPADs could potentially be used as a point-of care (PoC) diagnostic tool for the detection of Hepatitis C Virus. In addition to its detection capacity, it also provides more advantages compared to conventional ELISA. As clearly seen in the Table 3.3, the µP-ELISA requires the paper instead of specialized ELISA plate. The detection, which depends on the colorimetric readout, is provided by either naked eye or smart-phone or bright-field microscopy; however, the plate reader is required for the conventional ELISA. Moreover, the analysis of samples via µP-ELISA is 14 times shorter and 45 times cheaper compared to conventional ELISA. In addition to being cost-effective and rapid analysis, the developed µPADs provide lower LoD values for HCV detection than conventional ELISA (Table 3.3). As the developed µPADs are produced from only paper, they could easily be disposed without requirement of any waste management; therefore, they can be used as a PoC diagnostic tool and can be converted to various disease detection platforms.

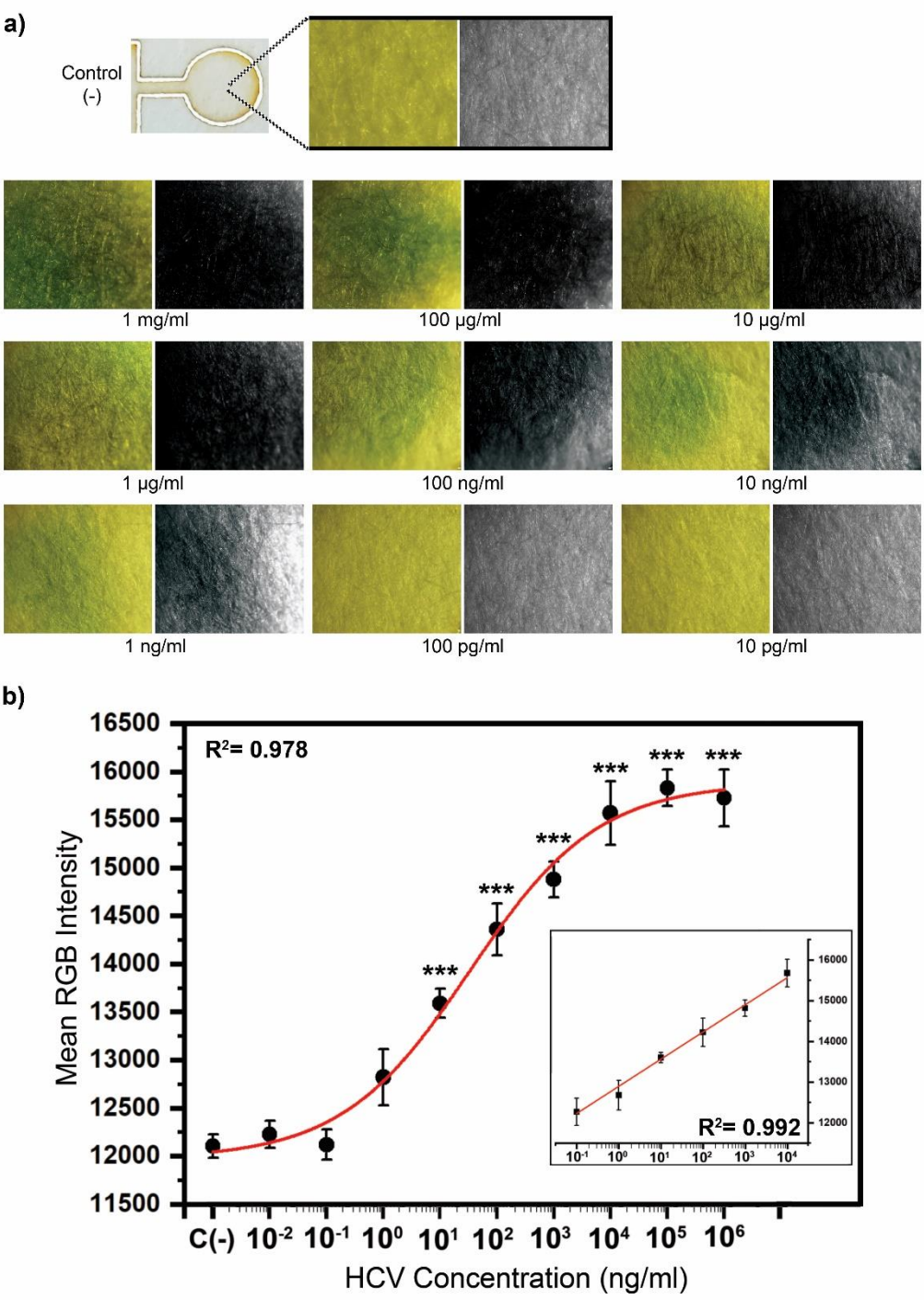

Figure 3.18. Limit of detection (LoD) measurement for HCV protein via bright-field microscope in 1S4T-Type2 µPADs. a) The colour bars represent the colour intensity of recombinant HCV NS3 protein with varying concentrations (from 0 to 1 mg/ml) in the presence of TMB substrate. b) The LoD curve was based on the mean RGB intensity of the test zones plotted against the various concentrations of recombinant HCV NS3 protein (from 0 to 1 mg/ml) in PBS. The error bars represent the standard deviations of eight replicates from two independent experiments. The inset chart shows the lineal calibration curve of HCV detection, and the linear range was from 1 ng/ml to 10 µg/ml.

Table 3.4. Comparison between µP-ELISA and conventional ELISA for HCV detection.

	µP-ELISA	**Conventional ELISA**
Antigen/antibody	Recombinant Hepatitis C Virus NS3 protein / anti-Hepatitis C Virus NS3 antibody	Recombinant Hepatitis C Virus NS3 protein / anti-Hepatitis C Virus NS3 antibody
Detection antibody	anti-goat IgG/HRP	anti-goat IgG/HRP
Enzyme/substrate	HRP-TMB	HRP-TMB
Test platform	Paper	ELISA plate
Detection device	Naked Eye Smart-phone Bright-field microscope	Plate reader
Sensitivity	1.00 ng/ml (Naked eye) 8.83 X 10^{-1} ng/ml (Smart-phone) 7.96 X 10^{-1} ng/ml (Microscope)	1.60 ng/ml[141]
Time	~1.5 hours	~21 hours
Cost	~0.122 $ / test	~5.544 $ / test

Table 3.5. Costs for µP-ELISA and conventional ELISA during the HCV detection.

	µP-ELISA / Test zone		**Conventional ELISA / Test Zone**	
Reagents	**Volume**	**Price ($)**	**Volume**	**Price ($)**
Test Platform	Filter Paper	0.00200	ELISA plate	4.00000
Capture antibody	1 µL	0.00584	100 µL	0.58400
Primary antibody	1 µL	0.00584	100 µL	0.58400
Secondary antibody	1 µL	0.00274	100 µL	0.27360
Blocking solution	1 µL	0.00014	200 µL	0.02800
Wash buffer	10 ml	0.09700	4 ml	0.03880
Substrate	22 µL	0.00792	100 µL	0.03600
Total		**~ 0.122**		**~ 5.54**

CHAPTER 4

CONCLUSION

Paper-based microfluidic devices, which are produced by utilization of paper to the microfluidic systems, have been gaining attention all around the world since 2007. As the paper-based microfluidic devices have been employed to total analysis systems, they have been especially developed for POC diagnostics due to their cost-effective and easy fabrication. In addition, the paper-based microfluidic devices, which are totally disposable, provide easy-to-operate and rapid detections for disease. In this thesis, paper-based microfluidic devices (μPADs), which could be used in POC applications, were designed and developed.

In the first section of this study, several μPAD models (1S1T, 1S2T, 1S4T-Type1, 1S4T-Type2, 1S4T-Type3, and 1S8T μPADs) were designed and then fabricated in different fabrication conditions through laser ablation methodology. The fabricated μPADs were characterized in many perspectives, such as the surface characteristics, condition dependent-barrier properties in μPADs, and liquid sample flows within channels of μPADs. It was determined that there were no significant changes on the surface properties of filter paper, after their back-sides were coated with aluminium. Then, the modified filter papers were used to fabricate μPADs via laser cutter engraving machine. The 1S1T μPADs were fabricated in a hundred different fabrication parameters in laser cutter engraving machine to determine optimized fabrication parameters. It was observed that the barrier integrities and thicknesses significantly differed in each 1S1T μPAD when the power and speed values were changed. The barriers in 1S1T μPADs became thinner by increasing the speed value at constant power value; however, it became thicker by increasing the power value at constant speed value. Also, the integrities of barriers in 1S1T μPADs, which were fabricated in high power value, were deteriorated. By comparing differently-fabricated 1S1T μPADs in terms of barrier integrities and thicknesses, nine different parameters were determined as optimized fabrication parameters, which were 10P40S (10%Power & 40%Speed), 10P60S, 20P90S, 30P50S, 30P100S, 40P80S, 40P100S, 70P80S, and 70P100S. After optimized fabrication

parameters were identified with 1S1T μPADs, different models of μPADs (1S2T, 1S4T-Type1, 1S4T-Type2, 1S4T-Type3, and 1S8T μPADs) were also fabricated in these determined parameters. Each μPAD was then loaded with the liquid sample to observe its flows through the hydrophilic channels of μPADs. It was determined that the barrier thickness in μPADs should be higher than 255.92 μm to prevent liquid leakages. Also, we noticed that the required amounts of liquid sample for full saturation of test zones in different models of μPADs were different than each other as 6 μL for 1S1T, 7 μL for 1S2T, 10 μL for 1S4T-Type1, 22 μL for 1S4T-Type2, 20 μL for 1S4T-Type3, and 16 μL for 1S8T. However, the required amounts of liquid sample did not dependent to fabrication parameters for each model of μPADs. Lastly, the timing of full saturation of liquid samples within the μPADs were measured as 30 seconds for 1S1T, 1S2T, 1S4T-Type1, and 1S8T, 90 seconds for 1S4T-Type2, and 240 seconds for 1S4T-Type3.

In the second section, the micro-paper enzyme linked immunosorbent assay (μP-ELISA) was optimized and then evaluated via BSA detection. The problems, which is related to colour formation in the sample input area of 1S2T, 1S4T-Type1 and 1S8T μPADs were observed due to undesired accumulation of antibodies during washing steps; that's why, 1S4T-Type2 and 1S4T-Type3 μPADs were designed and fabricated. In 1S4T-Type2 and 1S4T-Type3 μPADs, the μP-ELISA protocol was evaluated via BSA detection. It was confirmed that there were no signals in negative control groups, and the BSA (1 mg/ml) in PBS solution was successfully detected via naked eyes.

Later, HCV detection was performed in 1S4T-Type2 and 1S4T-Type3 μPADs through the evaluated μP-ELISA protocol. It was stated that the recombinant HCV protein (1 mg/ml) in PBS solution was successfully detected via naked eyes. To determine the limit of detection (LoD) value, the μP-ELISA protocol was repeated in 1S4T-Type2 μPAD for the recombinant HCV protein. The LoD curves were plotted from 0 to 1 mg/ml of recombinant HCV protein and had an excellent coefficient of determination, $R^2 = 0.993$ and $R^2 = 0.978$, when the smart-phone and bright-field microscope were used as detector, respectively. Moreover, the LoD values were calculated as 1.00 ng/ml (by naked eyes), $8.83 \text{ X } 10^{-1}$ ng/ml (by smart-phone), and $7.96 \text{ X } 10^{-1}$ ng/ml (by bright-field microscope).

In summary, we have successfully designed and fabricated the paper-based microfluidic device, which could be used in point-of-care applications. The developed μPAD was tested by the detection of recombinant HCV protein. According to results, the 1S4T-Type2 μPADs provided highly sensitive, rapid and cost-effective detection of recombinant HCV protein compared to conventional ELISA techniques.

REFERENCES

(1) Whitesides, G. M. The Origins and the Future of Microfluidics. *Nature* **2006**, *442* (7101), 368–373. https://doi.org/10.1038/nature05058.

(2) Kocharekar, A. M.; Dukhande, M. S. Paper Microfluidics in Microbial World. *Int. J. Sci. Res.* **2017**, *6* (3), 1909–1914. https://doi.org/10.21275/ART20171837.

(3) Mark, D.; Haeberle, S.; Roth, G.; Stetten, F. Von; Zengerle, R. Microfluidic Lab-on-a-Chip Platforms: Requirements, Characteristics and Applications. *Chem. Soc. Rev.* **2010**, *39*, 1153–1182. https://doi.org/10.1039/b820557b.

(4) A. A., M.; S. A., A.; T, A. Microfluidics Devices Manufacturing and Biomedical Applications. *J Biosens Bioelectron* **2019**, *10* (1), 1000265. https://doi.org/10.4172/2155-6210.1000265.

(5) Sackmann, E. K.; Fulton, A. L.; Beebe, D. J. The Present and Future Role of Microfluidics in Biomedical Research. *Nature* **2014**, *507* (7491), 181–189. https://doi.org/10.1038/nature13118.

(6) Terry, S. C.; Herman, J. H.; Angell, J. B. A Gas Chromatographic Air Analyzer Fabricated on a Silicon Wafer. *IEEE Trans. Electron Devices* **1979**, *26* (12), 1880–1886. https://doi.org/10.1109/T-ED.1979.19791.

(7) Shoji, S.; Esashi, M.; Matsuo, T. Prototype Miniature Blood Gas Analyser Fabricated on a Silicon Wafer. *Sensors and Actuators* **1988**, *14* (2), 101–107. https://doi.org/10.1016/0250-6874(88)80057-X.

(8) Van Lintel, H. T. G.; Van De Pol, F. C. M.; Bouwstra, S. A Piezoelectric Micropump Based on Micromachining of Silicon. *Sensors and Actuators* **1988**, *15* (2), 153–167. https://doi.org/10.1016/0250-6874(88)87005-7.

(9) Bragheri, F.; Vazguez, R. M.; Osellame, R. *Microfluidics*; Elsevier Inc., 2016. https://doi.org/10.1002/9783527633449.ch7.

(10) Manz, A.; Graber, N.; Widmer, H. M. Miniaturized Total Chemical Analysis Systems: A Novel Concept for Chemical Sensing. *Sensors actuators B Chem.* **1990**, *1* (1–6), 244–248. https://doi.org/10.1109/34.387509.

(11) Manz, A.; Miyahara, Y.; Miura, J.; Watanabe, Y.; Miyagi, H.; Sato, K. Design of an Open-Tubular Column Liquid Cbromatograpb Using Silicon Chip Technology. *Sensors actuators B Chem.* **1990**, *1* (1–6), 249–255.

(12) Harrison, D. J.; Fluri, K.; Seiler, K.; Fan, Z.; Effenhauser, C. S.; Manz, A. Micromachining a Miniaturized Capillary Electrophoresis-Based Chemical Analysis System on a Chip. *Science (80-.).* **1993**, *261*, 895–897. https://doi.org/10.1126/science.261.5123.895.

(13) Litman, D. J.; Lee, R. H.; Jeong, H. J.; Tom, H. K.; Stiso, S. N.; Sizto, N. C.; Ullman, E. F. An Internally Referenced Test Strip Immunoassay for Morphine. *Clin. Chem.* **1983**, *29* (9), 1598–1603. https://doi.org/10.1093/clinchem/29.9.1598.

(14) Pacifici, R.; Farré, M.; Pichini, S.; Ortuño, J.; Roset, P. N.; Zuccaro, P.; Segura, J.; De La Torre, R. Sweat Testing MDMA with the Drugwipe® Analytical Device: A Controlled Study with Two Volunteers. *J. Anal. Toxicol.* **2001**, *25* (2), 144–146. https://doi.org/10.1093/jat/25.2.144.

(15) Balagaddé, F. K.; You, L.; Hansen, C. L.; Arnold, F. H.; Quake, S. R. Long-Term Monitoring of Bacteria Undergoing Programmed Population Control in a Microchemostat. *Science (80-.).* **2005**, *309* (5731), 137–140. https://doi.org/10.1126/science.1109173.

(16) Harrison, D. J.; Manz, A.; Fan, Z.; Lüdi, H.; Widmer, H. M. Capillary Electrophoresis and Sample Injection Systems Integrated on a Planar Glass Chip. *Anal. Chem.* **1992**, *64* (17), 1926–1932. https://doi.org/10.1021/ac00041a030.

(17) Whitesides, G. *Microfluidics in Late Adolescence*; 2018.

(18) Duffy, D. C.; McDonald, J. C.; Schueller, O. J. A.; Whitesides, G. M. Rapid Prototyping of Microfluidic Systems in Poly(Dimethylsiloxane). *Anal. Chem.* **1998**, *70* (23), 4974–4984. https://doi.org/10.1021/ac980656z.

(19) Hulme, S. E.; Shevkoplyas, S. S.; Apfeld, J.; Fontana, W.; Whitesides, G. M. A Microfabricated Array of Clamps for Immobilizing and Imaging C. Elegans. *Lab Chip* **2007**, *7* (11), 1515–1523. https://doi.org/10.1039/b707861g.

(20) Ostuni, E.; Chen, C. S.; Ingber, D. E.; Whitesides, G. M. Selective Deposition of Proteins and Cells in Arrays of Microwells. *Langmuir* **2001**, *17* (9), 2828–2834. https://doi.org/10.1021/la001372o.

(21) Whitesides, G. M.; Ostuni, E.; Takayama, S.; Jiang, X.; Ingber, D. E. SOFT LITHOGRAPHY IN BIOLOGY AND BIOCHEMISTRY. *Annu. Rev. Biomed. Eng.* **2001**, *3*, 335–373. https://doi.org/10.1146/annurev.bioeng.3.1.335.

(22) McDonald, J. C.; Duffy, D. C.; Anderson, J. R.; Chiu, D. T.; Wu, H.; Schueller, O. J. A.; Whitesides, G. M. Fabrication of Microfluidic Systems in Poly(Dimethylsiloxane). *Electrophoresis* **2000**, *21* (1), 27–40. https://doi.org/10.1002/(sici)1522-2683(20000101)21:1<27::aid-elps27>3.3.co;2-3.

(23) Folch, A.; Toner, M. Cellular Micropatterns on Biocompatible Materials. *Biotechnol. Prog.* **1998**, *14* (3), 388–392. https://doi.org/10.1021/bp980037b.

(24) Folch, A.; Ayon, A.; Hurtado, O.; Schmidt, M. A.; Toner, M. Molding of Deep Polydimethylsiloxane Microstructures for Microfluidics and Biological Applications. *J. Biomech. Eng.* **1999**, *121* (1), 28–34. https://doi.org/10.1115/1.2798038.

(25) Ghaemmaghami, A. M.; Hancock, M. J.; Harrington, H.; Kaji, H.; Khademhosseini, A. Biomimetic Tissues on a Chip for Drug Discovery. *Drug Discov. Today* **2012**, *17* (3–4), 173–181. https://doi.org/10.1016/j.drudis.2011.10.029.

(26) Huh, D.; Matthews, B. D.; Mammoto, A.; Montoya-Zavala, M.; Yuan Hsin, H.; Ingber, D. E. Reconstituting Organ-Level Lung Functions on a Chip. *Science (80-.).* **2010**, *328*, 1662–1668. https://doi.org/10.1126/science.1188302.

(27) Zhang, J. X. J.; Hoshino, K. *Microfluidics and Micro Total Analytical Systems*, 2nd Editio.; Academic Press, 2019. https://doi.org/10.1016/b978-0-12-814862-4.00003-x.

(28) Das, T.; Chakraborty, S. Biomicrofluidics: Recent Trends and Future Challenges. *Sadhana* **2009**, *34* (4), 573–590. https://doi.org/10.1007/s12046-009-0035-8.

(29) Regehr, K. J.; Domenech, M.; Koepsel, J. T.; Carver, K. C.; Ellison-Zelski, S. J.; Murphy, W. L.; Schuler, L. A.; Alarid, E. T.; Beebe, D. J. Biological Implications of Polydimethylsiloxane-Based Microfluidic Cell Culture. *Lab Chip* **2009**, *9* (15), 2132–2139. https://doi.org/10.1039/b903043c.

(30) Lee, J. N.; Park, C.; Whitesides, G. M. Solvent Compatibility of Poly(Dimethylsiloxane)-Based Microfluidic Devices. *Anal. Chem.* **2003**, *75* (23),

6544–6554. https://doi.org/10.1021/ac0346712.

(31) Toepke, M. W.; Beebe, D. J. PDMS Absorption of Small Molecules and Consequences in Microfluidic Applications. *Lab Chip* **2006**, *6* (12), 1484–1486. https://doi.org/10.1039/b612140c.

(32) Berthier, E.; Warrick, J.; Yu, H.; Beebe, D. J. Managing Evaporation for More Robust Microscale Assays: Part 1. Volume Loss in High Throughput Assays. *Lab Chip* **2008**, *8* (6), 852–859. https://doi.org/10.1039/b717422e.

(33) Wu, M.-H.; Dimopoulos, G.; Mantalaris, A.; Varley, J. The Effect of Hyperosmotic Pressure on Antibody Production and Gene Expression in the GS-NS0 Cell Line. *Biotechnol. Appl. Biochem.* **2004**, *40* (1), 41–46. https://doi.org/10.1042/ba20030170.

(34) Chin, C. D.; Laksanasopin, T.; Cheung, Y. K.; Steinmiller, D.; Linder, V.; Parsa, H.; Wang, J.; Moore, H.; Rouse, R.; Umviligihozo, G.; et al. Microfluidics-Based Diagnostics of Infectious Diseases in the Developing World. *Nat. Med.* **2011**, *17* (8), 1015–1019. https://doi.org/10.1038/nm.2408.

(35) Martynova, L.; Locascio, L. E.; Gaitan, M.; Kramer, G. W.; Christensen, R. G.; MacCrehan, W. A. Fabrication of Plastic Microfluid Channels by Imprinting Methods. *Anal. Chem.* **1997**, *69* (23), 4783–4789. https://doi.org/10.1021/ac970558y.

(36) Becker, H.; Heim, U. Hot Embossing as a Method for the Fabrication of Polymer High Aspect Ratio Structures. *Sensors Actuators, A Phys.* **2000**, *83* (1–3), 130–135. https://doi.org/10.1016/S0924-4247(00)00296-X.

(37) Martinez, A. W.; Phillips, S. T.; Whitesides, G. M. Diagnostics for the Developing World: Microfluidic Paper-Based Analytical Devices. *Anal. Chem.* **2010**, *82*, 3–10.

(38) Díaz-González, M.; Baldi, A. Fabrication of Biofunctionalized Microfluidic Structures by Low-Temperature Wax Bonding. *Anal. Chem.* **2012**, *84* (18), 7838–7844. https://doi.org/10.1021/ac301512f.

(39) Pelton, R. Bioactive Paper Provides a Low-Cost Platform for Diagnostics. *TrAC - Trends Anal. Chem.* **2009**, *28* (8), 925–942. https://doi.org/10.1016/j.trac.2009.05.005.

(40) Zhao, W.; Van Den Berg, A. Lab on Paper. *Lab Chip* **2008**, *8* (12), 1988–1991. https://doi.org/10.1039/b814043j.

(41) Yetisen, A. K.; Akram, M. S.; Lowe, C. R. Paper-Based Microfluidic Point-of-Care Diagnostic Devices. *Lab Chip* **2013**, *13* (12), 2210–2251. https://doi.org/10.1039/c3lc50169h.

(42) Khan, M. S.; Misra, S. K.; Wang, Z.; Daza, E.; Schwartz-Duval, A. S.; Kus, J. M.; Pan, D.; Pan, D. Paper-Based Analytical Biosensor Chip Designed from Graphene-Nanoplatelet-Amphiphilic-Diblock-Co-Polymer Composite for Cortisol Detection in Human Saliva. *Anal. Chem.* **2017**, *89* (3), 2107–2115. https://doi.org/10.1021/acs.analchem.6b04769.

(43) Fu, E.; Liang, T.; Spicar-Mihalic, P.; Houghtaling, J.; Ramachandran, S.; Yager, P. Two-Dimensional Paper Network Format That Enables Simple Multistep Assays for Use in Low-Resource Settings in the Context of Malaria Antigen Detection. *Anal. Chem.* **2012**, *84* (10), 4574–4579. https://doi.org/10.1021/ac300689s.

(44) Martinez, A. W.; Phillips, S. T.; Butte, M. J.; Whitesides, G. M. Patterned Paper as a Platform for Inexpensive, Low-Volume, Portable Bioassays. *Angew. Chemie - Int. Ed.* **2007**, *46* (8), 1318–1320. https://doi.org/10.1002/anie.200603817.

(45) Stroock, A. D. Microfluidics. In *Optical Biosensors: Today and Tomorrow*; Elsevier B.V., 2008; pp 659–682.

(46) Costa, M. N.; Veigas, B.; Jacob, J. M.; Santos, D. S.; Gomes, J.; Baptista, P. V.; Martins, R.; Inácio, J.; Fortunato, E. A Low Cost, Safe, Disposable, Rapid and Self-Sustainable Paper-Based Platform for Diagnostic Testing: Lab-on-Paper. *Nanotechnology* **2014**, *25* (9), 094006. https://doi.org/10.1088/0957-4484/25/9/094006.

(47) Akyazi, T.; Basabe-Desmonts, L.; Benito-Lopez, F. Review on Microfluidic Paper-Based Analytical Devices towards Commercialisation. *Anal. Chim. Acta* **2018**, *1001*, 1–17. https://doi.org/10.1016/j.aca.2017.11.010.

(48) Zhong, Q.; Ding, H.; Gao, B.; He, Z.; Gu, Z. Advances of Microfluidics in Biomedical Engineering. *Adv. Mater. Technol.* **2019**, *4* (6), 1800663. https://doi.org/10.1002/admt.201800663.

(49) Martinez, A. W.; Phillips, S. T.; Carrilho, E.; Thomas, S. W.; Sindi, H.;

Whitesides, G. M. Simple Telemedicine for Developing Regions: Camera Phones and Paper-Based Microfluidic Devices for Real-Time, off-Site Diagnosis. *Anal. Chem.* **2008**, *80* (10), 3699–3707. https://doi.org/10.1021/ac800112r.

(50) Verma, M. S.; Tsaloglou, M. N.; Sisley, T.; Christodouleas, D.; Chen, A.; Milette, J.; Whitesides, G. M. Sliding-Strip Microfluidic Device Enables ELISA on Paper. *Biosens. Bioelectron.* **2018**, *99*, 77–84. https://doi.org/10.1016/j.bios.2017.07.034.

(51) Cheng, C.-M.; Martinez, A. W.; Gong, J.; Mace, C. R.; Phillips, S. T.; Carrilho, E.; Mirica, K. A.; Whitesides, G. M. Paper-Based ELISA. *Angew. Chemie* **2010**, *122* (28), 4881–4884. https://doi.org/10.1002/anie.201001005.

(52) Lopez-Ruiz, N.; Curto, V. F.; Erenas, M. M.; Benito-Lopez, F.; Diamond, D.; Palma, A. J.; Capitan-Vallvey, L. F. Smartphone-Based Simultaneous PH and Nitrite Colorimetric Determination for Paper Microfluidic Devices. *Anal. Chem.* **2014**, *86* (19), 9554–9562. https://doi.org/10.1021/ac5019205.

(53) Yagoda, H. Applications of Confined Spot Tests in Analytical Chemistry: Preliminary Paper. *Ind. Eng. Chem. - Anal. Ed.* **1937**, *9* (2), 79–82. https://doi.org/10.1021/ac50106a012.

(54) Müller, R. H.; Clegg, D. L. Automatic Paper Chromatography. *Anal. Chem.* **1949**, *21* (9), 1123–1125. https://doi.org/10.1021/ac60033a032.

(55) NobelPrize.org. The Nobel Prize in Chemistry https://www.nobelprize.org/prizes/chemistry/1952/summary/ (accessed Sep 3, 2020).

(56) Comer, J. P. Semiquantitative Specific Test Paper for Glucose in Urine. *Anal. Chem.* **1956**, *28* (11), 1748–1750. https://doi.org/10.1021/ac60119a030.

(57) Nygaard, A. P.; Hall, B. D. A Method For The Detection of RNA-DNA Complexes. *Biochem. Biophys. Res. Commun.* **1963**, *12* (2), 98–104. https://doi.org/10.1016/0006-291X(63)90242-0.

(58) Farrell, B. O. *Evolution in Lateral Flow-Based Immunoassay Systems*; Wong, R. C., Tse, H. Y., Eds.; Humana Press, 2009; Vol. 57. https://doi.org/10.1007/978-1-59745-240-3.

(59) Leuvering, J. H. W. Metal Sol Particle Immunoassay. US4313734A, 1982.

(60) Campbell, R. L.; Wagner, D. B.; O'Connell, J. P. Solid Phase Assay with Visual Readout. US4703017A, 1987.

(61) Rosenstein, R. W.; Bloomster, T. G. Solid Phase Assay Employing Capillary Flow. US4855240A, 1989.

(62) Yang, Y.; Noviana, E.; Nguyen, M. P.; Geiss, B. J.; Dandy, D. S.; Henry, C. S. Paper-Based Microfluidic Devices: Emerging Themes and Applications. *Anal. Chem.* **2017**, *89* (1), 71–91. https://doi.org/10.1021/acs.analchem.6b04581.

(63) Xia, Y.; Si, J.; Li, Z. Fabrication Techniques for Microfluidic Paper-Based Analytical Devices and Their Applications for Biological Testing: A Review. *Biosens. Bioelectron.* **2016**, *77*, 774–789. https://doi.org/10.1016/j.bios.2015.10.032.

(64) Mu, X.; Zhang, Y. S. Fabrication and Applications of Paper-Based Microfluidics. *Diagnostic Devices with Microfluid.* **2019**, No. 1, 45–64. https://doi.org/10.1201/9781315154442-3.

(65) Fenton, E. M.; Mascarenas, M. R.; Lopez, G. P.; Sibbert, S. S. Multiplex Lateral-Flow Test Strips Fabricated by Two-Dimensional Shaping. *Appl. Mater. Interfaces* **2009**, *1* (1), 124–129. https://doi.org/10.1021/am800043z.

(66) Fu, E.; Lutz, B.; Kauffman, P.; Yager, P. Controlled Reagent Transport in Disposable 2D Paper NetworksNo Title. *Lab Chip* **2010**, *10*, 918–920. https://doi.org/10.1039/B919614E.

(67) Dungchai, W.; Chailapakul, O.; Henry, C. S. A Low-Cost, Simple, and Rapid Fabrication Method for Paper-Based Microfluidics Using Wax Screen-Printing. *Analyst* **2011**, *136* (1), 77–82. https://doi.org/10.1039/c0an00406e.

(68) Songjaroen, T.; Dungchai, W.; Chailapakul, O.; Laiwattanapaisal, W. Novel, Simple and Low-Cost Alternative Method for Fabrication of Paper-Based Microfluidics by Wax Dipping. *Talanta* **2011**, *85* (5), 2587–2593. https://doi.org/10.1016/j.talanta.2011.08.024.

(69) Songjaroen, T.; Dungchai, W.; Chailapakul, O.; Henry, C. S.; Laiwattanapaisal, W. Blood Separation on Microfluidic Paper-Based Analytical Devices. *Lab Chip* **2012**, *12* (18), 3392–3398. https://doi.org/10.1039/c2lc21299d.

(70) Lu, R.; Shi, W.; Jiang, L.; Qin, J.; Lin, B. Rapid Prototyping of Paper-Based Microfluidics with Wax for Low-Cost, Portable Bioassay. *Electrophoresis* **2009**, *30* (9), 1497–1500. https://doi.org/10.1002/elps.200800563.

(71) Bruzewicz, D. A.; Reches, M.; Whitesides, G. M. Low-Cost Printing of Poly(Dimethylsiloxane) Barriers To Define Microchannels in Paper. *Anal. Chem.* **2008**, *80* (9), 3387–3392. https://doi.org/10.1021/ac801251y.

(72) Curto, V. F.; Lopez-Ruiz, N.; Capitan-Vallvey, L. F.; Palma, A. J.; Benito-Lopez, F.; Diamond, D. Fast Prototyping of Paper-Based Microfluidic Devices by Contact Stamping Using Indelible Ink. *RSC Adv.* **2013**, *3* (41), 18811–18816. https://doi.org/10.1039/c3ra43825b.

(73) Akyazi, T.; Saez, J.; Elizalde, J.; Benito-Lopez, F. Fluidic Flow Delay by Ionogel Passive Pumps in Microfluidic Paper-Based Analytical Devices. *Sensors Actuators, B Chem.* **2016**, *233*, 402–408. https://doi.org/10.1016/j.snb.2016.04.116.

(74) Li, X.; Tian, J.; Nguyen, T.; Shen, W. Paper-Based Microfluidic Devices by Plasma. *Anal. Chem.* **2008**, *80* (23), 9131–9134. https://doi.org/10.1039/b811135a.10.1021/ac801729t.

(75) Li, X.; Tian, J.; Garnier, G.; Shen, W. Fabrication of Paper-Based Microfluidic Sensors by Printing. *Colloids Surfaces B Biointerfaces* **2010**, *76* (2), 564–570. https://doi.org/10.1016/j.colsurfb.2009.12.023.

(76) Abe, K.; Suzuki, K.; Citterio, D. Inkjet-Printed Microfluidic Multianalyte Chemical Sensing Paper. *Anal. Chem.* **2008**, *80* (18), 6928–6934. https://doi.org/10.1021/ac800604v.

(77) Apilux, A.; Ukita, Y.; Chikae, M.; Chailapakul, O.; Takamura, Y. Development of Automated Paper-Based Devices for Sequential Multistep Sandwich Enzyme-Linked Immunosorbent Assays Using Inkjet Printing. *Lab Chip* **2013**, *13* (1), 126–135. https://doi.org/10.1039/c2lc40690j.

(78) Wang, J.; Monton, M. R. N.; Zhang, X.; Filipe, C. D. M.; Pelton, R.; Brennan, J. D. Hydrophobic Sol-Gel Channel Patterning Strategies for Paper-Based Microfluidics. *Lab Chip* **2014**, *14* (4), 691–695. https://doi.org/10.1039/c3lc51313k.

(79) Deiss, F.; Matochko, W. L.; Govindasamy, N.; Lin, E. Y.; Derda, R. Flow-through

Synthesis on Teflon-Patterned Paper to Produce Peptide Arrays for Cell-Based Assays. *Angew. Chemie - Int. Ed.* **2014**, *53* (25), 6374–6377. https://doi.org/10.1002/anie.201402037.

(80) Haller, P. D.; Flowers, C. A.; Gupta, M. Three-Dimensional Patterning of Porous Materials Using Vapor Phase Polymerization. *Soft Matter* **2011**, *7* (6), 2428–2432. https://doi.org/10.1039/c0sm01214a.

(81) Olkkonen, J.; Lehtinen, K.; Erho, T. Flexographically Printed Fluidic Structures in Paper. *Anal. Chem.* **2010**, *82* (24), 10246–10250. https://doi.org/10.1021/ac1027066.

(82) Abe, K.; Kotera, K.; Suzuki, K.; Citterio, D. Inkjet-Printed Paperfluidic Immuno-Chemical Sensing Device. *Anal. Bioanal. Chem.* **2010**, *398* (2), 885–893. https://doi.org/10.1007/s00216-010-4011-2.

(83) He, Q.; Ma, C.; Hu, X.; Chen, H. Method for Fabrication of Paper-Based Microfluidic Devices by Alkylsilane Self-Assembling and UV/O3-Patterning. *Anal. Chem.* **2013**, *85* (3), 1327–1331. https://doi.org/10.1021/ac303138x.

(84) Zhang, A. L.; Zha, Y. Fabrication of Paper-Based Microfluidic Device Using Printed Circuit Technology. *AIP Adv.* **2012**, *2* (2), 022171. https://doi.org/10.1063/1.4733346.

(85) Chitnis, G.; Ding, Z.; Chang, C. L.; Savran, C. A.; Ziaie, B. Laser-Treated Hydrophobic Paper: An Inexpensive Microfluidic Platform. *Lab Chip* **2011**, *11* (6), 1161–1165. https://doi.org/10.1039/c0lc00512f.

(86) Cate, D. M.; Adkins, J. A.; Mettakoonpitak, J.; Henry, C. S. Recent Developments in Paper-Based Microfluidic Devices. *Anal. Chem.* **2015**, *87* (1), 19–41. https://doi.org/10.1021/ac503968p.

(87) Alkasir, R. S. J.; Rossner, A.; Andreescu, S. Portable Colorimetric Paper-Based Biosensing Device for the Assessment of Bisphenol A in Indoor Dust. *Environ. Sci. Technol.* **2015**, *49* (16), 9889–9897. https://doi.org/10.1021/acs.est.5b01588.

(88) Wang, W.; Wu, W. Y.; Wang, W.; Zhu, J. J. Tree-Shaped Paper Strip for Semiquantitative Colorimetric Detection of Protein with Self-Calibration. *J. Chromatogr. A* **2010**, *1217* (24), 3896–3899. https://doi.org/10.1016/j.chroma.2010.04.017.

(89) Dungchai, W.; Chailapakul, O.; Henry, C. S. Use of Multiple Colorimetric Indicators for Paper-Based Microfluidic Devices. *Anal. Chim. Acta* **2010**, *674* (2), 227–233. https://doi.org/10.1016/j.aca.2010.06.019.

(90) Ornatska, M.; Sharpe, E.; Andreescu, D.; Andreescu, S. Paper Bioassay Based on Ceria Nanoparticles as Colorimetric Probes. *Anal. Chem.* **2011**, *83* (11), 4273–4280. https://doi.org/10.1021/ac200697y.

(91) Klasner, S. A.; Price, A. K.; Hoeman, K. W.; Wilson, R. S.; Bell, K. J.; Culbertson, C. T. Paper-Based Microfluidic Devices for Analysis of Clinically Relevant Analytes Present in Urine and Saliva. *Anal. Bioanal. Chem.* **2010**, *397* (5), 1821–1829. https://doi.org/10.1007/s00216-010-3718-4.

(92) Chen, X.; Chen, J.; Wang, F.; Xiang, X.; Luo, M.; Ji, X.; He, Z. Determination of Glucose and Uric Acid with Bienzyme Colorimetry on Microfluidic Paper-Based Analysis Devices. *Biosens. Bioelectron.* **2012**, *35* (1), 363–368. https://doi.org/10.1016/j.bios.2012.03.018.

(93) Mentele, M. M.; Cunningham, J.; Koehler, K.; Volckens, J.; Henry, C. S. Microfluidic Paper-Based Analytical Device for Particulate Metals. *Anal. Chem.* **2012**, *84* (10), 4474–4480. https://doi.org/10.1021/ac300309c.

(94) Li, M.; Cao, R.; Nilghaz, A.; Guan, L.; Zhang, X.; Shen, W. "Periodic-Table-Style" Paper Device for Monitoring Heavy Metals in Water. *Anal. Chem.* **2015**, *87* (5), 2555–2559. https://doi.org/10.1021/acs.analchem.5b00040.

(95) Chen, W.; Fang, X.; Li, H.; Cao, H.; Kong, J. A Simple Paper-Based Colorimetric Device for Rapid Mercury(II) Assay. *Sci. Rep.* **2016**, *6* (June), 31948. https://doi.org/10.1038/srep31948.

(96) Wei, X.; Tian, T.; Jia, S.; Zhu, Z.; Ma, Y.; Sun, J.; Lin, Z.; Yang, C. J. Microfluidic Distance Readout Sweet Hydrogel Integrated Paper-Based Analytical Device (MDiSH-PAD) for Visual Quantitative Point-of-Care Testing. *Anal. Chem.* **2016**, *88* (4), 2345–2352. https://doi.org/10.1021/acs.analchem.5b04294.

(97) Liu, X. Y.; Cheng, C. M.; Martinez, A. W.; Mirica, K. A.; Li, X. J.; Phillips, S. T.; Mascareñas, M.; Whitesides, G. M. A Portable Microfluidic Paper-Based Device for Elisa. *Proc. IEEE Int. Conf. Micro Electro Mech. Syst.* **2011**, 75–78. https://doi.org/10.1109/MEMSYS.2011.5734365.

(98) Jokerst, J. C.; Adkins, J. A.; Bisha, B.; Mentele, M. M.; Goodridge, L. D.; Henry,

C. S. Development of a Paper-Based Analytical Device for Colorimetric Detection of Select Foodborne Pathogens. *Anal. Chem.* **2012**, *84* (6), 2900–2907. https://doi.org/10.1021/ac203466y.

(99) Hossain, S. M. Z.; Brennan, J. D. β-Galactosidase-Based Colorimetric Paper Sensor for Determination of Heavy Metals. *Anal. Chem.* **2011**, *83* (22), 8772–8778. https://doi.org/10.1021/ac202290d.

(100) Nie, Z.; Deiss, F.; Liu, X.; Akbulut, O.; Whitesides, G. M. Integration of Paper-Based Microfluidic Devices with Commercial Electrochemical Readers. *Lab Chip* **2010**, *10* (22), 3163–3169. https://doi.org/10.1039/c0lc00237b.

(101) Dungchai, W.; Chailapakul, O.; Henry, C. S. Electrochemical Detection for Paper-Based Microfluidic. *Anal. Chem.* **2009**, *81*, 5821–5826. https://doi.org/10.1016/j.snb.2012.11.002.

(102) Cunningham, J. C.; Brenes, N. J.; Crooks, R. M. Paper Electrochemical Device for Detection of DNA and Thrombin by Target-Induced Conformational Switching. *18th Int. Conf. Miniaturized Syst. Chem. Life Sci. MicroTAS 2014* **2014**, *86*, 6166–6170.

(103) Carvalhal, R. F.; Kfouri, M. S.; De Piazetta, M. H. O.; Gobbi, A. L.; Kubota, L. T. Electrochemical Detection in a Paper-Based Separation Device. *Anal. Chem.* **2010**, *82* (3), 1162–1165. https://doi.org/10.1021/ac902647r.

(104) Liu, H.; Crooks, R. M. Paper-Based Electrochemical Sensing Platform with Integral Battery and Electrochromic Read-Out. *Anal. Chem.* **2012**, *84* (5), 2528–2532. https://doi.org/10.1021/ac203457h.

(105) Ruecha, N.; Rodthongkum, N.; Cate, D. M.; Volckens, J.; Chailapakul, O.; Henry, C. S. Sensitive Electrochemical Sensor Using a Graphene-Polyaniline Nanocomposite for Simultaneous Detection of Zn(II), Cd(II), and Pb(II). *Anal. Chim. Acta* **2015**, *874*, 40–48. https://doi.org/10.1016/j.aca.2015.02.064.

(106) Wang, Y.; Xu, H.; Luo, J.; Liu, J.; Wang, L.; Fan, Y.; Yan, S.; Yang, Y.; Cai, X. A Novel Label-Free Microfluidic Paper-Based Immunosensor for Highly Sensitive Electrochemical Detection of Carcinoembryonic Antigen. *Biosens. Bioelectron.* **2016**, *83*, 319–326. https://doi.org/10.1016/j.bios.2016.04.062.

(107) Glavan, A. C.; Christodouleas, D. C.; Mosadegh, B.; Yu, H. D.; Smith, B. S.; Lessing, J.; Fernández-Abedul, M. T.; Whitesides, G. M. Folding Analytical

Devices for Electrochemical ELISA in Hydrophobic RH Paper. *Anal. Chem.* **2014**, *86* (24), 11999–12007. https://doi.org/10.1021/ac5020782.

(108) Ge, S.; Ge, L.; Yan, M.; Song, X.; Yu, J.; Huang, J. A Disposable Paper-Based Electrochemical Sensor with an Addressable Electrode Array for Cancer Screening. *Chem. Commun.* **2012**, *48* (75), 9397–9399. https://doi.org/10.1039/c2cc34887j.

(109) Carrilho, E.; Phillips, S. T.; Vella, S. J.; Martinez, A. W.; Whitesides, G. M. Paper Microzone Plates. *Anal. Chem.* **2009**, *81* (15), 5990–5998. https://doi.org/10.1021/ac900847g.

(110) Ali, M. M.; Aguirre, S. D.; Xu, Y.; Filipe, C. D. M.; Pelton, R.; Li, Y. Detection of DNA Using Bioactive Paper Strips. *Chem. Commun.* **2009**, No. 43, 6640–6642. https://doi.org/10.1039/b911559e.

(111) Thom, N. K.; Yeung, K.; Pillion, M. B.; Phillips, S. T. "Fluidic Batteries" as Low-Cost Sources of Power in Paper-Based Microfluidic Devices. *Lab Chip* **2012**, *12* (10), 1768–1770. https://doi.org/10.1039/c2lc40126f.

(112) Rosa, A. M. M.; Louro, A. F.; Martins, S. A. M.; Inácio, J.; Azevedo, A. M.; Prazeres, D. M. F. Capture and Detection of DNA Hybrids on Paper via the Anchoring of Antibodies with Fusions of Carbohydrate Binding Modules and ZZ-Domains. *Anal. Chem.* **2014**, *86* (9), 4340–4347. https://doi.org/10.1021/ac5001288.

(113) Liang, L.; Su, M.; Li, L.; Lan, F.; Yang, G.; Ge, S.; Yu, J.; Song, X. Aptamer-Based Fluorescent and Visual Biosensor for Multiplexed Monitoring of Cancer Cells in Microfluidic Paper-Based Analytical Devices. *Sensors Actuators, B Chem.* **2016**, *229*, 347–354. https://doi.org/10.1016/j.snb.2016.01.137.

(114) Liang, J.; Wang, Y.; Liu, B. Paper-Based Fluoroimmunoassay for Rapid and Sensitive Detection of Antigen. *RSC Adv.* **2012**, *2* (9), 3878–3884. https://doi.org/10.1039/c2ra20156a.

(115) Nery, E. W.; Kubota, L. T. Sensing Approaches on Paper-Based Devices: A Review. *Anal. Bioanal. Chem.* **2013**, *405* (24), 7573–7595. https://doi.org/10.1007/s00216-013-6911-4.

(116) Nuchtavorn, N.; Macka, M. A Novel Highly Flexible, Simple, Rapid and Low-Cost Fabrication Tool for Paper-Based Microfluidic Devices (MPADs) Using

Technical Drawing Pens and in-House Formulated Aqueous Inks. *Anal. Chim. Acta* **2016**, *919*, 70–77. https://doi.org/10.1016/j.aca.2016.03.018.

(117) Alahmad, W.; Uraisin, K.; Nacapricha, D.; Kaneta, T. Miniaturized Chemiluminescence Detection System for a Microfluidic Paper-Based Analytical Device and Its Application to the Determination of Chromium(III). *Anal. Methods* **2016**, *8* (27), 5414–5420. https://doi.org/10.1039/c6ay00954a.

(118) Yu, J.; Ge, L.; Huang, J.; Wang, S.; Ge, S. Microfluidic Paper-Based Chemiluminescence Biosensor for Simultaneous Determination of Glucose and Uric Acid. *Lab Chip* **2011**, *11* (7), 1286–1291. https://doi.org/10.1039/c0lc00524j.

(119) Yu, J.; Wang, S.; Ge, L.; Ge, S. A Novel Chemiluminescence Paper Microfluidic Biosensor Based on Enzymatic Reaction for Uric Acid Determination. *Biosens. Bioelectron.* **2011**, *26* (7), 3284–3289. https://doi.org/10.1016/j.bios.2010.12.044.

(120) Wang, Y.; Ge, L.; Wang, P.; Yan, M.; Ge, S.; Li, N.; Yu, J.; Huang, J. Photoelectrochemical Lab-on-Paper Device Equipped with a Porous Au-Paper Electrode and Fluidic Delay-Switch for Sensitive Detection of DNA Hybridization. *Lab Chip* **2013**, *13* (19), 3945–3955. https://doi.org/10.1039/c3lc50430a.

(121) Ge, L.; Wang, S.; Song, X.; Ge, S.; Yu, J. 3D Origami-Based Multifunction-Integrated Immunodevice: Low-Cost and Multiplexed Sandwich Chemiluminescence Immunoassay on Microfluidic Paper-Based Analytical Device. *Lab Chip* **2012**, *12* (17), 3150–3158. https://doi.org/10.1039/c2lc40325k.

(122) Wang, S.; Ge, L.; Song, X.; Yan, M.; Ge, S.; Yu, J.; Zeng, F. Simple and Covalent Fabrication of a Paper Device and Its Application in Sensitive Chemiluminescence Immunoassay. *Analyst* **2012**, *137* (16), 3821–3827. https://doi.org/10.1039/c2an35266d.

(123) Chinnadayyala, S. R.; Park, J.; Le, H. T. N.; Santhosh, M.; Kadam, A. N.; Cho, S. Recent Advances in Microfluidic Paper-Based Electrochemiluminescence Analytical Devices for Point-of-Care Testing Applications. *Biosens. Bioelectron.* **2019**, *126* (July 2018), 68–81. https://doi.org/10.1016/j.bios.2018.10.038.

(124) Delaney, J. L.; Hogan, C. F.; Tian, J.; Shen, W. Electrogenerated Chemiluminescence Detection in Paper-Based Microfluidic Sensors. *Anal. Chem.* **2011**, *83* (4), 1300–1306. https://doi.org/10.1021/ac102392t.

(125) Shi, J.; Tang, F.; Xing, H.; Zheng, H.; Bi, L.; Wang, W. Electrochemical Detection of Pb and Cd in Paper-Based Microfluidic Devices. *J. Braz. Chem. Soc.* **2012**, *23* (6), 1124–1130. https://doi.org/10.1590/S0103-50532012000600018.

(126) Bertoncello, P.; Stewart, A. J.; Dennany, L. Analytical Applications of Nanomaterials in Electrogenerated Chemiluminescence. *Anal. Bioanal. Chem.* **2014**, *406* (23), 5573–5587. https://doi.org/10.1007/s00216-014-7946-x.

(127) Deng, S.; Ju, H. Electrogenerated Chemiluminescence of Nanomaterials for Bioanalysis. *Analyst* **2013**, *138*, 43–61. https://doi.org/10.1039/b000000x.

(128) Zhou, Y.; Yan, D.; Wei, M. A 2D Quantum Dot-Based Electrochemiluminescence Film Sensor towards Reversible Temperature-Sensitive Response and Nitrite Detection. *J. Mater. Chem. C* **2015**, *3* (39), 10099–10106. https://doi.org/10.1039/c5tc02002f.

(129) Dalla Marta, S.; Novara, C.; Giorgis, F.; Bonifacio, A.; Sergo, V. Optimization and Characterization of Paper-Made Surface Enhanced Raman Scattering (SERS) Substrates with Au and Ag NPs for Quantitative Analysis. *Materials (Basel).* **2017**, *10* (12), 1365. https://doi.org/10.3390/ma10121365.

(130) Rohrman, B. A.; Richards-Kortum, R. R. A Paper and Plastic Device for Performing Recombinase Polymerase Amplification of HIV DNA. *Lab Chip* **2012**, *12* (17), 3082–3088. https://doi.org/10.1039/c2lc40423k.

(131) Li, C. Z.; Vandenberg, K.; Prabhulkar, S.; Zhu, X.; Schneper, L.; Methee, K.; Rosser, C. J.; Almeide, E. Paper Based Point-of-Care Testing Disc for Multiplex Whole Cell Bacteria Analysis. *Biosens. Bioelectron.* **2011**, *26* (11), 4342–4348. https://doi.org/10.1016/j.bios.2011.04.035.

(132) Parolo, C.; Merkoçi, A. Paper-Based Nanobiosensors for Diagnostics. *Chem. Soc. Rev.* **2013**, *42* (2), 450–457. https://doi.org/10.1039/c2cs35255a.

(133) Hu, J.; Wang, S. Q.; Wang, L.; Li, F.; Pingguan-Murphy, B.; Lu, T. J.; Xu, F. Advances in Paper-Based Point-of-Care Diagnostics. *Biosens. Bioelectron.* **2014**, *54*, 585–597. https://doi.org/10.1016/j.bios.2013.10.075.

(134) Schonhorn, J. E.; Fernandes, S. C.; Rajaratnam, A.; Deraney, R. N.; Rollanda, J. P.; Mace, C. R. A Device Architecture for Three-Dimensional, Patterned Paper Immunoassays. *Lab Chip* **2014**, *14* (24), 4653–4658. https://doi.org/10.1039/c4lc00876f.

(135) Li, M.; Tian, J.; Al-Tamimi, M.; Shen, W. Paper-Based Blood Typing Device That Reports Patient's Blood Type "in Writing." *Angew. Chemie - Int. Ed.* **2012**, *51* (22), 1–6. https://doi.org/10.1002/anie.201201822.

(136) Zhang, Y.; Ma, H.; Wu, D.; Li, Y.; Du, B.; Wei, Q. Label-Free Immunosensor Based on Au@Ag2S Nanoparticles/Magnetic Chitosan Matrix for Sensitive Determination of Ractopamine. *J. Electroanal. Chem.* **2015**, *741*, 14–19. https://doi.org/10.1016/j.jelechem.2015.01.007.

(137) Liu, W.; Kou, J.; Xing, H.; Li, B. Paper-Based Chromatographic Chemiluminescence Chip for the Detection of Dichlorvos in Vegetables. *Biosens. Bioelectron.* **2014**, *52*, 76–81. https://doi.org/10.1016/j.bios.2013.08.024.

(138) Nouanthavong, S.; Nacapricha, D.; Henry, C. S.; Sameenoi, Y. Pesticide Analysis Using Nanoceria-Coated Paper-Based Devices as a Detection Platform. *Analyst* **2016**, *141* (5), 1837–1846. https://doi.org/10.1039/c5an02403j.

(139) Armbruster, D. A.; Pry, T. Limit of Blank, Limit of Detection and Limit of Quantitation. *Clin. Biochem. Rev.* **2008**, *29* (August), S49-52.

(140) Anderson, D. J. Determination of the Lower Limit of Detection. *Clin. Chem.* **1989**, *35* (10), 2152–2153. https://doi.org/10.1093/clinchem/35.10.2152.

(141) Xi, Y.; Zhang, Y.; Fang, J.; Whittaker, K.; Luo, S.; Huang, R. P. Prokaryotic Expression of Hepatitis C Virus-NS3 Protein and Preparation of a Monoclonal Antibody. *Monoclon. Antib. Immunodiagn. Immunother.* **2017**, *36* (6), 251–258. https://doi.org/10.1089/mab.2017.0033.